UNIVERSITY OF ALBERTA

METHODS FOR DETECTING SOURCES OF POWER QUALITY DISTURBANCES

By

Thavatchai Tayjasanant 

A thesis
submitted to the Faculty of Graduate Studies and Research
in partial fulfillment of the requirements for the degree of
Doctor of Philosophy

Department of Electrical and Computer Engineering

Edmonton, Alberta
Spring 2006

Your file Votre référence
ISBN: 0-494-14050-X
Our file Notre référence
ISBN: 0-494-14050-X

ABSTRACT

Power quality has attracted a great deal of attention in recent years due to an increasing utilization of sensitive power electronic-based loads in power systems. Power disturbances can cause severe damage to equipment and costly problems for customers. One of the important steps for power quality management is to determine the locations of disturbances. Only after a disturbance-source location is known can disturbance mitigation be further carried out. With the deregulation of the power industry, utilities have become increasingly interested in quantifying the responsibility for power quality problems. Consequently, research on how to identify which customer load or supply system is responsible for a power quality disturbance has become an important topic.

Voltage sag is one of the main power quality disturbances. This thesis presents a novel method for voltage sag-source detection. Its principle is to estimate the equivalent impedance of the non-disturbance side by utilizing voltage and current changes caused by the sag. The impedance estimation is derived using system identification and least-squares methods. The sign of the estimated resistance can reveal the location of the sag disturbance. Extensive tests using the method have shown that it is effective and reliable. A comparison of sag-source results with other published sag-source detection methods is also provided.

Voltage flicker is another type of power quality disturbance. It can be considered as repetitive voltage sags. The proposed system identification-based method is extended for flicker-source detection in this thesis. This research work further

analyzes interharmonic-caused voltage flickers and proposes a method to determine the interharmonic-related flicker sources.

Relationships between interharmonics and flickers are also investigated. A limit for interharmonic emission is proposed by utilizing the published limits on voltage flicker. The limit is represented as an interharmonic-magnitude versus interharmonic-frequency curve and is called an interharmonic-flicker curve. A systematic method to derive the limits for interharmonics is presented. Potential applications of the results are discussed.

ACKNOWLEDGEMENTS

First and foremost, I would like to express my sincerest gratitude and appreciation to my supervisor, Prof. Wilsun Xu, for his invaluable guidance, great patience, and consistent encouragement. It has been my honour and privilege to be one of his students. My gratitude extends to other members of my thesis committee, for their useful comments and suggestions: Dr. Andy Knight, Dr. Venkata Dinavahi, Dr. Mike MacGregor, and Prof. Sherif Faried. I am thankful to Dr. Ray DeCorby, who served as a chairman.

I also would like to thank the Department of Electrical Engineering, Chulalongkorn University, for granting me a leave of absence to pursue the Ph.D. degree, and Prof. Mathias H. J. Bollen, Prof. Mongkol Dejnakarinda, and Chaiya Chamchoy for helping me to come to University of Alberta. I am indebted to my uncles (especially Booncharn Tayjasanant), aunts, parents, and grandmothers, who financially supported me when I first came to study here. I gratefully acknowledge the financial support from the National Sciences and Engineering Research Council of Canada in the form of Research Assistantships and conference funding made available by Prof. Wilsun Xu, and Graduate Tuition scholarship and Dissertation fellowship from the University of Alberta.

I would like to thank the following people: Dr. Chun Li for his critical discussions and invaluable explanations that help me understand many issues in this work; Albert Terheide for laboratory assistance; Dr. Emad Ahmed for his useful discussions and suggestions; Dr. Zhenyu Huang, Dr. Guibin Zhang, Dr. Walmir Freitas, Prof. Washington Neves, and all my colleagues at Power Lab for our fruitful discussions; Dianne Cameron, Brian Gibson, Claudio Bringas, and Ontima Wasusri for their feedback and proofreading; and Dr. Suresh Kapoor for his kind hospitality, comments and encouragement. Finally, I would like to thank my parents, brother, and grandmothers for their eternal love, support, and confidence in me.

CONTENTS

Page

LIST OF TABLES

Page

LIST OF FIGURES

Page

LIST OF SYMBOLS AND ABBREVIATIONS

1P	Single line-to-ground fault
3P	Three-phase fault
Δf	Frequency difference
$\Delta i(t)$ and $\Delta v(t)$	Instantaneous current and voltage changes
$\Delta \boldsymbol{I}$ and $\Delta \boldsymbol{V}$	Complex current and voltage changes
ΔI	Magnitude of current change
ΔP	Active power change
$\Delta V/V$	Relative voltage fluctuation
$\lvert\boldsymbol{I}\rvert$ or I	Magnitude of complex current
$\lvert\boldsymbol{V}\rvert$ or V	Magnitude of complex voltage
$\lvert\boldsymbol{Z}\rvert$	Magnitude of complex impedance
$\angle\boldsymbol{Z}$	Phase angle of complex impedance
Φ	Frequency-response identification function
θ	Phase angle
$\mathbf{A}^{\mathrm{T}}$	Transpose of matrix **A**
AC	Alternating-current quantities
ASD	Adjustable speed drive
Cap	Capacitor
CPL	Constant power load
d	Per unit distance
DC	Direct-current quantities
DE	Disturbance energy
DFT	Discrete Fourier transform
DP	Disturbance power
DP-DE method	Disturbance Power-Disturbance Energy method
DS	Downstream
$\boldsymbol{E}$	Complex voltage source

f	Frequency in hertz
f_1	Fundamental frequency
f_d	Predominant frequency
f_h	Harmonic frequency
f_{IH}	Interharmonic frequency
h	Order of harmonic
HP	Horsepower
HV	High voltage
$ip_{3\phi}(t)$	Total three-phase instantaneous power
$ip_{ss}(t)$	Pre-disturbance, steady-state, three-phase instantaneous power
j	$\sqrt{-1}$
IEC	The International Electrotechnical Commission
IEEE	The Institute of Electrical and Electronics Engineers
IH or interh	Interharmonic
IM	Induction motor
IP(DP)	Initial peak of disturbance power
IZ method	Incremental Impedance method
L	Reactance
LL	Linear load
LLF	Line-to-line fault
LS	Least-squares method
LV	Low voltage
m	Interharmonic relative magnitude
n	Number of cycles during sag
N	Total number of samples in one cycle
P	Active power
P_1	Fundamental-frequency active power
PNF	Phase-to-neutral fault
PQ	Power quality

P_{st}	Short-term flicker level
P_t and Q_t	Active and reactive powers during the transient period
pu	Per unit quantities
r	Correlation coefficient
R	Resistance
R_e or R_{eq}	Equivalent resistance
$\Re$eal(.)	Real part of a complex value
RMS	Root-mean-square or effective value
R-X plane	Impedance plane
subscripts X and Y	Real and imaginary parts
superscript +	Pseudoinverse
T_1	Period of the fundamental-frequency component
US	Upstream
$v(t)$	Instantaneous voltage
$\boldsymbol{V}$ and $\boldsymbol{I}$	RMS complex voltage and current values
$\boldsymbol{V}_+$ and $\boldsymbol{I}_+$	Complex fundamental-frequency positive-sequence voltage and current
V_1	Fundamental-frequency voltage magnitude
V_{RMS} and V_{peak}	Root-mean-square and peak voltage magnitudes
VCC method	Voltage and Current Changes method
VFD	Variable frequency drive
X	Reactance
Xfmr	Transformer
$\boldsymbol{Z}$	Complex impedance value
$\boldsymbol{Z}_e$	Complex equivalent impedance value
$\boldsymbol{Z}_+$	Complex fundamental-frequency positive-sequence impedance
ZMP method	Impedance Magnitude and Phase method

CHAPTER 1

Introduction

The topic of electric power quality has attracted a great deal of interest over the last two decades. This is mainly because sensitive equipment and nonlinear loads are more commonplace in industrial, commercial, and residential sectors. Most older electromechanical equipment was robust and could handle minor changes in voltage with little or no effect on operations. However, recent technological advancement in electronics has led to an influx of power electronic-based devices and other sophisticated equipment that is very sensitive to minor voltage changes. These minor changes can easily cause malfunctions or disrupt sensitive loads. The disruption can lead to shutdowns of industrial processes resulting in tremendous economic losses. With today's high competition among utilities, power quality issues are more important than ever. The level of power quality delivered to end-users can be degraded by power quality disturbances which can originate anywhere in the power system. Although it is critically important to develop mitigation devices to keep disturbances to a minimum, locating the source of a disturbance needs to be the first step. Only after information about a disturbance-source detection is available can power quality troubleshooting, diagnosis, and mitigation be carried out. This chapter will explain the background of power quality and disturbances and power quality-source detection. The objective and scope of this thesis and the thesis outline are provided.

1.1 Power Quality and Disturbances

The term "power quality" (PQ) can mean different things to different people, depending on one's frame of reference. PQ for the electric utility could mean the integrity of the sinusoidal aspect of the voltage wave, while PQ for the industrial customer could mean the relative absence of voltage variations as measured at the point of service [1] or mean the continuity of power [2]. Although the term power quality is used, it is actually the quality of the voltage that is being addressed in most cases because the power supply system can only control the quality of the voltage and has no control over the currents that specific loads might draw [3]. PQ disturbances are generally any phenomena which can deteriorate the quality of the power delivered to end-users. These disturbances can occur anywhere in electrical systems. Two widely referenced organizations—The Institute of Electrical and Electronics Engineers (IEEE) and The International Electrotechnical Commission (IEC)—define power quality and disturbance as summarized in Table 1.1.

Table 1.1: Power quality and disturbance definitions by IEEE and IEC standards

Power Quality Definitions	Disturbance Definitions
IEEE 1100 [4]: The concept of powering and grounding electronic equipment in a manner that is suitable to the operation of that equipment and compatible with the premise wiring system and other connected equipment.	IEEE 1100 [4]: Any deviation from the nominal value (or from some selected thresholds based on load tolerance) of the input AC power characteristics.
IEC 61000-4-30 [5]: Characteristics of the electricity at a given point on an electrical system, evaluated against a set of reference technical parameters.	IEC 61000-2-5 [6]: Any electromagnetic phenomenon which might degrade the performance of a device, equipment or system or adversely affect living or inert matter.

IEEE 1159 [7] and IEC 61000-2-5 [6] classify PQ disturbances into various categories. IEEE 1159 puts PQ disturbances into seven categories based on information about typical spectral content, duration, and magnitude. A further subdivision of some disturbances is possible. Table 1.2 summarizes the classification in order of the increased duration.

Table 1.2: Classification of PQ disturbances according to IEEE 1159

Categories	Typical Spectral Content	Typical Magnitude	Typical Duration
1. Transients			
– Impulsive	5 ns - 0.1 ms rise		50 ns less - 1ms plus
– Oscillatory	0.5 MHz - 5 kHz less	0 - 8 pu*	5 μs - 0.3 ms
2. Short-duration variations			
– Interruptions		< 0.1 pu	0.5 cycles - 1 min
– Sags		0.1 - 0.9 pu	0.5 cycles - 1 min
– Swells		1.1 - 1.8 pu	0.5 cycles - 1 min
3. Long-duration variations			
– Sustained interruptions		0.0 pu	> 1 min
– Undervoltages		0.8 - 0.9 pu	> 1 min
– Overvoltages		1.1 - 1.2 pu	> 1 min
4. Voltage fluctuations	< 25 Hz	0.1 - 7%	Intermittent
5. Power-frequency variations			< 10 s
6. Voltage imbalances		0.5 - 2%	Steady-state
7. Waveform distortions			
– DC offset	0 - 0.1%		Steady-state
– Harmonics	0 - 20%	0 - 100th H	Steady-state
– Interharmonics	0 - 2%	0 - 6 kHz	Steady-state
– Notching			Steady-state
– Noise	0 - 1%	Broadband	Steady-state

* The per-unit (pu) value of any quantity is defined as the ratio of that quantity to its base (nominal) value expressed as a decimal.

IEC 61000-2-5 classifies PQ disturbances into three categories of environment phenomena. Each phenomenon is then divided into radiated and conducted disturbances depending on the medium within which they occur. Radiated

disturbances occur in the medium surrounding the equipment, while conducted disturbances occur in various metallic media. The boundary frequency between the low and high frequencies is generally understood as being 9 kHz. Table 1.3 lists the types of phenomena.

Table 1.3: Principal phenomena causing electromagnetic disturbances according to IEC 61000-2-5

1.1 Conducted low-frequency phenomena	– Harmonics and interharmonics – Signalling voltages – Voltage fluctuations – Voltage dips and interruptions – Voltage unbalance – Power-frequency variations – Induced low-frequency voltages – DC in AC networks
1.2 Radiated low-frequency phenomena	– Magnetic fields – Electric fields
2.1 Conducted high-frequency phenomena	– Induced continuous wave voltages and currents – Unidirectional transients – Oscillatory transients
2.2 Radiated high-frequency phenomena	– Magnetic fields – Electric fields – Electromagnetic fields: Continuous wave and Transient
3 Electrostatic discharge phenomena	

Among various PQ disturbances, only voltage sags (dips in IEC terms) and voltage fluctuations will be considered in this thesis. Voltage sags are considered to be the most important PQ problem [8] and voltage fluctuations can cause voltage flicker which is also another PQ problem [9, 10]. Details of voltage sag and flicker will be presented in Sections 2.1 and 5.1, respectively.

1.2 Disturbance-Source Detection

Poor power quality is normally associated with high cost. For example, an interruption of less than a tenth of a second at one glass plant can cost about $200,000 and a two-second outage at a computer centre can cost up to $600,000 [11]. As a result, both electric utilities and their customers have a great financial incentive to reduce the severity and frequency of PQ disturbances in the power system. In order to understand and diagnose the nature of disturbances, PQ monitoring is required. Generally, the monitoring point for a meter is at the service entrance of an industrial plant. Recorded voltage and current waveforms cannot directly tell on which side of the meter a disturbance occurs. Further analysis of these waveforms is needed to develop a method of determining the location of a disturbance, otherwise known as disturbance-source detection. PQ troubleshooting, diagnosis, and mitigation can only be carried out after the disturbance-source detection is completed. Then any disputes about the major responsible party can be resolved fairly and the standard compliance can be fully accessed. The PQ disturbances described in the previous section can originate anywhere in the power system from the utility system to inside the customer's premises. Figure 1.1 illustrates the problem of disturbance-source detection. The objective of disturbance-source detection is to determine whether a disturbance originates upstream or downstream from the monitoring point. It is assumed that the fundamental-frequency active power flows from the upstream side to the downstream side. Further practical applications of the disturbance-source detection will be described in Section 2.2.

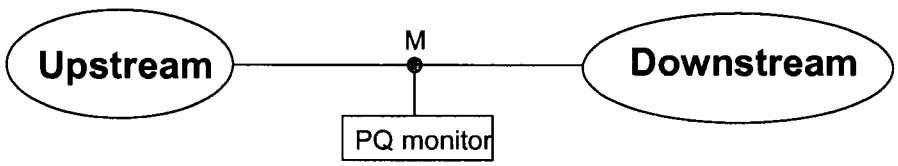

Figure 1.1: The disturbance-source detection problem

1.3 Objective and Scope

As explained earlier, PQ disturbances can have a huge economic impact. Attempts to reduce PQ disturbances to a minimum will be very beneficial. Most studies of PQ issues involve disturbance measurement and mitigation methods. Little work has been done on methods to locate the sources of PQ disturbances. Electric utilities and customers have become increasingly interested in quantifying the responsibilities for PQ problems. Consequently, research on how to locate disturbance sources has become a significant issue recently. One of the primary goals of any PQ investigation is to determine the source of any problem-causing disturbances [12]. In spite of various efforts, there is still no reliable and technically sound method for locating PQ disturbance sources. Available methods have limitations and still lack concrete theoretical supports. The objective of the research work in this thesis is to develop a theoretically justifiable and practically useful method for PQ disturbance-source detection. The PQ disturbances that will be considered are voltage sags and voltage fluctuations. The proposed method will not only help industry to correctly identify source directions of PQ disturbances, but also fairly settle disputes between responsible parties.

The scope of this thesis can be summarized as follows:

- Conducting a literature review on published methods to determine sag-source detection and comparing results of sag-source detection from published methods using available data from computer simulations, experimental tests, and field measurements. This task also requires a development of source codes to simulate the algorithms of published methods.

- Developing a method for sag-source detection. The method should be effective and practical for general-purpose sag-source detection. Sags from faults, transformer energization, and induction motor starting will be investigated.

- Verifying the proposed sag-source detection method with data from computer simulations, experimental tests, and field measurements. Limitations of the proposed sag-source detection method will be discussed.

- Developing a method for flicker-source detection. Voltage flicker is another type of disturbance and a result of voltage fluctuation. Flickers caused by two major sources—fluctuating and interharmonic-producing loads—will be investigated.

- Verifying the proposed flicker-source detection method with data from experimental tests and field measurements. Limitations of the proposed flicker-source detection method will be discussed.

1.4 Outline of the Thesis

This research work offers more reliable and accurate method for PQ disturbance-source detection. Computer simulations and experimental tests in the laboratory were conducted to verify the validity of the proposed method. Verification studies of data from field measurements could yield some practical limitations of the proposed method. The contents of the thesis are organized as follows:

Chapter 2 describes voltage sag disturbances and their causes. The problem of disturbance-source detection is discussed in more detail. A summary of the literature review of published methods for sag-source detection is provided.

Chapter 3 proposes a method for sag-source detection. The proposed method is motivated by the incremental-impedance concept, one of the published sag-source detection methods summarized in Chapter 2. System identification and least-squares methods are applied for the analysis. Verification studies using available data from computer simulations, experimental tests, and field measurements are conducted. Limitations of the proposed method are also discussed.

Chapter 4 compares results from the published sag-source detection methods summarized in Chapter 2 using the same sag data from faults, transformer energization, and induction motor starting in Chapter 3.

Chapter 5 proposes a method for flicker-source detection. Voltage flicker is another type of power quality disturbance. The first section explains voltage flicker disturbances and their causes. The system identification-based method presented in Chapter 3 is extended to the problem of flicker-source detection. The power direction-based method is also proposed to tackle another type of flicker-producing load where the system identification-based method has a limitation. Case studies are used to verify the validity of two proposed methods. A general-purpose flicker-source detection method combining two proposed schemes is also provided.

Chapter 6 presents a systematic method to derive limits for interharmonics from the published limits on voltage flicker. Further inherent relationships between interharmonics and flickers are described, other than those briefly mentioned in Chapter 5. Both RMS and peak magnitude fluctuations caused by a single interharmonic are investigated. The limit for interharmonic level is represented as an interharmonic-magnitude versus interharmonic-frequency and is called an interharmonic-flicker curve. Potential applications and discussions are also provided.

Chapter 7 provides the conclusions drawn from the research work conducted in this thesis and offers some suggestions for future work.

CHAPTER 2

Problem Definition and Literature Review

Voltage sags are considered as the most important power quality disturbances in the power system because sags can propagate to a wide area and result in serious financial losses. This chapter provides necessary background on voltage sag disturbances and their causes. The problem of sag-source detection will be further described in detail. Available published methods for sag-source detection are reviewed and summarized.

2.1 Voltage Sag Disturbances and Their Causes

IEEE 1159 [7] classifies power system electromagnetic phenomena that can cause power quality (PQ) problems into seven categories (Table 1.2 in Chapter 1). The category that is related to voltage sags belongs to short-duration variations. A voltage sag according to [7] is defined as "a decrease to between 0.1 per unit and 0.9 per unit in root-mean-square (RMS) voltage at the power frequency for a duration from 0.5 cycles to 1 minute". IEC 61000-2-8 [13] refers to voltage sag as voltage dip and defines it as "sudden reduction of the voltage at a particular point on an electricity supply system below a specified dip threshold followed by its recovery after a brief interval". This thesis will only use the term voltage sag or sag.

Voltage sags are usually associated with system faults, but can also be caused by the energization of transformers or starting of heavy loads such as large induction motors that require high starting currents. Faults are considered the main source of voltage sags. A fault somewhere in the system can result in voltage sag over a wide area. Figure 2.1 shows a sag waveform (top) and RMS plot (bottom) caused by a fault from one of the available field measurements. The sag in RMS voltage magnitude can be clearly noticed. The duration of the sag is dependent on the fault-clearing times of the circuit breakers and protection settings. Typical fault-clearing times range from 3 to 30 cycles, depending on the fault-current magnitude and the type of overcurrent protection [7].

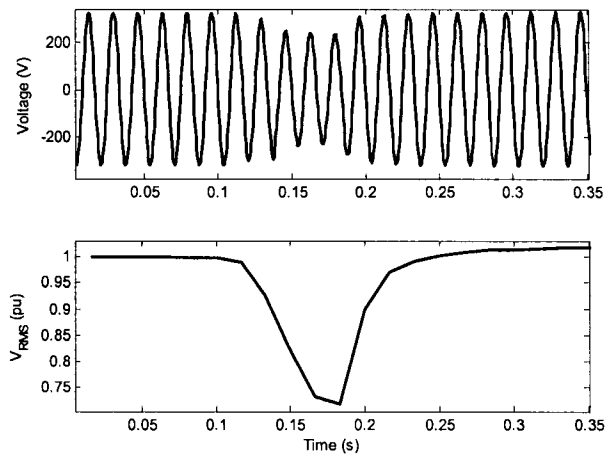

Figure 2.1: Voltage sag waveform and RMS plot caused by a fault

In certain system faults, voltage swells can happen with voltage sags. But voltage swells are less common than voltage sags. A swell according to [7] is defined as "an increase to between 1.1 per unit and 1.8 per unit in RMS voltage at the power frequency for a duration from 0.5 cycles to 1 minute". A common cause of swells is the temporary voltage rise on unfaulted phases during a single line-to-ground fault [7]. Figure 2.2 illustrates such the situation. The severity of a voltage swell during a fault condition is a function of the fault location, system impedance, and grounding. Swells can also be caused by switching off a large load or by energizing a large

capacitor bank. Figure 2.3 shows a swell waveform and RMS plot caused by energization of a capacitor bank from one of our experimental tests. Voltage swells do not normally disrupt sensitive loads, but they can harm equipment due to their large voltage magnitudes.

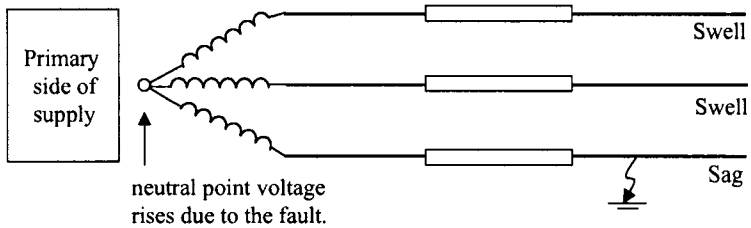

Figure 2.2: Voltage swells on unfaulted phases caused by a single line-to-ground fault

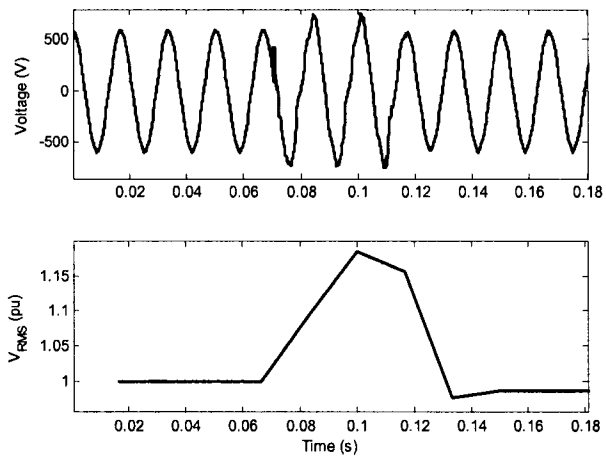

Figure 2.3: Voltage swell waveform and RMS plot caused by capacitor energization

Motor starting can cause noticeable voltage sag because an induction motor will draw 6 to 10 times its full-load current during the starting. If the current magnitude is large relative to the available fault current in the system, the resulting voltage sag can be significant. Figure 2.4 shows RMS voltage characteristics of a large motor-starting sag [7]. The duration of such sags is a function of motor acceleration. Typical values are in the range of a few seconds.

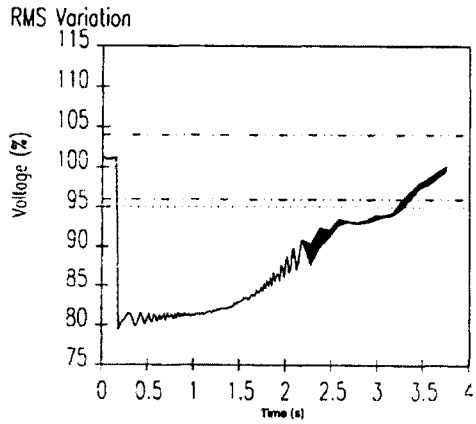

Figure 2.4: Voltage sag caused by motor starting

Transformer energization can also result in voltage sag. During energization, iron cores of a transformer can be driven into saturation. This causes high inrush current during an energization. This undesirable and high inrush current can result in a severe sag [14]. The inrush current of a transformer mainly depends on the instant of switching and the residual magnetization. Figure 2.5 shows a sag waveform and RMS plot caused by transformer energization from one of our experimental tests.

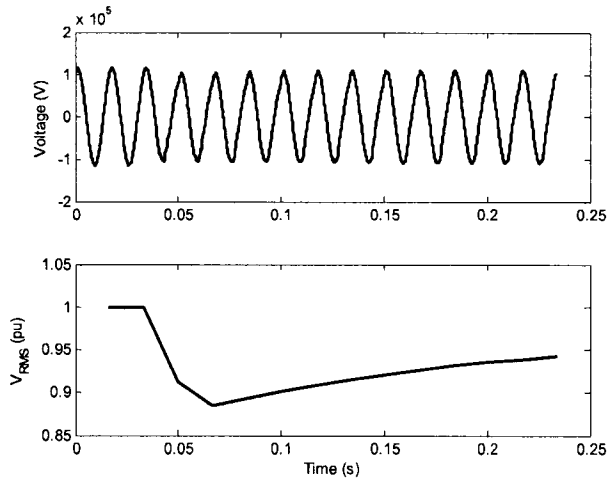

Figure 2.5: Voltage sag waveform and RMS plot caused by transformer energization

Sags are probably the most significant PQ concerns. Sags can propagate to a relatively large area in the power system. For example, various customers could experience voltage sags although a fault is not on the feeder directly supplying them.

Furthermore, modern electronics used in industrial plants are now low-cost and high-capacity equipment which can significantly increase productivity. These modern electronics tend to be more sensitive to voltage sags themselves because their lower voltage and power levels can be easily disturbed. Sags normally do not damage equipment, but they can easily disrupt the operation of these sensitive loads. A failure or malfunction of one computer-controlled unit in the product line can trouble or stop the whole automatic process in industrial plants. One shutdown could result in a huge financial loss. Therefore, many industrial customers consider voltage sags as the most important PQ problem [8]. The extent of sag propagation is not too difficult to predict. It can be determined by using well known short-circuit analysis methods. Case-specific studies have shown that sensitive loads can be affected by faults 5 to 10 miles away. The severity of a sag or swell event is measured by two parameters—the magnitude and duration—as shown in previously mentioned RMS plots.

2.2 Detection of Sag Sources

This section describes the problem of sag-source detection in detail. A typical situation that requires the detection of sag sources is depicted in Figure 2.6. In this figure, a PQ monitor is placed at point M. The monitor measures (three-phase) voltages and currents. If a voltage sag is detected by the monitor, it is required to determine if the source of the voltage sag is on the upstream or downstream side of the monitor. Upstream side is defined as the side that supplies the fundamental-frequency active power to the other side as shown in the figure.

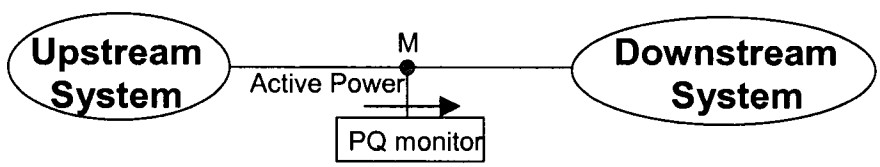

Figure 2.6: The problem of sag-source detection

A PQ monitor that can determine the location of sag sources can be considerably useful to the users. It can facilitate the troubleshooting of PQ problems because sags may easily propagate from one customer and affect neighboring customers. Locating sag sources has to be done as the first step although it is critically important to develop sag-mitigation devices to keep sags as small as possible. PQ troubleshooting, diagnosis, and mitigation can only be carried out after the disturbance-source detection is completed. With the deregulation of the power industry, utilities have become increasingly interested in quantifying the responsibilities for PQ problems, with voltage sag as the most prominent concern. Therefore, accurate and reliable sag-source results can fairly settle disputes between responsible parties.

In a typical application, point M is the utility-customer interface point. Ideally, the algorithm of sag-source detection should be implemented in a digital revenue meter connected at M. For example, the downstream side is the customer of interest, while the upstream side is the rest of the system, i.e. the utility system and other neighboring customers. As a result, both the supply utility and customer can obtain a list of sags, their severity, and their directions. Such information will greatly facilitate the resolution of disputes between the two parties if a sag results in financial losses to either party.

Based on the circuit theory, the above sag-source problem can be illustrated as shown in Figure 2.7. The upstream and downstream systems can be modeled as equivalent voltage sources in series with equivalent impedances. For example, $\boldsymbol{E_1}$ and $\boldsymbol{Z_1}$ can be the equivalent voltage source and impedance of the upstream system, while $\boldsymbol{E_2}$ and $\boldsymbol{Z_2}$ on the downstream side can be equivalent voltage source and impedance of the customer of interest. The impedance $\boldsymbol{Z_2}$ will be an equivalent of all loads in the customer facility such as linear loads (heaters and air-conditioners) and nonlinear loads (variable frequency drives and induction motors). Figure 2.8 shows sample voltage and current waveforms recorded at the service entrance of an industrial plant.

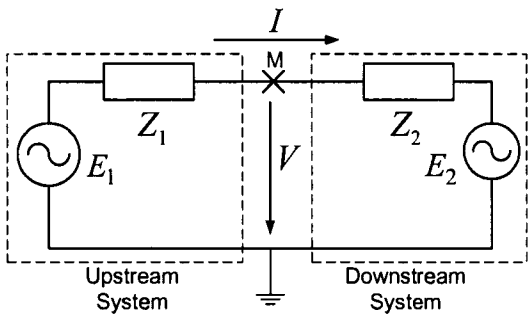

Figure 2.7: Equivalent circuit for the problem of sag-source detection

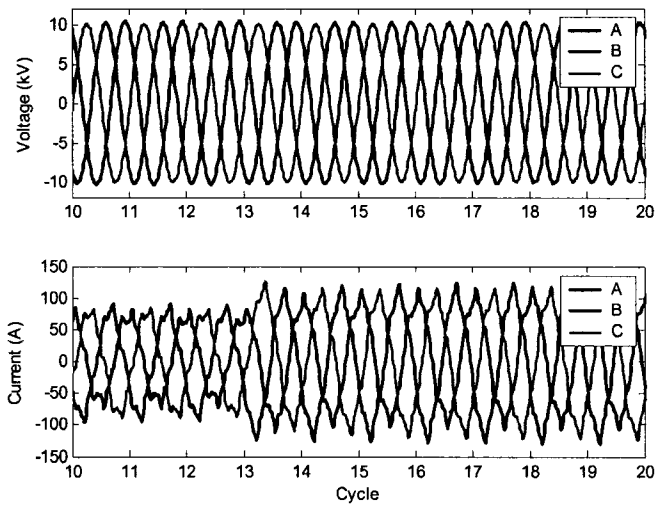

Figure 2.8: Sample three-phase voltage and current waveforms

In summary, the problem of determining sag source can be stated as follows (Figure 2.9): a PQ monitor captures sag-containing voltage and current waveforms at point M. The objective is to determine if the sag comes from the upstream or downstream system. In practice, point M should be chosen as the utility-customer interface point. So it can be checked whether the customer of interest is the source of the captured sag. If PQ monitors can be installed at all utility-customer interface points, it will be easy to pinpoint which customer in the system was responsible for the sags. Then PQ troubleshooting, diagnosis, and mitigation can proceed.

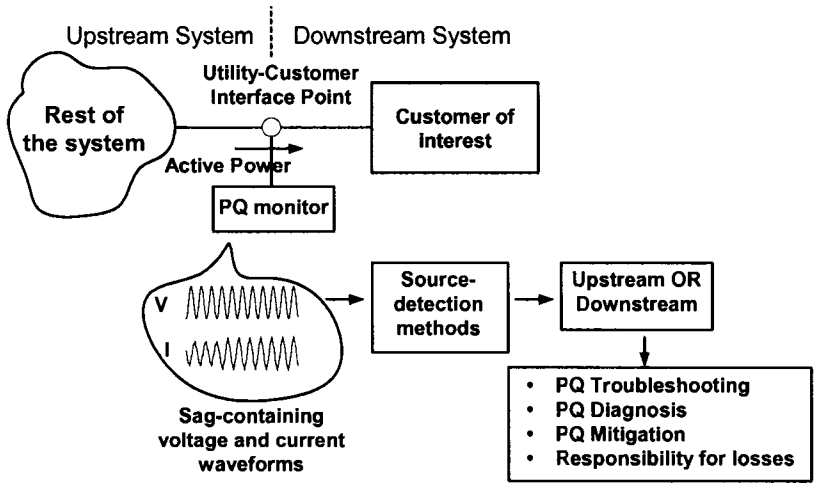

Figure 2.9: The typical application of the sag-source-detection problem

2.3 Review of Published Methods

This section reviews published methods for sag-source detection. Several methods have been published in order to solve the sag-source detection problem. A literature survey revealed that published methods can be categorized into three major groups: 1) power quality-based methods, 2) protection-based methods, and 3) other methods. Power quality-based methods rely on engineering experience and intuitive understanding of voltage sag phenomena. These methods were developed from the perspective of PQ troubleshooting and diagnosis. The first subsection will review concepts and variations in this category. Since voltage sags are mainly related to faults, some authors have adopted power system protection methods such as the directional-relay concept to sag-source detection. Because two-thirds of faults in the power system occur in the transmission-line networks [15], it is therefore useful to examine methods for transmission-line protection. The subsection on protection-based methods describes these concepts and variations. Finally, there was also an attempt to apply artificial intelligence algorithm such as artificial neural network and advanced transform such as wavelet transform to analyze the fault location. These methods are grouped in the last category although the review found that there are no real applications using these methods for general-purpose sag-source detection.

The published methods for sag-source detection can be illustrated in Figure 2.10. Three groups with concepts belonging to each group are shown. The last row represents names (first author) and reference numbers of variations under the concept on which each is based.

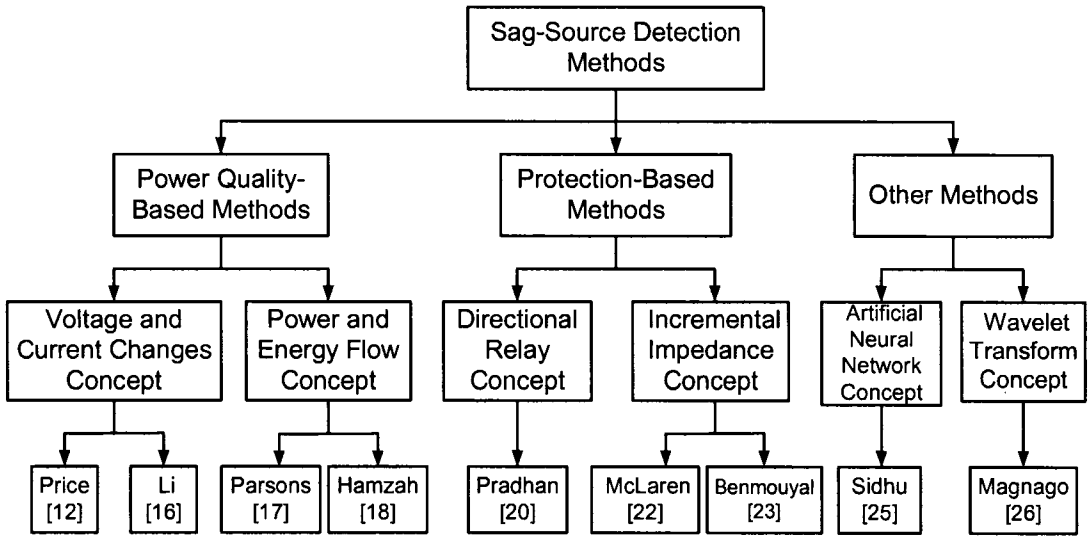

Figure 2.10: The classification diagram of sag-source detection methods

2.3.1 Power Quality-Based Methods

Unique characteristics of voltage sags can provide useful information for sag-source detection. Methods that are derived based on these unique characteristics are classified as power quality-based methods. These methods are based on intuitive understanding of voltage sag phenomena and engineering experience. Thus, it is rather difficult to assess the reliability and limitations of these methods. There are two main available concepts for sag-source detection developed for PQ purpose. The first concept considers voltage and current changes during a sag, while the second concept relies on the power and energy flow during a sag. There are also other variations based on these two main concepts. These concepts are summarized in the following subsections.

2.3.1.1 Voltage and Current Changes Concept

The first concept examines the relationship between voltage and current magnitude changes during a sag to determine the direction of sag source. A decrease in the current magnitude indicates a sag source is located upstream, while a current increase means it is downstream [12]. Though this simple rule is easy to apply to most general cases, this concept may not perform for certain loads such as constant power loads (CPLs). This is because the current magnitude drawn by CPLs normally increases for both upstream and downstream faults in an attempt to keep the power consumption constant. As a result, the relationship between voltage and current magnitude changes during a sag may not be reliable for sag-source detection of CPLs.

The above observation of voltage and current changes can be interpreted by considering the slope between the two parameters or $|V|$-$|I|$ trajectory. Figure 2.11 shows this observation graphically where pre-sag and post-sag conditions are characterized by dots. It can be seen that slopes of voltage magnitude versus current magnitude have opposite signs depending on the sag-source location. By examining the slope sign, one may be able to tell if the sag source is located upstream or downstream.

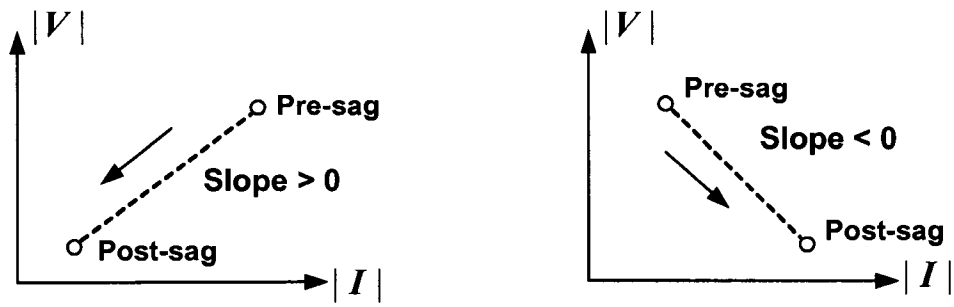

(a) Upstream sag (b) Downstream sag

Figure 2.11: Slope characteristic of the $|V|$-$|I|$ trajectory

A variation of this concept was presented in [16]. The method was formulated based on this aforementioned concept and interpreted the slope sign of a fitting line between the product of voltage magnitude and power factor against current magnitude during a sag. A negative slope indicates a downstream sag, while a positive slope indicates an upstream sag. Although the method utilizes multiple data points to improve its reliability and robustness, the method may not work well under some circumstances. This is because the method assumes that the phase angle of current may not change significantly during a sag which does not hold true for some practical cases. Furthermore, unbalanced sags were not discussed.

2.3.1.2 Power and Energy Flow Concept

The second concept is based on the flow of power and energy during a sag. The method applied the initial peak of the disturbance power [IP(DP)] and the disturbance energy (DE) to determine directions of sag sources [17]. The concept relies on the facts that energy tends to flow towards a disturbance source and the non-zero disturbance power indicates the change caused by the disturbance. Thus, IP(DP) and the change in DE are used as two key indices for sag-source detection. The disturbance power (DP) can be calculated from

$$\mathrm{DP} = ip_{3\phi}(t) - ip_{ss}(t) \tag{2.1}$$

where $ip_{3\phi}(t)$ is the total three-phase instantaneous power and $ip_{ss}(t)$ is the pre-disturbance, steady-state, three-phase instantaneous power. The DE is an integration of the DP over the sag period. Negative IP(DP) and DE indicate an upstream sag, while positive IP(DP) and DE indicate a downstream sag. The method needs a threshold for the DE to achieve reliable sag-source interpretation. If the final value of DE is less than 80% of the peak value of DE during a sag, only the IP(DP) will be used to determine the location of a sag source with a lesser degree of confidence. Although the method is reliable for single-source systems, there are no discussions

on two-source systems. The aforementioned observations on IP(DP) and DE may not be valid for two-source systems as in single-source systems.

A variation of this concept was presented in [18] where a sag source in the power distribution system was determined by the polarity of the real current component. The method relies on the active power flow direction at the measuring point. If the active power at the measuring point is positive, a sag source is located downstream; if the active power is negative, a sag source is located upstream. The product of the RMS current and the power factor or $Icos(\theta_V-\theta_I)$ at the monitoring point is used as an index where θ_V and θ_I are voltage and current phase angles, respectively. The sign of $Icos(\theta_V-\theta_I)$ is actually the same as the sign of $VIcos(\theta_V-\theta_I)$ or the active power. As a result, this sag-source detection is equivalent to considering the flow of active power at the beginning of a sag.

2.3.2 Protection-Based Methods

Because faults often happen on transmission-line networks, methods for transmission-line protection should be reviewed. Among the available protection schemes, the concepts of directional relay and incremental impedance relay are the most relevant to sag-source detection. These two concepts perform well for fault detection on transmission lines.

2.3.2.1 Directional-Relay Concept

Directional-relay concept is a conventional concept where the direction of a fault is based on the phase angle between the fault current and some reference quantities [19]. Typically, the voltage at the relay is chosen as the reference quantity. This reference voltage must be the voltage that is driving the fault current, e.g. for a phase A-to-ground fault, the current and voltage of phase A must be used. Therefore, the operation of this concept depends on the direction of the fault current with respect to the driving voltage. The concept can be explained by Figure 2.12. It is assumed that

the current flows into the line. E_S and E_R are sending and receiving end supply voltages.

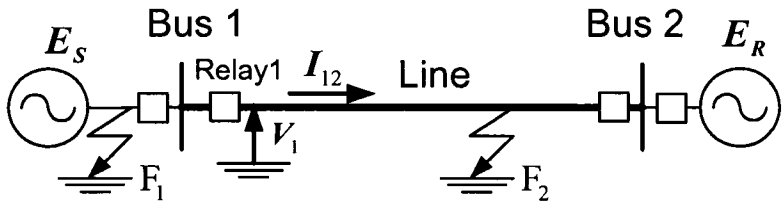

Figure 2.12: The directional-relay concept

Because the transmission-line impedance is mostly reactive, a fault in a downstream (forward) direction at F_2 will have a fault current flowing from Bus 1 to F_2 or I_{12} that lags the voltage V_1 at the Relay1 by an angle of almost 90°. On the other hand, a fault in an upstream (reverse) direction at F_1 will have a fault current I_{12} that leads V_1 by an angle of about 90°. Figure 2.13 shows the operation of the relay based on the phase angle difference in the complex plane. For all forward faults producing fault current phasors in the shaded region, the relay would trip, while the relay would block or not operate for all other reverse faults. The value of θ_m defines the boundary between the trip and block regions, typically 2° to 8°.

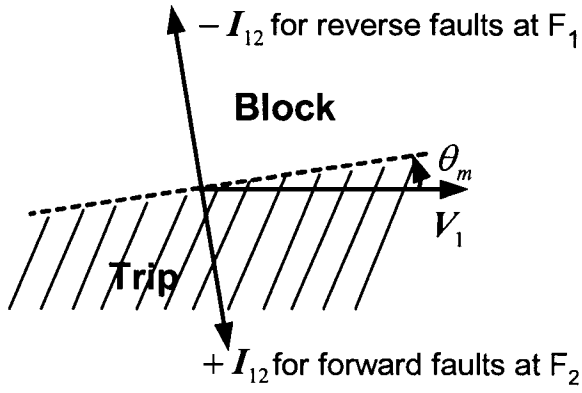

Figure 2.13: The operation region of directional-relay concept in the complex plane

It can be seen that directions of fault current I_{12} are different for forward and reverse faults. Due to this unique characteristic of phase angle difference between fault current and voltage for two different fault locations, the direction of a fault on a transmission line can be correctly determined. This concept works well for the transmission-line protection, however, it may not be directly applicable in some single-source radial systems. For example, if we replace remote source E_R in Figure 2.12 with a passive load impedance, it can be shown that the current I_{12} always lags the voltage V_1 for both faults at F_1 and F_2 assuming the system is purely reactive. As a result, the reverse-direction fault cannot be detected properly by this conventional directional-relay concept for single-source radial systems.

The work in [20] presented a sag-source-detection algorithm based on directional-relay and distance-relay concepts. A downstream sag is identified when the magnitude of the impedance seen from a relay at pre-sag condition is greater than during-sag condition and the phase angle of the during-sag impedance is greater than zero. For other situations, sag is considered to be in the upstream direction. A distance relay is a relay that trips when the impedance magnitude which is proportional to the distance from the relay to the fault is less than a setting value, $|Z_r|$ [21]. This impedance magnitude is calculated from the ratio of voltage and current phasors at the relay. Since the load current under the normal condition is much smaller than the fault current, this ratio is large and located outside the circle of radius $|Z_r|$ in the complex R-X plane as shown by a black dot in the blocking region in Figure 2.14. A standard distance relay cannot specify the direction of a fault (non-directional) since it is only based on the comparison of impedance magnitude. The relay would trip for either forward or reverse faults that give the impedance magnitude less than $|Z_r|$ as shown in the tripping region. This algorithm simply adds the directionality from the directional-relay concept with the impedance magnitude comparison from the distance-relay concept.

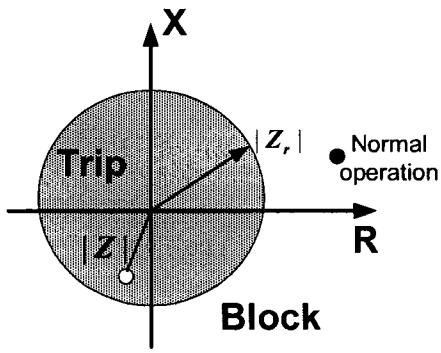

Figure 2.14: The operation region of distance-relay concept in the complex plane

2.3.2.2 Incremental-Impedance Concept

Voltage and current changes during a fault can yield useful information for fault detection on a transmission line. These voltage and current changes generated from a fault are called incremental quantities. The incremental impedance can be calculated from these available quantities when there is a fault. If incremental quantities are too small, impedance results could be unreliable. It will be shown later that faults at different locations give different impedance signs. Therefore, the incremental-impedance concept determines the direction of a fault by the sign of impedance calculated from incremental voltage and current quantities [22-24]. Figure 2.15 is the superimposed system (using superposition theorem) of Figure 2.12 for a downstream (forward) fault at F_2 (per unit distance d of the total line length from Bus 1) [24]. V_f is the pre-fault voltage at the fault point and R_f is the fault resistance. Z_L, Z_S and Z_R are line, source and remote impedances, respectively.

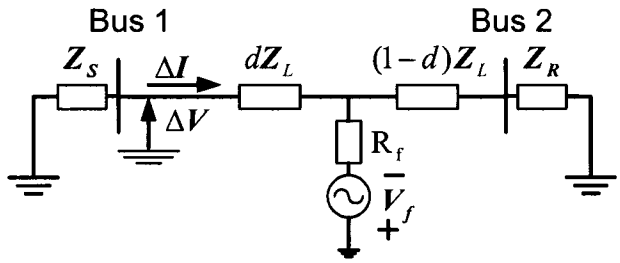

Figure 2.15: Superimposed system for a forward fault

Considering the left-hand section of Bus 1, the equivalent impedance (Z_e) for a forward fault can be estimated from

$$Z_e = \frac{\Delta V}{\Delta I} = \frac{V_{during} - V_{pre}}{I_{during} - I_{pre}} = -Z_S \tag{2.2}$$

where

ΔV the phasor difference between the voltage during the fault and immediately prior to the fault,

ΔI the phasor difference between the current during the fault and immediately prior to the fault,

V_{during} the phasor voltage during the fault,

V_{pre} the phasor voltage immediately prior to the fault,

I_{during} the phasor current during the fault,

I_{pre} the phasor current immediately prior to the fault,

Z_S the source impedance at Bus 1.

In a similar way, the equivalent impedance seen by the relay at Bus 1 for a reverse fault is the sum of line impedance plus the impedance of remote source (Z_R):

$$Z_e = Z_L + Z_R \tag{2.3}$$

It can be seen that this concept estimates the impedance of the unfaulted side from incremental voltage and current quantities generated by a fault. Because of distinctive impedance signs in equations (2.2) and (2.3), the direction to a fault can be determined. The sign difference of the equivalent impedance can be exploited in two different ways.

The first variation based on this concept utilizes the location of the equivalent impedance on the impedance plane (R-X plane) [22]. The directional element determines the direction of a fault by checking where the equivalent impedance lies in the R-X plane. In order to be applicable to all types of faults, the fundamental-frequency positive-sequence impedance is used. Equivalent impedances from forward faults will lie in the third quadrant, while equivalent impedances will lie in the first quadrant for reverse faults. Figure 2.16 shows incremental impedance positions on the R-X plane. This relationship assumes that the amount of series compensation is less than 100%. It can be seen that the equivalent impedance is the negative value of the source impedance at Bus 1 and lies in the third quadrant of the R-X plane for forward faults. For reverse faults, the equivalent impedance is the summation of the line and remote source impedances and lies in the first quadrant of the R-X plane.

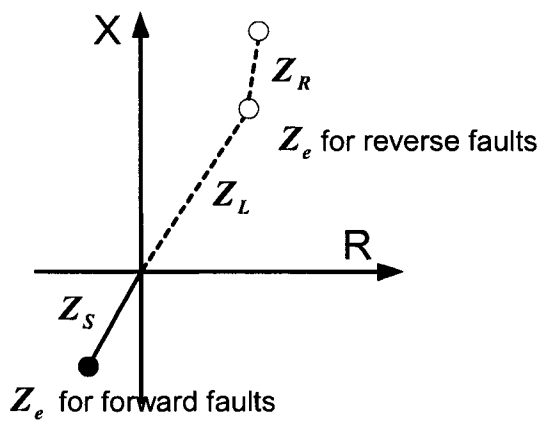

Figure 2.16: Incremental impedances on the impedance plane

The second variation determines the direction of a sag by using phase and amplitude comparators [23]. The equivalent impedance is a complex number that can be converted to a polar form containing the magnitude and phase angle. The phase comparator compares the phase angle between two phasors, incremental voltage and the product of incremental current and the negative of positive-sequence source impedance. The amplitude comparator checks the amplitude between two complex

numbers derived from incremental voltage, incremental current, and the negative of positive-sequence source impedance. The algorithm is performed in the time-domain because it is fast and suitable for ultra-high speed transmission-line protection. However, a prior knowledge of the magnitudes of incremental voltage and current quantities is necessary and the method does not work with some complex networks such as double-circuit networks. The limitation of this concept is due to the fact that the equivalent impedance from the incremental voltage and current is not equal to the negative of local source impedance when there is a forward fault on a double-circuit transmission line [23].

2.3.3 Other Methods

There are other methods applying artificial intelligence algorithm such as artificial neural network [25] and advanced transform such as wavelet transform [26] to the fault-location analysis. The fault-location problem is treated as the conventional pattern classification problem. The proposed artificial neural network was trained using the training patterns and the back-propagation algorithm. The result yields a direction discriminator for forward and reverse faults on transmission lines. For the transmission-line fault location using wavelet transform, the distance to fault can be computed from travel times between fault and relay locations. These travel times are obtained from wavelet transform. The wavelet transform is believed to be advantageous for the analysis of signals containing short-lived high-frequency disturbance generated by a fault superimposed on the fundamental-frequency component. Results from these methods are promising, however, it was found that there are no real applications using these methods for general-purpose sag-source detection.

2.4 Summary

Voltage sags are considered as the most important PQ problem in the power system. Sags can propagate over a wide area and affect many customers. Although sags do not cause equipment damage, they can disrupt automatic processes and cause significant financial losses. Major sources of sags are system faults, transformer energization, and starting of large induction motors. Magnitude and duration are two important parameters that characterize sags.

The problem for sag-source detection is to determine if the sag source is located on the upstream or downstream side of a PQ monitor. In practice, the PQ monitor is located at the interface point between utility and customer. Thus, it can be known if the sag originates from the customer of interest or not. After sag-source detection is available, other procedures such as PQ troubleshooting, diagnosis, and mitigation can be further carried out. The dispute for the responsibility for losses from sags can be fairly resolved.

Published sag-source methods can be mainly classified into three groups: methods developed for power quality, methods borrowed from power system protection, and other methods that use advanced algorithms. Methods in all three groups can be further categorized based on different concepts. Power quality-based methods are empirical methods based on intuitive understanding of sag phenomena and engineering experience. As a result, the reliability and limitations of power quality-based methods are not easy to assess. Voltage and current changes and power and energy flow concepts are two principal concepts in this group. On the other hand, protection-based methods are mainly derived from transmission-line protection because faults normally occur in transmission-line networks. Directional-relay and incremental-impedance concepts are two major concepts in this group. These methods have concrete theoretical background. They have been used in transmission-line protection. There are other methods applying advanced algorithms such as

artificial neural network and wavelet transform, but there are no real applications using these methods for general-purpose sag-source detection.

Based on this review, we find that there is still no reliable and accurate method for general-purpose sag-source detection. However, it is found that the incremental-impedance concept is promising and will be further developed for general-purpose sag-source detection for this thesis. The next chapter will present the proposed method for sag-source detection motivated by the incremental-impedance concept with some improvements.

CHAPTER 3

A System Identification-Based Method for Sag-Source Detection[1]

This chapter presents a system identification-based method for determining the origin of voltage sag disturbance. The proposed method is motivated by the incremental-impedance concept described in Chapter 2. Frequency-domain system identification and least-squares methods are applied for the analysis. The concept of the proposed method is to estimate the equivalent impedance of the non-sag side utilizing voltage and current changes caused by the sag. The real part sign of the estimated impedance can reveal whether the sag source is from upstream or downstream. Case studies from computer simulations of real power systems, experimental tests, and field measurements are used to verify the effectiveness and robustness of the proposed method. Discussions of practical issues are also provided.

---

[1] The work in this chapter has been published: T. Tayjasanant, C. Li, and W. Xu, "A Resistance Sign-Based Method for Voltage Sag Source Detection," *IEEE Trans. Power Delivery*, Vol. 20, No. 4, October 2005, pp. 2544-2551.

3.1 Introduction

System faults, switching of heavy loads, and starting of large motors can cause sags in a power system. Sags can propagate a long distance from the source location and affect many customers in large areas. Many methods were tried to increase the ride-through capability of sensitive loads in order to survive the PQ disturbances. A lot of PQ-enhancement equipment has been studied and developed. However, there is no absolute solution to prevent PQ disturbances completely. Over the past many years, research work in voltage sag diagnosis has been focused on developing protocols and systems to measure the disturbance. Little work has been reported on locating the origins of voltage sags. With the deregulation of the power industry, utilities have become increasingly interested in quantifying the responsibilities for PQ problems, with voltage sag as the most prominent concern. As a result, research on how to detect sag source has become an important topic recently. In spite of various efforts, there is still no reliable and technically sound method available for locating sag sources.

Reference [17] is probably the pioneering work in this subject. It uses disturbance energy and the initial peak of the disturbance power to determine directions of disturbances. The method is based on intuitive understanding of the disturbance phenomena. Theoretical support for the method is not available. As a result, it is difficult to assess the reliability and limitations of the method. Reference [16] proposed a method based on the observation that the slopes of the voltage versus current plot can have opposite signs depending on the sag-source location. By examining the sign of the slope, one may be able to tell if a disturbance is located upstream or downstream. Again, this is an empirical method and it is difficult to assess its application range.

Since voltage sags are mainly related to faults, it would be useful to examine the knowledge accumulated in the area of power system protection and fault locations. It is found that the concept of incremental impedance used in directional relays is the

most relevant to the problem of sag-source detection [24]. The method is based on the observation that the equivalent impedance obtained from incremental voltage and current quantities at different fault locations will lie in different quadrants of the impedance plane. One of the problems of this method is that the impedance is sensitive to the selections of pre- and post-fault cycles [27]. Different cycle selection may give opposite results.

This chapter introduces a theoretically justifiable method for sag-source detection. The method is inspired by the impedance-estimation concept, but can overcome its limitations. Furthermore, it is shown that the method presented in [16] is a variation of this more general method. The basic idea of the proposed method is as follows. We can use the sag disturbance to estimate the (fundamental-frequency positive-sequence) equivalent impedance of the portion of the system where the sag source does not reside. The sign of the resistive component of this equivalent impedance can reveal the sag-source location. This conclusion can be proven theoretically for linear systems. Extensive tests on the proposed method using simulations, experimental tests, and field measurements have shown that it is a more robust and reliable method.

3.2 The Proposed Method for Sag-Source Detection

3.2.1 The Concept of Impedance Estimation

This section describes the proposed system identification-based method for sag-source detection in detail. The proposed method is motivated by the incremental-impedance concept summarized in Chapter 2. The incremental-impedance concept calculates the equivalent impedance of the non-sag side from voltage and current changes generated by the sag. The main concept of the proposed method is to estimate the frequency response of the equivalent impedance of the non-sag side as follows:

$$\boldsymbol{Z}(f) = \Phi[\Delta v(t), \Delta i(t)] \tag{3.1}$$

where $\Delta v(t)$ and $\Delta i(t)$ are the voltage and current changes caused by the sag measured at the monitoring point and Φ represents a frequency-response identification function. The impedance estimation can be described as follows. Time-domain voltage and current data that includes the sag event is transformed into the frequency response using the discrete Fourier transform (DFT). The DFT provides complex values of voltage and current at various frequencies in the frequency domain. The impedance frequency response is then estimated using the least-squares method which will be described in more detail. The best choice of frequency f in equation (3.1) for sag-source detection is the fundamental frequency because voltage and current changes by the sag are predominant at the fundamental frequency. In order to deal with all types of faults, positive-sequence quantities will be used. Positive-sequence quantities can be calculated by the symmetrical components transformation[2]. Therefore, only fundamental-frequency positive-sequence quantities will be considered for the estimation of impedance frequency response.

The concept of impedance estimation using only two data points is first introduced in order to show how the sign of the real-part of the impedance frequency response can determine the sag source. The application of multiple data points to improve the accuracy of the proposed method using the least-squares method is later described.

Figure 3.1 is the equivalent fundamental-frequency positive-sequence circuit for the analysis of sag-source detection. This equivalent circuit model is valid if one assumes that the system consists of linear elements. It is required to determine whether a sag originates on the left (upstream) or right (downstream) of point M

---

[2] The positive-sequence voltage and current can be calculated from three-phase quantities as follows: $(1/3)\times(\boldsymbol{V}_A + a\boldsymbol{V}_B + a^2\boldsymbol{V}_C)$ and $(1/3)\times(\boldsymbol{I}_A + a\boldsymbol{I}_B + a^2\boldsymbol{I}_C)$, where $a = -0.5+j0.866$.

where voltage and current waveforms are measured. The most practical location for the PQ monitor for disturbance-source detection is at the utility-customer interface because both the utility and the customer can check if a disturbance occurs inside or outside facilities of a particular customer. Complex parameters $\boldsymbol{Z_1}$ and $\boldsymbol{E_1}$ are equivalent impedance and internal voltage source of the supply (upstream) system, while $\boldsymbol{Z_2}$ and $\boldsymbol{E_2}$ are the similar parameters for the customer (downstream) system.

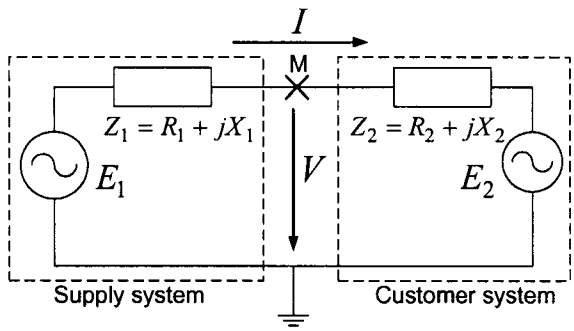

Figure 3.1: Equivalent circuit for sag-source analysis

Assume a sag occurs on the customer side and leads to a voltage sag at M, the measurements at M satisfy this equation before the occurrence of the event:

$$\boldsymbol{V = E_1 - I Z_1} \tag{3.2}$$

When a sag occurs, the voltage and current are changed to $\boldsymbol{V}+\Delta\boldsymbol{V}$ and $\boldsymbol{I}+\Delta\boldsymbol{I}$, where $\Delta\boldsymbol{V}$ and $\Delta\boldsymbol{I}$ are voltage and current changes due to the customer-side event. If we assume that the parameters on the supply side ($\boldsymbol{Z_1}$ and $\boldsymbol{E_1}$) remain unchanged during the sag period, a similar equation can be written as

$$\boldsymbol{V} + \Delta\boldsymbol{V} = \boldsymbol{E_1} - (\boldsymbol{I} + \Delta\boldsymbol{I})\, \boldsymbol{Z_1} \tag{3.3}$$

Since the probability that a sag occurs on both sides simultaneously is practically very small, the above assumption that the parameters of the non-sag side are constant is justifiable.

Subtracting equation (3.2) from equation (3.3), the impedance of the non-sag side (supply side) can be computed from

$$Z_1 = -\frac{\Delta V}{\Delta I} \tag{3.4}$$

Similarly, if a sag occurs on the supply side, the customer-side impedance can be obtained as

$$Z_2 = \frac{\Delta V}{\Delta I} \tag{3.5}$$

It can be seen that the quantity $Z_e = \Delta V/\Delta I$ gives different signs depending on the origin of the sag. The basic idea proposed is, therefore, to estimate Z_e. In fact, Z_e has a physical meaning. It is the equivalent impedance of the non-sag side. If a sag occurs on the supply side, Z_e is the customer impedance; if a sag occurs on the customer side, Z_e is the supply impedance multiplied by a negative sign.

Since the resistance should always be positive, we could determine the direction of sag source by checking the sign of the real part of the impedance Z_e or $\Re\text{eal}(Z_e)$. This forms the basis of the proposed method:

1) Calculate the equivalent impedance once a sag is detected at the monitoring point

$$Z_e = \frac{\Delta V}{\Delta I} = \frac{V_{during} - V_{pre}}{I_{during} - I_{pre}} \tag{3.6}$$

where V_{pre} and I_{pre} are pre-sag voltage and current and V_{during} and I_{during} are during-sag voltage and current.

2) If $\Re\text{eal}(Z_e) > 0$, the source of sag is on the supply side (upstream system).
3) If $\Re\text{eal}(Z_e) < 0$, the source of sag is on the customer side (downstream system).

Note that the above conclusion is valid with respect to the current direction shown in Figure 3.1. In actual implementation, the current direction can be established as the same direction as the fundamental-frequency active power. For

example, if $\Re\text{eal}(\boldsymbol{Z}_e) > 0$, the sag source will be the upstream (US) direction; if $\Re\text{eal}(\boldsymbol{Z}_e) < 0$, the sag source will be the downstream (DS) direction.

The above method can be graphically illustrated on the impedance plane (R-X plane) as shown in Figure 3.2. If the equivalent impedance $\boldsymbol{Z}_e$ lies in either the first or fourth quadrant ($R_e > 0$), the sag source is on the supply side; if the impedance lies in either the second or third quadrant ($R_e < 0$), the sag source is on the customer side. Since the equivalent impedances of a power network are generally reactive at the fundamental frequency, the impedance results will mostly reside in either the first or third quadrant of the R-X plane [22].

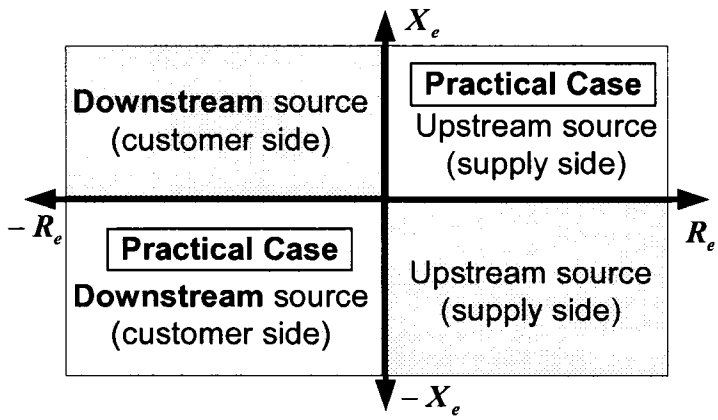

Figure 3.2: Impedance plane illustration for sag-source interpretation

3.2.2 Improving The Accuracy of Impedance Estimation

The aforementioned impedance-based method is theoretically sound, but there is one major difficulty in its practical implementation: the results could be inconsistent if different pre- or during-sag cycles are selected. According to our several months' field measurement results, source locations for almost 20% of the disturbances cannot be correctly identified if during-event cycle is selected too close or too far from the pre-event cycle. This is because the estimated impedance would vary during the disturbance period. Therefore, using a single during-event cycle in the analysis could yield unreliable results. In order to improve the estimation of the equivalent

impedance, we propose to utilize multiple cycles of data by using the least-squares (LS) method. This can be done as follows. Equation (3.2) can be rewritten as

$$V_X + jV_Y = (E_{1X} + jE_{1Y}) - (I_X + jI_Y)(R_1 + jX_1) \tag{3.7}$$

where subscripts X and Y represent real and imaginary parts of a variable, respectively. If n cycles of (V, I) data are measured during the development of a sag, equation (3.7) becomes

$$\begin{bmatrix} V_X(1) \\ \vdots \\ V_X(n) \end{bmatrix} = \begin{bmatrix} I_X(1) & I_Y(1) & 1 \\ \vdots & \vdots & \vdots \\ I_X(n) & I_Y(n) & 1 \end{bmatrix} \begin{bmatrix} -R_1 \\ X_1 \\ E_{1X} \end{bmatrix} \tag{3.8}$$

and

$$\begin{bmatrix} V_Y(1) \\ \vdots \\ V_Y(n) \end{bmatrix} = \begin{bmatrix} I_Y(1) & I_X(1) & 1 \\ \vdots & \vdots & \vdots \\ I_Y(n) & I_X(n) & 1 \end{bmatrix} \begin{bmatrix} -R_1 \\ -X_1 \\ E_{1Y} \end{bmatrix} \tag{3.9}$$

Most PQ monitors provide three cycles or more pre-sag and post-sag data. Data recorded during the sag can be as long as the duration of the sag. As a result, n is typically greater than three. The equivalent impedance can then be estimated by using the LS method:

$$\begin{bmatrix} -R_1 \\ X_1 \\ E_{1X} \end{bmatrix} = \begin{bmatrix} I_X(1) & I_Y(1) & 1 \\ \vdots & \vdots & \vdots \\ I_X(n) & I_Y(n) & 1 \end{bmatrix}^{+} \begin{bmatrix} V_X(1) \\ \vdots \\ V_X(n) \end{bmatrix} \tag{3.10}$$

and

$$\begin{bmatrix} -R_1 \\ -X_1 \\ E_{1Y} \end{bmatrix} = \begin{bmatrix} I_Y(1) & I_X(1) & 1 \\ \vdots & \vdots & \vdots \\ I_Y(n) & I_X(n) & 1 \end{bmatrix}^{+} \begin{bmatrix} V_Y(1) \\ \vdots \\ V_Y(n) \end{bmatrix} \tag{3.11}$$

where the superscript symbol '+' indicates pseudoinverse[3] [28].

From equations (3.10) and (3.11), it can be seen that the impedance calculated from the right-hand side will always have a negative real part. This implies that for a customer-side (downstream) sag, if we try to estimate impedance by calculating the right-hand side of equation (3.10) or equation (3.11), the result will drop into the second or third quadrant of the impedance plane ($R_e < 0$) as shown in Figure 3.2.

Similarly, if a sag originates from the supply side (upstream system), one obtains

$$\begin{bmatrix} R_2 \\ -X_2 \\ E_{2X} \end{bmatrix} = \begin{bmatrix} I_X(1) & I_Y(1) & 1 \\ \vdots & \vdots & \vdots \\ I_X(n) & I_Y(n) & 1 \end{bmatrix}^{+} \begin{bmatrix} V_X(1) \\ \vdots \\ V_X(n) \end{bmatrix} \tag{3.12}$$

and

$$\begin{bmatrix} R_2 \\ X_2 \\ E_{2Y} \end{bmatrix} = \begin{bmatrix} I_Y(1) & I_X(1) & 1 \\ \vdots & \vdots & \vdots \\ I_Y(n) & I_X(n) & 1 \end{bmatrix}^{+} \begin{bmatrix} V_Y(1) \\ \vdots \\ V_Y(n) \end{bmatrix} \tag{3.13}$$

Therefore, it can be concluded that for a supply-side sag, the equivalent impedance estimated from equation (3.12) or equation (3.13) will lie in the first or fourth quadrant of the impedance plane ($R_e > 0$) as shown in Figure 3.2. The calculated impedance will always have a positive real part. Note the terms on the right of equations (3.12) and (3.13) are exactly the same as those of equations (3.10) and (3.11), respectively.

Accordingly, the source direction of sag can be detected by checking signs of the real part of the impedance calculated by system identification and LS methods. Positive real part of the fundamental-frequency positive-sequence impedance

---

[3] If the dimension of **A** is $p \times q$ with $p > q$ and full rank, then the solution of $\mathbf{Ax} = \mathbf{b}$ is $\mathbf{x} = (\mathbf{A}^T\mathbf{A})^{-1}\mathbf{A}^T\mathbf{b}$. For the sag-source detection, the dimension of **A** is $n \times 3$ where n is the total number of cycles during sag.

indicates that the sag originated upstream, while negative real part implies the sag source originated downstream.

In order to determine the sag-source detection, two resistance signs are estimated and checked as previously mentioned. When two signs are consistent, sag source can be determined with a high level of confidence. But when there is no consistency of two resistance signs, we introduce an alternative to estimate the impedance by combining equations of real and imaginary parts together. This step would give only one single R_e value. Though the luxury of having two R_e values to crosscheck each other is lost, the sag source can still be interpreted. The procedure can be achieved as follows. Considering a downstream sag and combining equations (3.8) and (3.9) into one equation:

$$\begin{bmatrix} V_X(1) \\ \vdots \\ V_X(n) \\ V_Y(1) \\ \vdots \\ V_Y(n) \end{bmatrix} = \begin{bmatrix} I_X(1) & -I_Y(1) & 1 & 0 \\ \vdots & \vdots & \vdots & \vdots \\ I_X(n) & -I_Y(n) & 1 & 0 \\ I_Y(1) & I_X(1) & 0 & 1 \\ \vdots & \vdots & \vdots & \vdots \\ I_Y(n) & I_X(n) & 0 & 1 \end{bmatrix} \begin{bmatrix} -R_1 \\ -X_1 \\ E_{1X} \\ E_{1Y} \end{bmatrix} \tag{3.14}$$

The supply-side equivalent impedance can then be computed using the LS method:

$$\begin{bmatrix} -R_1 \\ -X_1 \\ E_{1X} \\ E_{1Y} \end{bmatrix} = \begin{bmatrix} I_X(1) & -I_Y(1) & 1 & 0 \\ \vdots & \vdots & \vdots & \vdots \\ I_X(n) & -I_Y(n) & 1 & 0 \\ I_Y(1) & I_X(1) & 0 & 1 \\ \vdots & \vdots & \vdots & \vdots \\ I_Y(n) & I_X(n) & 0 & 1 \end{bmatrix}^{+} \begin{bmatrix} V_X(1) \\ \vdots \\ V_X(n) \\ V_Y(1) \\ \vdots \\ V_Y(n) \end{bmatrix} \tag{3.15}$$

It can be observed that the impedance calculated from the right-hand side of equation (3.15) is the equivalent supply-side impedance with a negative sign.

For an upstream sag, the customer-side impedance can also be estimated in the similar way. The customer-side equivalent impedance can be estimated from

$$\begin{bmatrix} R_2 \\ X_2 \\ E_{2X} \\ E_{2Y} \end{bmatrix} = \begin{bmatrix} I_X(1) & -I_Y(1) & 1 & 0 \\ \vdots & \vdots & \vdots & \vdots \\ I_X(n) & -I_Y(n) & 1 & 0 \\ I_Y(1) & I_X(1) & 0 & 1 \\ \vdots & \vdots & \vdots & \vdots \\ I_Y(n) & I_X(n) & 0 & 1 \end{bmatrix}^{+} \begin{bmatrix} V_X(1) \\ \vdots \\ V_X(n) \\ V_Y(1) \\ \vdots \\ V_Y(n) \end{bmatrix} \tag{3.16}$$

Similarly, it can be observed that the impedance calculated from the right-hand side of equation (3.16) is the equivalent customer-side impedance. Also note the terms on the right of equations (3.15) and (3.16) are exactly the same.

In practice, values of voltage and current from measurements could be in the range of kV and kA. An initial procedure known as scaling is recommended for such a case. The scaling is introduced to the impedance estimation in order to reduce these practically large values of voltage and current to be comparable to each other. This scaling can be achieved by dividing all fundamental-frequency positive-sequence voltages and currents during the sag with pre-sag quantities. The scaled voltage and current will be in the range of one. As a result, estimated resistance values from the proposed method will have no unit.

In summary, the proposed sag-source detection method can be implemented in the following steps.

Step 1: Perform Fourier analysis and symmetrical components transformation to extract the fundamental-frequency positive-sequence voltage and current during the voltage sag.

Step 2: Scale the voltage and current obtained from Step 1 by dividing with the pre-sag voltage and current accordingly.

Step 3: Separate real and imaginary parts of voltage and current and calculate two values of R_e from

$$\begin{bmatrix} R_e \\ X_e \\ E_X \end{bmatrix} = \begin{bmatrix} I_X(1) & I_Y(1) & 1 \\ \vdots & \vdots & \vdots \\ I_X(n) & I_Y(n) & 1 \end{bmatrix}^{+} \begin{bmatrix} V_X(1) \\ \vdots \\ V_X(n) \end{bmatrix} \tag{3.17}$$

and

$$\begin{bmatrix} R_e \\ X_e \\ E_Y \end{bmatrix} = \begin{bmatrix} I_Y(1) & I_X(1) & 1 \\ \vdots & \vdots & \vdots \\ I_Y(n) & I_X(n) & 1 \end{bmatrix}^{+} \begin{bmatrix} V_Y(1) \\ \vdots \\ V_Y(n) \end{bmatrix} \tag{3.18}$$

Step 4: Check the consistency of two resistance signs determined from Step 3. If two R_e signs are consistent, sag source can be interpreted reliably. Positive signs indicate a supply-side sag, while negative signs indicate a customer-side sag.

Step 5: If two R_e signs are not consistent (opposite), sag source can still be interpreted from

$$\begin{bmatrix} R_e \\ X_e \\ E_X \\ E_Y \end{bmatrix} = \begin{bmatrix} I_X(1) & -I_Y(1) & 1 & 0 \\ \vdots & \vdots & \vdots & \vdots \\ I_X(n) & -I_Y(n) & 1 & 0 \\ I_Y(1) & I_X(1) & 0 & 1 \\ \vdots & \vdots & \vdots & \vdots \\ I_Y(n) & I_X(n) & 0 & 1 \end{bmatrix}^{+} \begin{bmatrix} V_X(1) \\ \vdots \\ V_X(n) \\ V_Y(1) \\ \vdots \\ V_Y(n) \end{bmatrix} \tag{3.19}$$

Step 6: Check the sign of the single value of R_e from Step 5. Positive sign indicates a supply-side sag, while negative sign indicates a customer-side sag.

3.3 Nonlinear or Constant Power Loads

Another issue that could render the proposed method less reliable is the assumption of linear systems. In reality, there often exist nonlinear loads such as variable frequency drives (VFDs) and induction motors (IMs) in customer facilities. Both types of loads could behave as constant power loads (CPLs) [12, 29]. Their response during the voltage sag can be quite different from linear loads. In order to clarify this issue, experimental studies were conducted. Results are presented in this section.

3.3.1 Experimental Setup

A laboratory experiment consisting of a VFD or an IM load was set up for this purpose (Figure 3.3). The VFD or IM has a rating of 2 HP. Various voltage sags ranging from 5% to 20% drop were introduced by switching R_f in and out of the circuit. The sag started at the 0^{th} cycle and lasted for about 10 cycles. Voltage and current signals were recorded at M_1 and M_2 giving downstream (DS) and upstream (US) sag-source data, respectively. Figure 3.4 shows voltage and current waveforms for the case of 20% sag. The data was obtained using a Data Acquisition Nicolet Transient Recorder. This equipment can record the data simultaneously with adjustable sampling rate by connecting a laptop via IEEE-488 interface unit. The recorder has special software called Transient Evaluation and Analysis Manager (TEAM256) installed on the laptop to control the recording process. The voltage and current waveforms were measured using voltage and current probes. The test data was then manipulated by MATLAB program for the sag-source analysis.

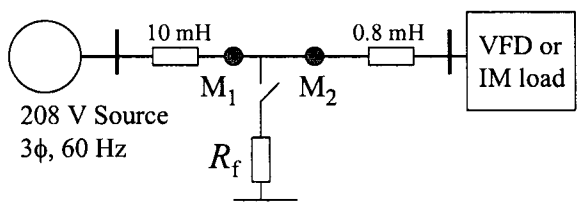

Figure 3.3: Test circuit for constant power loads

Since the supply system is dominated by linear components, the proposed method has no difficulties to identify downstream sag sources. The difficulties arise when a sag originates from upstream. The proposed method essentially attempts to estimate an equivalent impedance for the downstream which is a constant power load. The upstream disturbance is therefore the focus of this investigation.

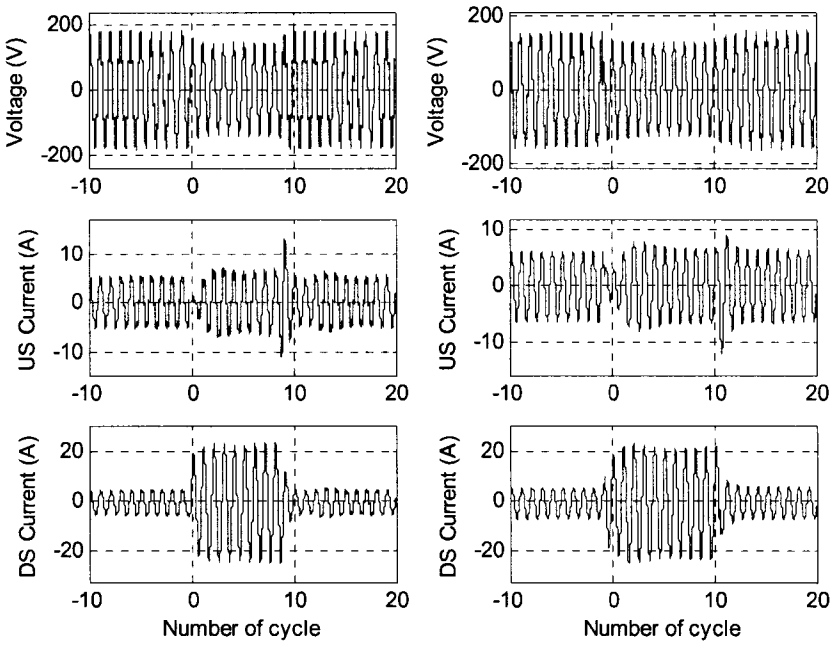

(a) VFD load (b) IM load

Figure 3.4: Voltage and current waveforms of constant power loads

Figure 3.5 shows the fundamental-frequency positive-sequence voltage, current, and powers associated with an upstream sag. It can be seen that the active power and current decrease initially and then increase in order to compensate for the drop in the voltage for maintaining the constant power. Such a behavior has been well investigated in the voltage stability area [30, 31]. According to [31], the response can be represented using a dynamic load model with transient and steady-state load characteristic curves.

The transient characteristic curves in the form of $P_t(V) = P_0V^{\alpha}$ and $Q_t(V) = Q_0V^{\beta}$ are shown as dotted lines in the last row of Figure 3.5 where α and β are transient

load characteristic parameters and P_0 and Q_0 are pre-disturbance power quantities. The range of α is estimated to be 4.2 to 6.5 for a VFD and 11.0 to 16.1 for an IM. The range of β varies from 10.6 to 17.9 for a VFD and 3.5 to 4.5 for an IM. The transient response of the loads is, therefore, not the constant power type ($\alpha = \beta = 0$). In fact, the load is much more sensitive to voltage change than the linear load ($\alpha = \beta = 2$). Thus, if $\boldsymbol{Z}_e$ for the transient period is estimated, one may detect the sag source reliably. The theoretical justification for this approach is provided as follows. The load can be modeled as

$$P + jQ = P_0 V^{\alpha} + jQ_0 V^{\beta} \tag{3.20}$$

The corresponding load current is

$$I = \frac{P - jQ}{V} = P_0 V^{\alpha-1} - jQ_0 V^{\beta-1} \tag{3.21}$$

In the above equation, the phase angle of voltage V is used as the reference angle and is set to zero. If there is a voltage disturbance ΔV, the current change ΔI is

$$\Delta I = P_0 V^{\alpha-2}(\alpha - 1)\Delta V - jQ_0 V^{\beta-2}(\beta - 1)\Delta V \tag{3.22}$$

The equivalent incremental impedance of the load can thus be estimated as follows:

$$\begin{aligned} \Delta \boldsymbol{Z} = \frac{\Delta \boldsymbol{V}}{\Delta \boldsymbol{I}} &= \frac{1}{P_0 V^{\alpha-2}(\alpha-1) - jQ_0 V^{\beta-2}(\beta-1)} \\ &= kP_0 V^{\alpha-2}(\alpha-1) + jkQ_0 V^{\beta-2}(\beta-1) \\ &= R_{eq} + jX_{eq} \end{aligned} \tag{3.23}$$

where $k = \left[P_0 V^{\alpha-2}(\alpha-1)\right]^2 + \left[Q_0 V^{\beta-2}(\beta-1)\right]^2$. R_{eq} is the equivalent resistance to be determined by the sag-source detection algorithm. The resistance has the form of

$$R_{eq} = kP_0 V^{\alpha-2}(\alpha-1) \tag{3.24}$$

It can be seen that if $\alpha > 1$, R_{eq} will be positive. So the proposed method will work. Since α is much larger than one, R_{eq} will be larger and it will make the sign determination easier.

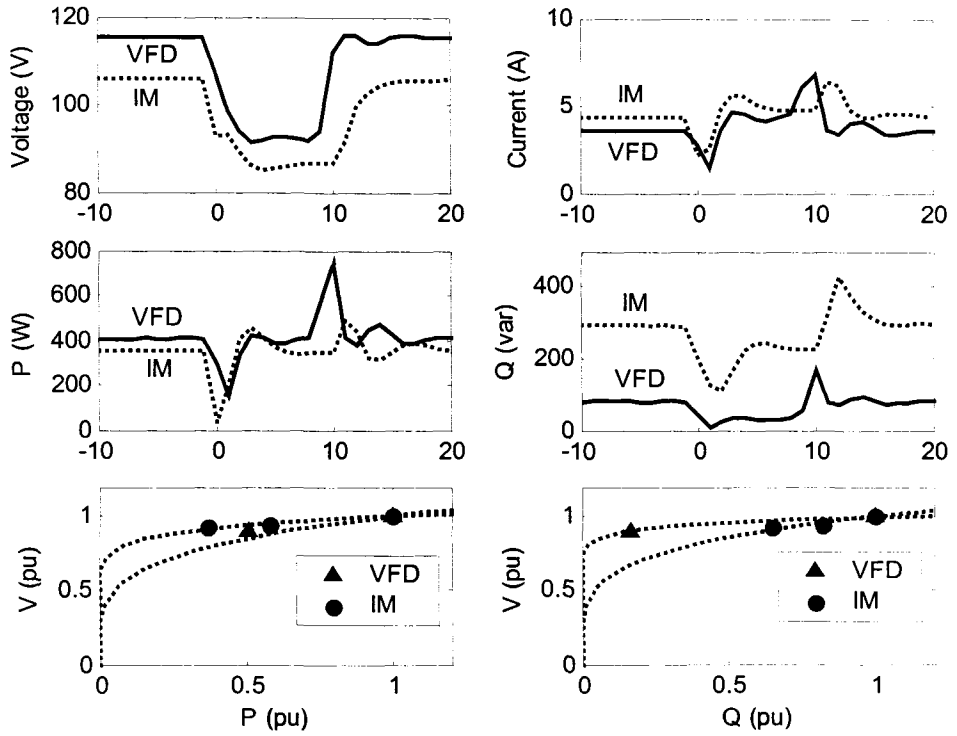

Figure 3.5: Fundamental-frequency positive-sequence voltage, current, powers, and characteristics of voltages against powers

3.3.2 Modified Sag-Source Detection Method

In order to determine how many cycles of data are sufficient to capture the transient characteristics of the load, a sensitivity study has been conducted. Figure 3.6 shows the calculated R_e results using different window lengths. The figures also plot the active power change defined as $\Delta P = P - P_{pre}$ where P is fundamental-frequency active power and P_{pre} is the pre-sag fundamental-frequency active power. This index can be used to monitor the power restoration behavior of a constant power load.

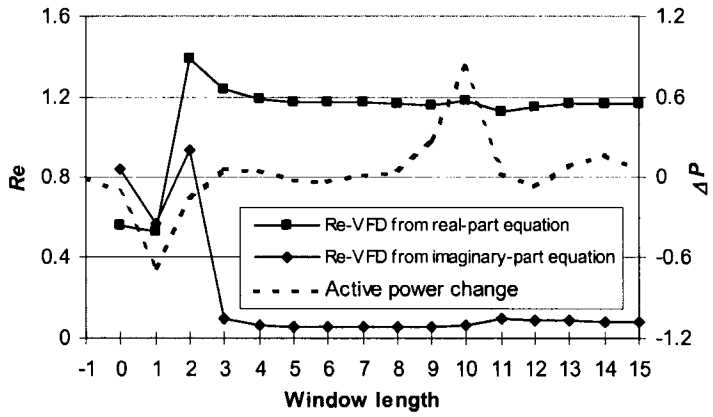

(a) VFD load

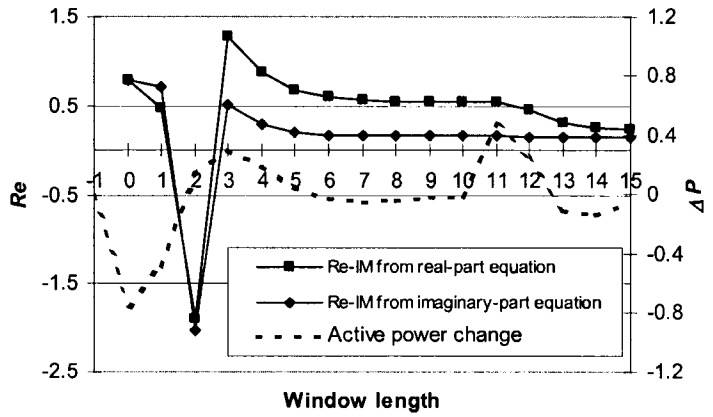

(b) IM load

Figure 3.6: Resistance plots using different window length

It can be seen that, if the window is less than three cycles, the two estimated R_e values are close to each other and their signs indicate sag locations correctly. The active power index starts to change sign after three cycles, which means that the load power has been restored after three cycles and the load no longer behaves as a linear load. Based on these observations and the inherent transient characteristics of the loads, the sag-source detection technique is further refined. The basic idea is to select the during-sag cycle properly for $\boldsymbol{Z}_e$ estimation. The criterion is to monitor the active power change with respect to its pre-disturbance value. If ΔP has only one sign, either positive or negative, the value of n for $\boldsymbol{Z}_e$ estimation can be selected as the sag

duration. If ΔP changes sign, the value of n should be selected as K–1, where K is the cycle when ΔP changes sign. The completed algorithm of the proposed sag source detector is thus shown in Figure 3.7.

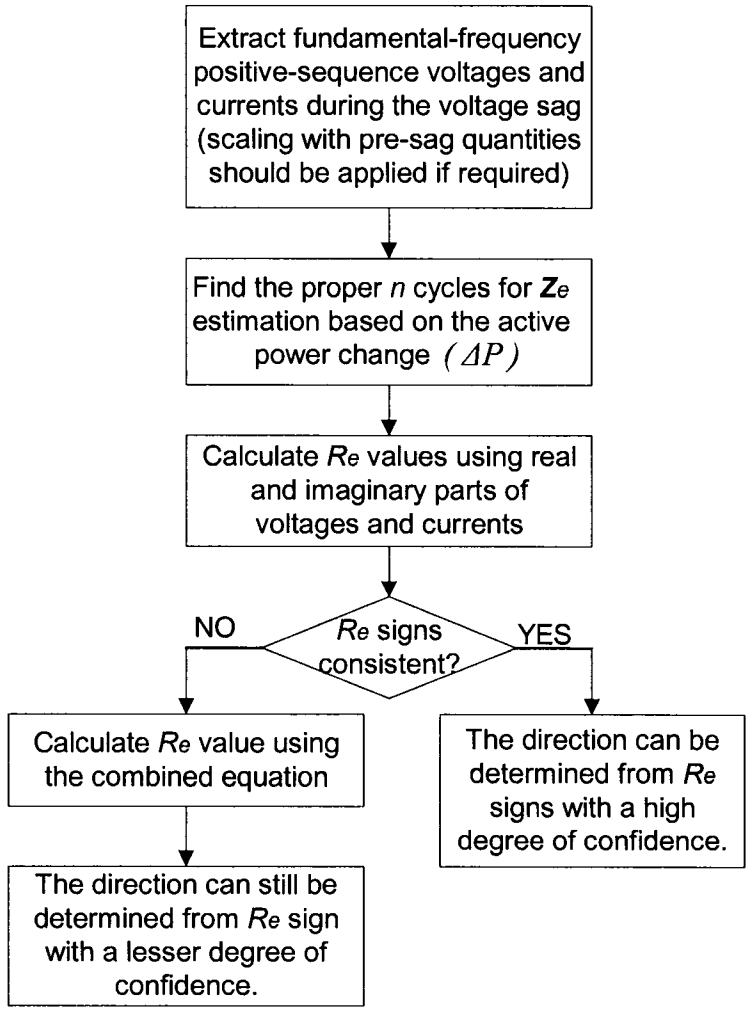

Figure 3.7: Flowchart of the modified proposed sag-source detection method

The above method assumes that a composite customer load has a transient power recovery characteristic. Extensive voltage stability oriented dynamic load research and measurement such as those shown in references [32, 33] supports the validity of this assumption. It is theoretically possible that some power electronic loads could respond faster than three cycles. Our extensive literature search on this subject has not found the existence of such a very fast response characteristic. It is important to

note as well that sag-source detection methods are not intended for application to individual power electronic loads. They are intended for the utility-customer interface points. The downstream loads are composite loads representing a whole customer facility. It is an accepted fact that such loads exhibit recovery characteristics.

3.4 Verification Studies

The proposed method has been verified using simulations, field measurements, and experimental tests. Details are provided as follows.

3.4.1 Simulation Results

Two actual power systems were modeled and simulated for the verification study. Analysis results and details are described next.

3.4.1.1 Case Study 1: 100-Bus System

Figure 3.8 illustrates the simplified system diagram of the first case study. Three-phase-to-ground faults causing balanced sags were simulated at five different locations in a 100-bus power system. Each fault/sag event was recorded at two monitoring buses, one sees the fault as the downstream source and the other as the upstream source. The simulation was performed using Visual PSA-H software. Visual PSA-H is an Excel-based program for the harmonic, power flow, fault, and power quality analysis of balanced transmission and distribution systems. The simulation data was then manipulated by MATLAB for the sag-source analysis. The fundamental-frequency resistance (R_1) values averaged from three phases are tabulated in Table 3.1. It can be seen that signs of R_1 can indicate sag sources (or fault bus directions) correctly.

Table 3.1: Bus selection details and resistance values

Fault bus	Monitoring buses		The average R_f values (pu)	
	fault seen as downstream	fault seen as upstream	fault seen as downstream	fault seen as upstream
262	61	57	–0.12	+1.55
150	62	76	–0.15	+1.31
84	43	55	–0.08	+4.25
51	48	56	–0.07	+4.04
116	60	65	–0.04	+3.73

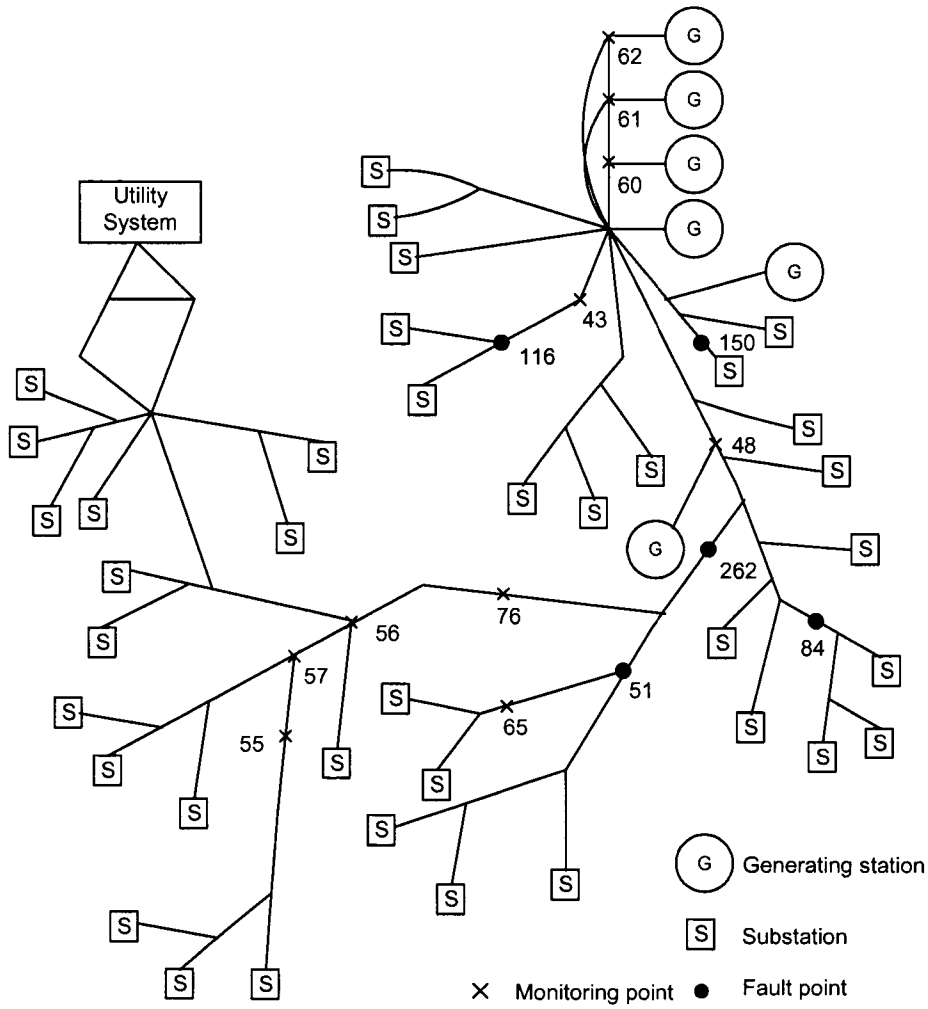

Figure 3.8: Simplified system diagram for the simulation (case study 1)

3.4.1.2 Case Study 2: Oil Field System

Figure 3.9 depicts the simplified system diagram of the second case study. The system is an oil field system installed with 21 distributed adjustable speed drives (ASDs), induction motors, and linear loads. The ASDs use a diode rectifier as a front end in addition to an inductance and a capacitor in the DC link. Induction motors were modeled as loads and grouped with linear loads (LLs). Nine capacitors (Caps) are distributed in the system for the voltage support. Load details connected at each bus through step-down transformers are given in Table 3.2. The system total active and reactive powers are 6.3 MW and 2.2 Mvar, respectively. The simulation was performed using PSCAD/EMTDC software. PSCAD is a power system simulator for the design and verification of various types of power systems and EMTDC is a general-purpose time-domain program. Together they can provide a fast, flexible, and accurate solution for the power system simulation. The simulation data was then manipulated by MATLAB for the sag-source analysis.

Table 3.2: Load details at each bus

Bus	Transformer rating	Load type	Load Size (HP)	Cap Size (kvar)
L1	0.3 MVA, 25/0.48 kV	LL	205	
L2	0.5 MVA, 25/0.48 kV	ASD	150	
L3	3 @ 0.5 MVA, 25/0.48 kV	LL and Caps	398	3 @ 50
L4	3 @ 0.3 MVA, 25/0.48 kV	ASDs, LL, and Cap	100 (ASD#1), 150 (ASD#2), and 203 (LL)	1 @ 40
L5	2 @ 0.3 MVA, 25/0.48 kV	ASD, LL, and Cap	115 (ASD) and 203 (LL)	1 @ 30
L6	0.3 MVA, 25/0.48 kV	LL and Cap	203	1 @ 40
L7	1.5 MVA, 25/4.16 kV and 1 MVA, 25/0.48 kV	LLs and ASD	450 (ASD), 900 (LL#1), and 398 (LL#2)	
L8	0.3 MVA, 25/0.48 kV	ASD	82	
L9	4 @ 0.3 MVA, 25/0.48 kV and 1 @ 0.5 MVA, 25/0.48 kV	ASDs, LL, and Cap	90 (ASD#1), 90 (ASD#2), 90 (ASD#3), 82 (ASD#4),	1 @ 40

			and 203 (LL)	
L10	3 @ 0.3 MVA, 25/0.48 kV	ASD, LLs, and Cap	450 (ASD), 150 (LL#1), and 150 (LL#2)	1 @ 40
L11	2 @ 0.3 MVA, 25/0.48 kV	ASD, LL, and Cap	115 (ASD) and 203 (LL)	1 @ 40
L12	0.3 MVA, 25/0.48 kV	ASD	120	
L13	2 @ 0.3 MVA, 25/0.48 kV and 1 @ 0.75 MVA, 25/0.48 kV	ASDs and LL	100 (ASD#1), 65 (ASD#2), 450 (ASD#3), and 203 (LL)	
L14	0.3 MVA, 25/0.48 kV	ASD	150	
L15	0.3 MVA, 25/0.48 kV	ASD	115	
L16	0.5 MVA, 25/0.48 kV	ASD	150	
L17	0.3 MVA, 25/0.48 kV	ASD	115	

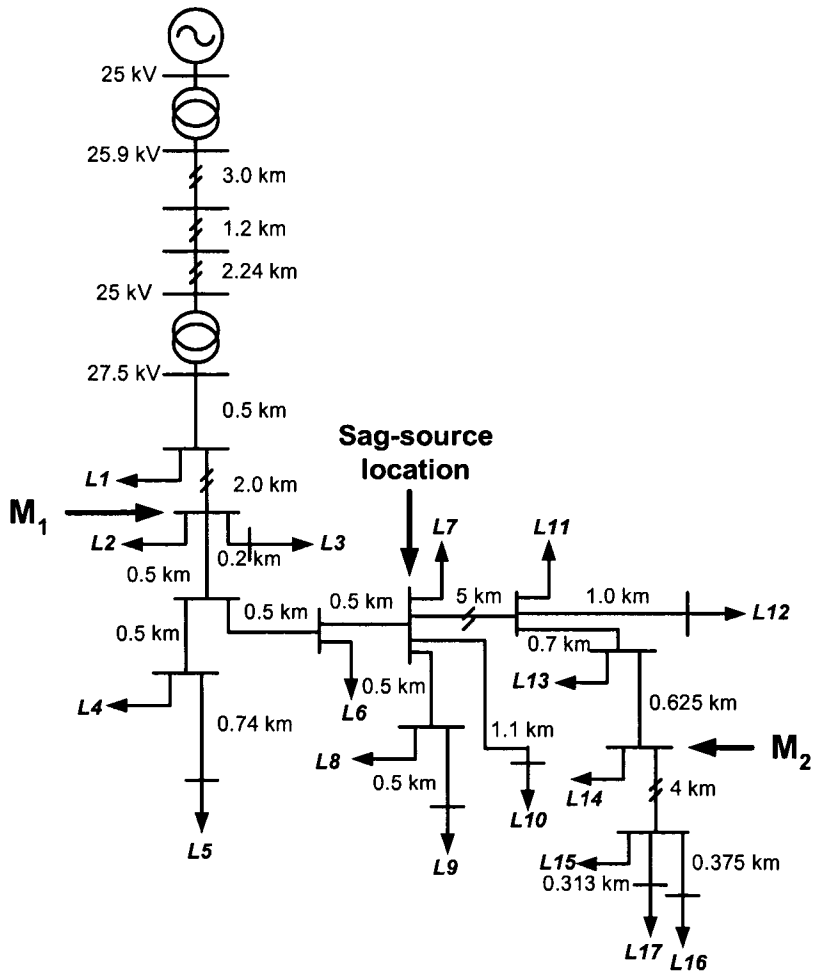

Figure 3.9: Simplified system diagram for the simulation (case study 2)

Three sources of sag—faults, transformer energization, and induction motor starting—were performed and simulated. Sag data was recorded at two locations, M_1 and M_2. The data from M_1 represents the downstream (DS) sag, while the data from M_2 represents the upstream (US) sag. These directions are referenced with the fundamental-frequency active power direction that flows from the 25 kV substation to loads through overhead distribution lines. Two types of faults—three-phase (3P) and single line-to-ground (1P) faults—were studied. 3P faults are typically the worst case and 1P faults are the most frequent occurred in the power system. These faults were short-circuited to ground with a fault resistance of 30 Ω in order to cause a reasonable sag level at the measurement locations. Four cases of faults were simulated.

For a sag caused by transformer energization, a transformer equipped with a circuit breaker for the switching was connected at the sag-source location to create DS and US sags at M_1 and M_2, respectively. A 30 MVA, 20/20 kV transformer with a leakage reactance of 0.05 per unit supplying a linear load (100 ohms in series with 0.05 H) was energized through a circuit breaker to cause a sag. Two cases of transformer energization were simulated.

For a sag caused by induction motor starting, an induction motor was connected at the sag-source location to create DS and US sags at M_1 and M_2, respectively. A 450 HP, 0.48 kV induction motor was supplied through a 1.2 MVA, 25/0.48 kV transformer and started through a circuit breaker to cause a sag. Two cases were simulated. Estimated equivalent resistance (R_e) results of all simulated cases are summarized in Table 3.3. Sag level was computed from the largest drop of the fundamental-frequency positive-sequence voltage magnitude during a sag as a percentage of the pre-sag voltage magnitude. R_e of all DS cases are expected to be theoretically close because the location of sag sources and the recording point (M_1) are the same. It is also expected to be true for R_e of all US cases. R_e results agree well with this observation and resistance signs can correctly determine the sag source.

Table 3.3: Sag-source analysis of simulation results

Case	Source location	Sag type	Sag level (%)	R_e
Fault				
1	Downstream	3P	25.6	–0.08
2	Downstream	1P	9.0	–0.07
3	Upstream	3P	29.3	+0.80
4	Upstream	1P	10.7	+0.75
Transformer Energization				
1	Downstream	3P	8.7	–0.05
2	Upstream	3P	9.6	+0.80
Induction Motor Starting				
1	Downstream	3P	2.9	–0.05
2	Upstream	3P	3.3	+0.75

3.4.2 Field Measurement Results

The proposed method has also been verified using field measurement data. There are three sets of data from field measurements. The first set contains downstream voltage ripples from load variations at an industrial plant. The second set contains four downstream faults: three faults on a transmission system and one fault on a distribution system. The third set contains one downstream transformer energization near a substation. Details and results are summarized as follows.

3.4.2.1 Case Study 1: Load Variations

A power quality monitor was placed at a 12.47 kV industrial plant which is fed from a 225 kV substation as shown in Figure 3.10. Both the supply and customer sides have power generation. The plant consists of two groups of variable frequency drives (VFDs), the fifth and seventh harmonic filters installed at 12.47 kV bus, and five local generators supplying six additional VFDs and commercial loads such as office-building loads and heating. Disturbance waveforms were monitored continuously for several months and lots of voltage variations were detected. Historical records and operation logs showed that the disturbances were mainly due

to switching of heavy loads causing voltage ripples on the customer side. Figure 3.11 shows a scatter plot of voltage magnitudes versus their duration. It can be seen that most ripples are not severe and the duration is around 15-25 cycles. The circles in the figure are the disturbances whose source cannot be detected by the proposed method due to inconsistent signs of the estimated R_e values.

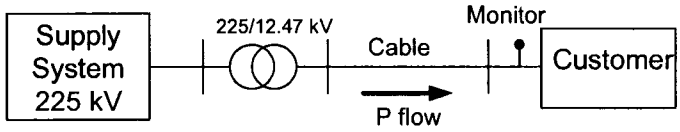

Figure 3.10: One-line diagram of the field measurement system

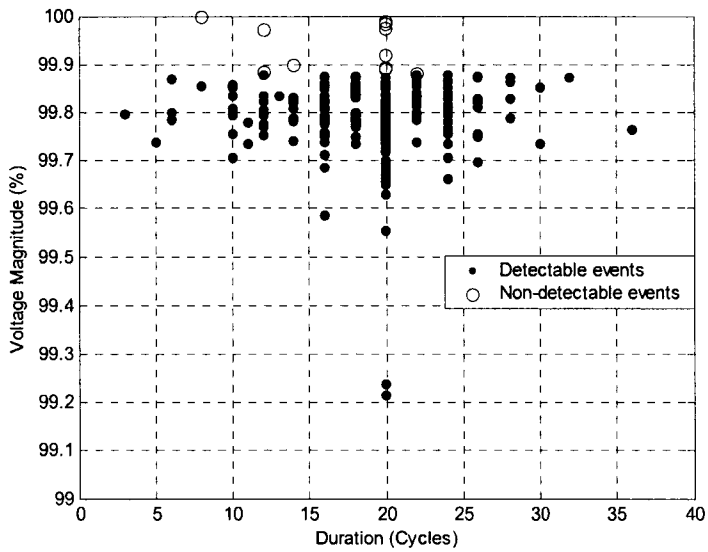

Figure 3.11: Voltage magnitudes as a function of their duration

Captured events were analyzed by calculating the equivalent impedance using two data points first. For all events, the first cycle before voltage drop and the last cycle of an event were selected for impedance calculations. The scaling has not been applied in the equivalent resistance estimation to this specific case study because we would like to compare the estimated impedance (in ohms) with the value from the detailed system modeling. The impedance comparison will be shown later. The results are plotted in an impedance plane as shown in Figure 3.12. Note that each impedance value is associated with the current change (ΔI) range. Reliable results

can be achieved when ΔI values are high. It can be seen that most impedances lie in the third quadrant, which indicates that sources of these ripples are from the customer side. The negative values of these impedances are supposed to be the driving-point impedances of the supply system ($\boldsymbol{Z}_1$ in Figure 3.1). However, there are still some impedances located in the fourth quadrant, which could be wrongly interpreted as supply-side disturbances. They cannot be trusted, however, if we examine the values of those impedances further. The points in the fourth quadrant are supposed to be the equivalent impedance of the customer side ($\boldsymbol{Z}_2$ in Figure 3.1), but their values are close to the supply system driving-point impedances as plotted in the third quadrant, and in addition, the impedances are capacitive. This is impossible in a practical distribution system. Therefore, it is very likely that all impedances should lie in the third quadrant. Errors are possibly caused by the improper selection of pre- and during-event cycles.

The results can be significantly improved by using more data cycles in the proposed least-squares method, as shown in Figure 3.13. The average of two consistent impedance values [one from equation (3.17) and the other one from equation (3.18)] was used to represent a single impedance value. Events with inconsistent resistance signs were considered as non-detectable by the proposed method. Their R_e results were not plotted in Figure 3.13, but the magnitude and duration of these disturbances were shown in Figure 3.11 as circles. It can be seen that such disturbances have very small magnitudes. Failure to detect their sources is caused by lower energy levels of the disturbance and should not be a major concern, since they are not significant events. It can be seen from Figure 3.13 that all the impedances now are only located in the third quadrant, which indicates that they were generated by customer-side disturbances. Their values are concentrated[4] around

---

[4] Values of total distances from equivalent impedances to the supply-side impedance (from detailed system model) in Figures 3.12 and 3.13 are 181.5 Ω and 154.53 Ω, respectively.

the actual supply-side driving-point impedance (0.78 + j1.70 Ω) which is derived from the detailed system model. The field-test results show great improvement, this is mainly due to the use of redundant information.

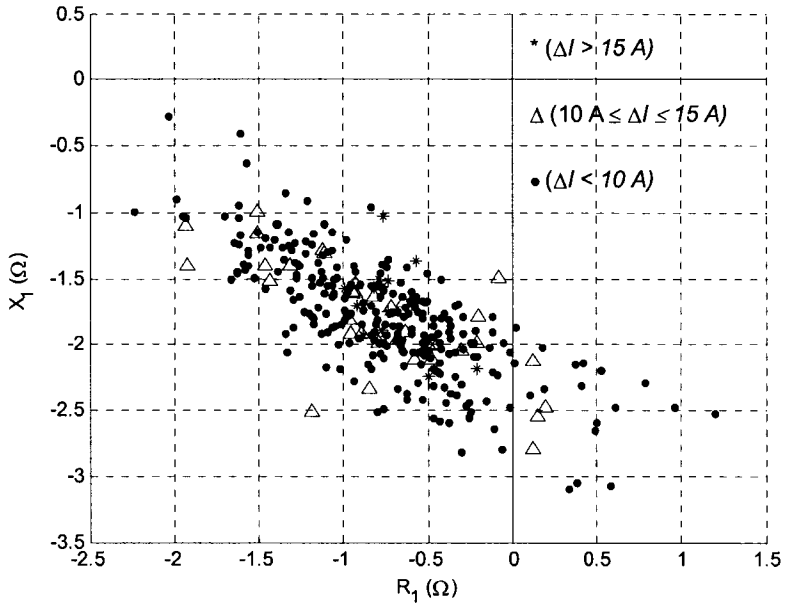

Figure 3.12: Impedances estimated using two cycles of data

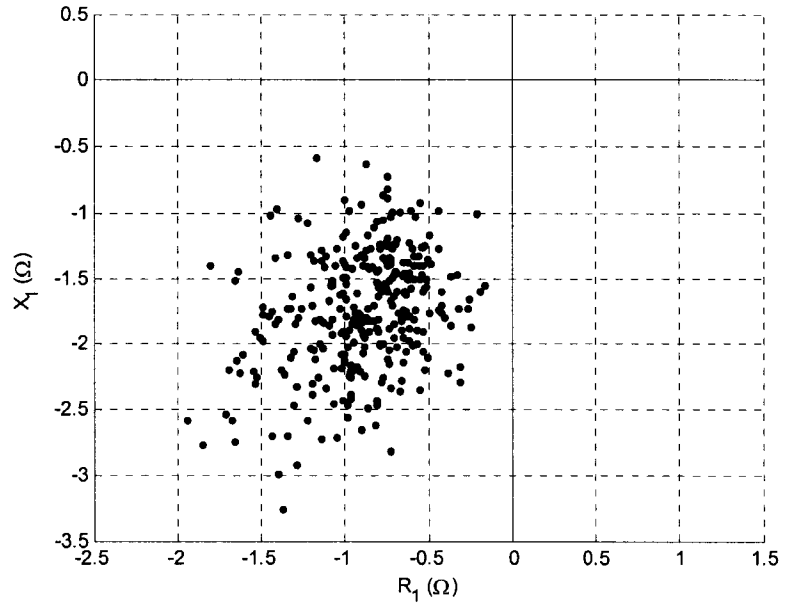

Figure 3.13: Impedances estimated using the proposed least-squares method

3.4.2.2 Case Study 2: Faults

Four downstream faults will be described in this section. The first fault (Fault 1) was a downstream line-to-line fault (LLF) on a transmission line connecting substations. Snow unloading from the line caused conductors to slap together. The second fault (Fault 2) was a downstream fault on a transmission line caused by a tree touching a line. The third fault (Fault 3) was a downstream phase-to-neutral fault (PNF) on a distribution line causing a fuse to clear. The fourth fault (Fault 4) was a downstream fault caused by a lightning strike on a transmission line. Because all faults are from downstream, negative signs of estimated R_e are expected. Table 3.4 summarizes sag-source analysis results for all four cases. All negative signs verify that the proposed method performs well with actual data from field measurements.

Table 3.4: Sag-source analysis of field measurement results

Case	Source location	Fault type	Sag level (%)	R_e
Fault 1	Downstream	LLF	45.5	–0.86
Fault 2	Downstream	3P	9.7	–0.001
Fault 3	Downstream	PNF	4.1	–0.05
Fault 4	Downstream	3P	85.5	–0.10

3.4.2.3 Case Study 3: Transformer Energization

A 315 MVA, 138/21 kV (HV grounded star/LV delta) generator transformer was energized through a breaker from the HV side. The transformer was energized radially from a short 138 kV line from one generating station. Downstream-sag waveforms were recorded at the end of the line connecting the transformer. The sag level is about 8.4%. The estimated R_e from the proposed method was estimated to be –0.02 which represented a downstream sag. The negative resistance sign shows that the location of the sag source has been correctly determined.

3.4.3 Experimental Results

There are three sets of data carried out by experimental tests. The first set contains sag data tested with linear and nonlinear loads. The second set contains sag data from transformer energization. The third set contains sag data from induction motor starting. Details and results are summarized as follows.

3.4.3.1 Case Study 1: Linear and nonlinear loads

Various tests (both upstream and downstream sags) with nonlinear loads—VFDs and IMs—were carried out experimentally in Section 3.3. Linear loads were also performed. Table 3.5 summarizes results of sag-source detection for all tests. Sag-source results confirm that the proposed method can work reliably for both linear and nonlinear loads.

Table 3.5: Experimental results (linear and nonlinear loads)

Event	Source location	Sag type	Sag level (%)	Duration (cycles)	R_e
Variable Frequency Drive (VFD load)					
1	Downstream	3P	4.1	12	–0.004
2	Downstream	3P	21.7	10	–0.002
3	Upstream	3P	4.1	12	+0.58
4	Upstream	3P	21.7	10	+0.57
5	Upstream	3P	3.4	120	+0.61
6	Upstream	3P	8.6	120	+0.62
7	Upstream	3P	13.8	120	+0.56
8	Upstream	3P	20.2	120	+0.69
9	Upstream	1P	2.9	120	+0.40
10	Upstream	1P	8.3	120	+0.48
11	Upstream	1P	17.2	120	+0.70
12	Upstream	1P	18.5	120	+0.60
Induction Motor (IM load)					
1	Downstream	3P	19.8	13	–0.003
2	Upstream	3P	19.8	13	+0.58

3	Upstream	3P	2.9	120	+0.77
4	Upstream	3P	8.1	120	+0.89
5	Upstream	3P	13.9	120	+0.61
6	Upstream	3P	20.1	120	+0.74
7	Upstream	1P	2.1	120	+0.97
8	Upstream	1P	6.0	120	+0.77
9	Upstream	1P	10.1	120	+0.46
10	Upstream	1P	14.4	120	+0.73
Linear Load					
1	Downstream	3P	4.2	12	–0.005
2	Upstream	3P	4.2	12	+1.02
3	Upstream	3P	4.4	7	+1.03
4	Upstream	3P	3.9	18	+1.01

3.4.3.2 Case Study 2: Transformer energization

Figure 3.14 illustrates the test circuit used to collect sags from transformer energization. The energization was conducted on 30 kVA, 120/208 V, 3-phase 3-limb, laboratory transformer with grounded Y primary and delta secondary. The linear load consists of 10-ohm resistance box and 46.5 mH coil. IM load rating is 1 HP. Nicolet device was used to record the data. Two measurement points (M_1 and M_2) collected downstream and upstream sag-source data. Table 3.6 summarizes sag-source analysis. Estimated R_e signs show the location of the sag source (transformer) correctly.

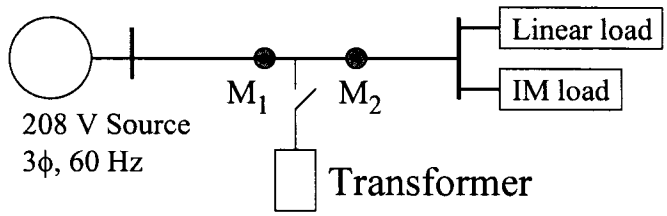

Figure 3.14: Test circuit for transformer energization

Table 3.6: Sag-source analysis of transformer energization

Case	Source location	Sag type	Sag level (%)	R_e
1	Downstream	3P	3.0	–0.0005
2	Upstream	3P	3.0	+0.63

3.4.3.3 Case Study 3: Induction motor starting

Figure 3.15 illustrates the test circuit used to collect sags from induction motor starting. The rating of switched IM is 1 HP. The starting time of IM is around one second. The linear load consists of 10-ohm resistance box and 46.5 mH coil. IM load rating is 0.23 HP. Nicolet device was used to record the data. Two measurement points (M_1 and M_2) collected downstream and upstream sag-source data. Table 3.7 summarizes sag-source analysis. Estimated R_e signs show the location of the sag source (induction motor) correctly.

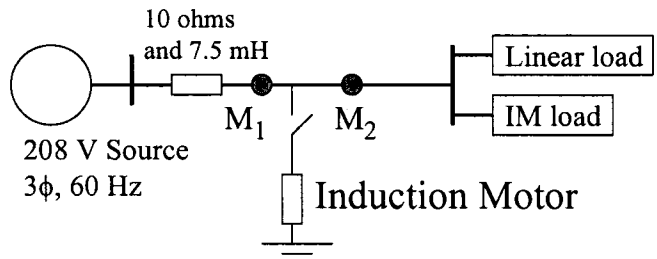

Figure 3.15: Test circuit for induction motor starting

Table 3.7: Sag-source analysis of induction motor starting

Case	Source location	Sag type	Sag level (%)	R_e
1	Downstream	3P	16.6	–0.44
2	Upstream	3P	16.6	+0.28

3.5 Discussions

This section discusses practical issues associated with the proposed method such as swells and unbalanced sags, the method simplification, applications for short-duration sags and meshed systems, and errors of instruments.

3.5.1 Swells and Unbalanced Sags

Unbalanced sags refer to those sags that exhibit different sag levels for different phases. One or two phases may even experience voltage swell. The proposed method applies to swells and unbalanced sags equally well because the estimation of the equivalent positive-sequence impedance is not dependent on the disturbance type. As long as there is a disturbance, the equivalent impedance can be estimated.

3.5.2 Simplification of the Method

Since the proposed method examines the sign of resistance only, there is no need to calculate the reactance. The impedance can be decoupled by introducing a rotating transformation, that is, selecting the fundamental-frequency current vector as reference axis. If we multiply both sides of equation (3.7) by $e^{-j\alpha}$ where $\alpha = tan^{-1}(I_Y / I_X)$ is the phase angle of the measured current, then equations (3.8) and (3.9) can be simplified as

$$\begin{bmatrix} V\cos\theta(1) \\ \vdots \\ V\cos\theta(n) \end{bmatrix} = \begin{bmatrix} I(1) & 1 \\ \vdots & \vdots \\ I(n) & 1 \end{bmatrix} \begin{bmatrix} -R_1 \\ E_1\cos\theta_1 \end{bmatrix} \tag{3.25}$$

and

$$\begin{bmatrix} V\sin\theta(1) \\ \vdots \\ V\sin\theta(n) \end{bmatrix} = \begin{bmatrix} I(1) & 1 \\ \vdots & \vdots \\ I(n) & 1 \end{bmatrix} \begin{bmatrix} -X_1 \\ E_1\sin\theta_1 \end{bmatrix} \tag{3.26}$$

where θ and θ_l are the phase angles by which $\boldsymbol{V}$ and $\boldsymbol{E}_l$ lead $\boldsymbol{I}$ respectively. In this transformation, it is assumed that θ_l will not change significantly during the event. The equivalent resistance can be obtained as follows by using the LS method:

$$\begin{bmatrix} -R_1 \\ E_1\cos\theta_1 \end{bmatrix} = \begin{bmatrix} I(1) & 1 \\ \vdots & \vdots \\ I(n) & 1 \end{bmatrix}^{+} \begin{bmatrix} V\cos\theta(1) \\ \vdots \\ V\cos\theta(n) \end{bmatrix} \tag{3.27}$$

Similarly, the parameters on the customer side can be found from a supply-side event as

$$\begin{bmatrix} R_2 \\ E_2 \cos\theta_2 \end{bmatrix} = \begin{bmatrix} I(1) & 1 \\ \vdots & \vdots \\ I(n) & 1 \end{bmatrix}^{+} \begin{bmatrix} V\cos\theta(1) \\ \vdots \\ V\cos\theta(n) \end{bmatrix} \tag{3.28}$$

where θ_2 is the phase by which $\boldsymbol{E}_2$ leads $\boldsymbol{I}$. θ_2 is also assumed to be constant during the disturbance.

It turns out that the above equation is very similar to that of reference [16]. Thus a theoretical foundation is established for the method in [16]. Note that, however, the method in [16] assumes θ_1 and θ_2 do not change significantly during a disturbance. This might not be true under some practical conditions. The system identification-based method proposed in this thesis, however, does not rely on this assumption and is therefore more reliable.

3.5.3 Applications for Short-Duration Sags and Meshed Systems

From equations (3.27) and (3.28), it can be seen that theoretically at least two sampling points during the event are required for the resistance estimation from which one point is a pre-disturbance measurement, . Since the majority of voltage sags last several cycles or longer, this requirement can be easily satisfied. If there are indeed only two data points, the results can be unreliable. This is a major drawback of the proposed method.

The proposed method has been developed for radial systems where upstream and downstream subsystems can be identified clearly. The interface point between a utility and a customer belongs to this type and the method is reliable to determine the sag responsibility. This is the most useful and the intended application of the proposed method. The proposed method may not be reliable for meshed systems. More research work is needed to confirm this suspicion.

3.5.4 Errors of Instruments

Measurement errors can be divided into three main groups: instrument errors, transducer errors, and errors due to the measured signal (low-level signals). In practice, the main errors are from the recording instrument, voltage and current transformers. The proposed method works on the fundamental-frequency components. Errors from these sources are very small at the fundamental frequency. Modern power quality meters generally possess sufficient sampling rate for the fundamental-frequency analysis. In summary, the proposed method does not impose additional accuracy requirements. The instrumentation circuits of modern digital revenue meters are sufficient for reliable implementation of the proposed method.

3.6 Summary

The sign of the fundamental-frequency positive-sequence resistance estimated from the data at a metering point is proposed as an indicator to determine the direction of voltage sag source. The equivalent resistance is derived using the frequency-domain system identification and the least-squares method. The main conclusions of this chapter are summarized as follows:

1. The principle of the proposed method is to estimate the equivalent impedance of the non-disturbance side by utilizing voltage and current changes caused by the disturbance.

2. The proposed method requires only measuring the voltage and current waveforms. The fundamental-frequency positive-sequence components of the waveforms are extracted for impedance estimation. As a result, the method can be easily implemented in modern digital revenue meters.

3. The proposed method has a solid theoretical foundation for linear systems and does not rely on empirical assumptions. For nonlinear loads, the method has been improved by taking into account the transient characteristics of the load.

The next chapter will compare sag-source results from the same case studies in this chapter with other published methods described in Chapter 2.

CHAPTER 4

Comparison of Methods

Chapter 3 covered the theoretical background and derivation of the proposed sag-source-detection method. The proposed method applied the frequency-domain system identification and the least-squares technique to estimate the impedance response of the non-sag side. The sag source can be determined from the sign of the equivalent resistance. This chapter will compare sag-source results from published methods summarized in Chapter 2 using same case studies in Chapter 3. Details of each case study can be found in Chapter 3.

4.1 Indices and Interpretations of Methods

Sag-source detection methods summarized in Chapter 2 mainly come from power quality-based and protection-based methods. Power quality-based methods rely on the intuitive understanding of sag phenomena, while protection-based methods are primarily developed from methods for transmission-line protection. Four methods—two that are power quality-based and two protection-based methods—will be considered for the sag-source comparison in this chapter. Indices and interpretations of methods are summarized as follows.

1) The method based on voltage and current changes: The slope sign of a fitting line between voltage and current magnitudes during a sag is used as an index. If the

slope is positive, the sag source is located upstream; if the slope is negative, the sag source is located downstream. This method is denoted Voltage and Current Changes method or VCC method.

2) The method based on the power and energy flow: The initial peak of disturbance power [IP(DP)] and the change in disturbance energy (DE) during a sag are used as indices. If IP(DP) and DE are negative, the sag source is located upstream; if IP(DP) and DE are positive, the sag source is located downstream. If results from IP(DP) and DE do not agree, the sag-source is found with lesser confidence by IP(DP). This method is denoted the Disturbance Power-Disturbance Energy method or DP-DE method.

3) The method based on directional-relay and distance-relay concepts: The magnitude and phase angle of impedance before and after sag are used as indices. If the impedance magnitude during the sag is less than the impedance magnitude before a sag and the phase angle of impedance during a sag is positive, the sag source is located downstream. Other cases which do not satisfy the aforementioned criteria will be considered as upstream sags. This method is denoted the Impedance Magnitude and Phase method or ZMP method.

4) The method based on the incremental-impedance concept: The fundamental-frequency positive-sequence impedance ($\boldsymbol{Z}_+$) is calculated from changes in voltage and current generated by a fault. The impedance location on the R-X plane is used as an index. If the impedance falls in the first quadrant (1^{st} Q) of R-X plane, the sag source is located upstream; if the impedance falls in the third quadrant (3^{rd} Q) of R-X plane, the sag source is located downstream. This method is denoted as Incremental Impedance method or IZ method.

Table 4.1 summarizes indices and interpretations of the four published sag-source-detection methods. Note that upstream (US) and downstream (DS) directions

are referenced to the fundamental-frequency active power flow at the measurement point.

Table 4.1: Indices and interpretations of published sag-source-detection methods

Methods	Index	Sag-source Interpretation
VCC	The slope sign of a fitting line between voltage and current magnitudes during a sag	If the slope > 0, US source. If the slope < 0, DS source.
DP-DE	The initial peak of disturbance power [IP(DP)] and a change in disturbance energy (DE) during a sag	If IP(DP) and DE < 0, US source. If IP(DP) and DE > 0, DS source.
ZMP	The impedance magnitude ($\|\boldsymbol{Z}_{sag}\|$) and phase angle ($\angle\boldsymbol{Z}_{sag}$) during a sag	If $\|\boldsymbol{Z}_{sag}\| < \|\boldsymbol{Z}_{presag}\|$ and $\angle\boldsymbol{Z}_{sag} > 0$ then DS source, else US source.
IZ	The estimated impedance ($\boldsymbol{Z}_+$) location on the R-X plane during a sag	If $\boldsymbol{Z}_+$ falls in the 1st Q, US source. If $\boldsymbol{Z}_+$ falls in the 3rd Q, DS source.

4.2 Case Study Results

Three major sag sources considered are faults, transformer energization, and induction motor starting. The sag data was obtained from computer simulations, experimental tests, and field measurements. The same case studies in Chapter 3 were used for the comparison. This section will present one example of the sag-source comparison in detail in order to reveal how conclusions of other case studies were drawn. A summary of result comparison will be presented in the next section.

A downstream sag caused by the load fluctuation (Load-Fluc 2) from an industrial plant in Section 3.4.2.1 is chosen as an example. Figure 4.1 contains six subplots used for the sag-source comparison. Subplots (a) and (b) show voltage and current waveforms and fundamental-frequency positive-sequence magnitudes and phase angles, respectively. Subplot (c) illustrates the DP and DE for sag-source analysis using the DP-DE method. IP(DP) and DE are positive so the sag source is downstream. Subplot (d) shows the result for the VCC method. The slope sign is negative so the sag source is downstream. The impedance magnitude and phase

angle are shown in subplot (e) for the ZMP method. The impedance magnitude during a sag is less than the pre-sag impedance magnitude and the impedance phase angle during a sag is positive so the sag source is downstream. Subplot (f) shows the incremental impedance trajectory on the impedance plane for the IZ method. The origin marked by a circle represents the pre-sag condition. The trajectory starts from this origin point. Each dot represents an incremental impedance using data from ten successive cycles after pre-sag cycle and the pre-sag cycle. For example, the second black dot on the trajectory is the incremental impedance calculated using the data from the second cycle after the pre-sag cycle (14^{th} cycle) and the pre-sag cycle (12^{th} cycle).

From the figure, sag-source interpretation and comparisons can be summarized as follows. VCC, DP-DE, and ZMP methods can correctly determine that the sag source is from downstream or the industrial plant. For the IZ method, it can be observed that if the during-sag cycle is selected too close or too far from the pre-sag cycle, unreliable sag-source can be obtained. As a result, the cycle selection is very important and has to be chosen carefully in order to achieve the reliable sag-source detection for the IZ method.

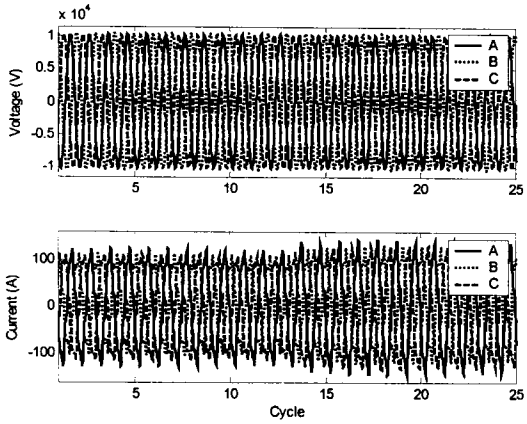

(a) Voltage and current waveforms

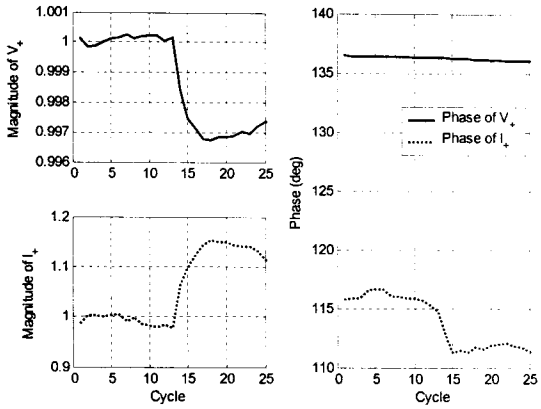

(b) Magnitudes and phases of V_+ and I_+

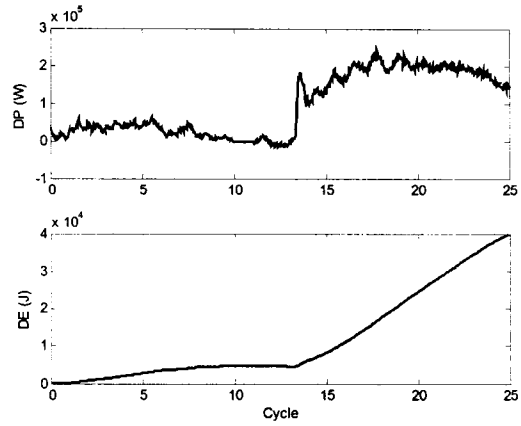

(c) DP-DE method

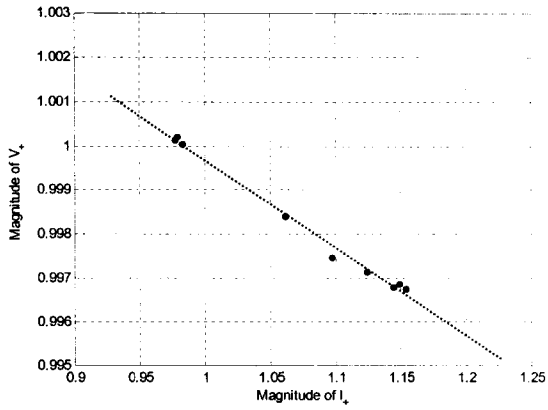

(d) VCC method

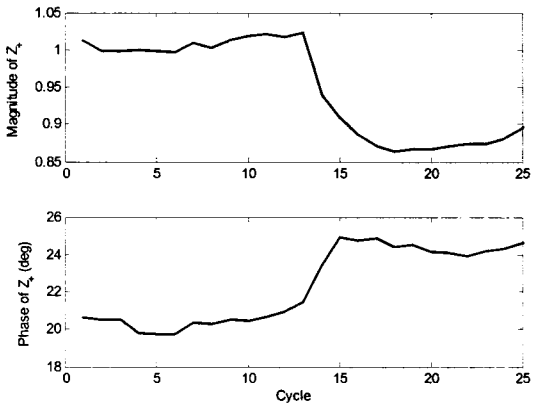

(e) ZMP method

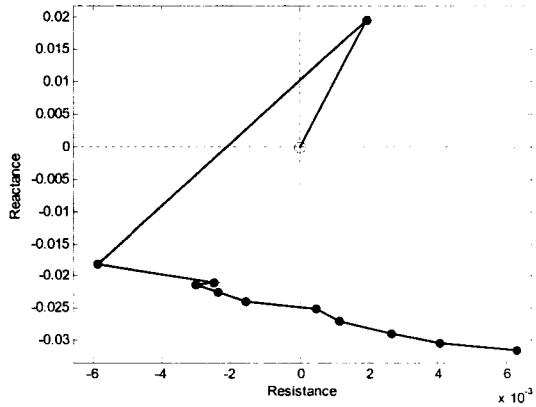

(f) IZ method

Figure 4.1: Results from published sag-source methods

4.3 Result Comparison

This section compares results of sag-source detection from the same case studies in Chapter 3. Sag sources were known beforehand so the correct sag-source detection can be verified. Table 4.2 summarizes sag-source results of the case studies.

Table 4.2: Comparison of sag-source interpretations of case studies

Case	VCC method	DP-DE method	ZMP method	IZ method
Fault				
3PSim-US	✓	✓	✓?	✓?
3PSim-DS	✓	IP(DP) ✘, DE ✓	✓	✓
1PSim-US	✓	✓	✓?	✓?
1PSim-DS	✓	✓	✓	✓
Rload-US	✓	✓	✓	✓
Rload-DS	✓	IP(DP) ✘, DE ✓	✓	✓?
VFDload-US	✘	✓	✓?	✓?
VFDload-DS	✓	IP(DP) ✘, DE ✓	✓	✓?
IMload-US	✘	✓	✓?	✓?
IMload-DS	✓	IP(DP) ✘, DE ✓	✓	✓?
Load-Fluc 1	✓	✓	✓	✓
Load-Fluc 2	✓	✓	✓	✓?
Fault 1	✓	✓	✓	✓?
Fault 2	✓	✓	✓	✓
Fault 3	✓	✓	✓	✓?
Fault 4	✓	✓	✓?	✓
Transformer (Xfmr) Energization				
XfmrSim-US	✓	✓	✓?	✓?
XfmrSim-DS	✓	IP(DP) ✘, DE ✓	✓	✓?
XfmrExp-US	✓	✓	✓?	✓?
XfmrExp-DS	✓	✓	✓	✓?
Xfmr-Field 1	✓	✓	✓	✓
Induction-Motor (IM) Starting				
IMSim-US	✓	✓	✓?	✓?
IMSim-DS	✓	✓	✓	✓
IMExp-US	✓	✓	✓	✓
IMExp-DS	✓	✓	✓	✓

where

Sim and Exp	simulation and experimental data,
✓	correct sag-source interpretation,
✘	wrong sag-source interpretation,
✓?	correct sag-source interpretation if proper judgement on the cycle selection is applied.

Table 4.2 shows that sag-source results from the four published methods can be summarized as follows. For the VCC method, the method can generally provide correct sag sources except US sources when constant power loads (VFDs and IMs) exist. The reason that the VCC method fails is that the behavior of constant power loads does not follow the voltage and current relationship observed by the method for US sags. This is the main limitation of the VCC method.

For the DP-DE method, sag sources detected from DE are all correct. However, there are a few DS cases where the initial peak of DP could not give the correct sag source. This disagreement reduces the confidence level in the sag-source interpretation of this method.

For the ZMP method, most US cases need proper judgement for the during-sag cycle selection. The difficulty occurs for the impedance magnitude criterion more often than the impedance phase angle criterion.

The IZ method also shows a good performance if proper during-sag cycle selection is chosen. It can be observed that if the during-sag cycle is selected such that it is too close or too far from the sag cycle, the results are unreliable as shown in Figure 4.1 (f).

4.4 Summary

In this chapter, a comparison of sag-source-detection methods was presented. Three major voltage sag sources—faults, transformer energization, and induction motor starting—were investigated. Case studies obtained from computer simulations, experimental tests, and field measurements were used for the comparison.

It is found that the method based on the voltage and current changes can give inaccurate upstream sag sources when constant power loads exist. For the method based on the disturbance power and energy, the disturbance energy is more reliable than the initial peak of disturbance power. For two methods based on the protection concept (ZMP and IZ methods), special attention is needed for the during-sag cycle selection. Unreliable results can be obtained if the during-sag cycle is selected too close or too far from the sag-cycle. As a result, the cycle selection is very important in order to obtain reliable sag-source interpretations for protection-based methods.

The next chapter will discuss the method to detect a voltage-flicker source. Voltage flicker is another type of important power quality disturbance. It has similar characteristics to voltage sag. The method is an extension of the system identification-based method presented in Chapter 3.

CHAPTER 5

Methods for Flicker-Source Detection

Chapter 3 presented a system identification-based method for sag-source detection that relies on fundamental-frequency positive-sequence resistance signs. Voltage sag is not the only power quality disturbance in the power system. Flicker is another common power quality disturbance and it is gaining attention due to an increase of flicker sources in the power system such as variable frequency drives. This chapter extends the system identification-based method in Chapter 3 to the problem of flicker-source detection. Flicker disturbances and their causes are described first. Flicker-source-detection methods are then proposed. The methods are verified using case studies. Guidelines for using the combined method are also developed.

5.1 Flicker Disturbances and Their Causes

Voltage fluctuations can be produced by various sources in the power system. If the fluctuation is sufficiently large and the fluctuation frequency falls within a range that is perceptible to the human eye, i.e. 0.5 Hz to 30 Hz, light flicker will occur. IEC 61000-4-30 [5] defines flicker as "the impression of unsteadiness of visual sensation induced by a light stimulus whose luminance or spectral distribution fluctuates with time". The IEEE Standard Dictionary of Electrical and Electronic Terms [34] defines flicker as "the impression of fluctuating brightness or color, occurring when the

frequency of observed variation lies between a few hertz and the fusion frequency of images". The fusion frequency is the frequency of intermittent stimulation of the eye at which flicker disappears. Because light flicker is so much related to supply-voltage fluctuation, voltage fluctuation is usually termed voltage flicker or flicker [35, 36]. In this chapter, the term flicker will be used.

In [36], flicker is classified into cyclic flicker and noncyclic flicker. Cyclic flicker is a result of periodic voltage fluctuations. Principal sources of cyclic flicker are arc furnaces, welders, variable frequency drives (VFDs), and cycloconverters. Noncyclic flicker corresponds to occasional voltage fluctuations such as that caused by the starting of a large motor. Cyclic flicker is a concern because it can result in more serious flicker-related problems than noncyclic flicker which does not happen very often. This chapter only considers cyclic flicker sources and categorizes them into two groups: fluctuating and interharmonic-producing loads.

Fluctuating loads include arc furnaces, welders, and motors. Arc furnaces are the most well-known flicker source [37-39]. An arc furnace operates by creating arcs between electrodes and the metal scrape. This is essentially a short-circuit of the power supply through an arc resistance. It can lead to voltage sag in the supply system. Since the arcing level varies randomly, the voltage sags caused by an arc furnace fluctuate randomly, which manifest as voltage flicker. The flicker caused by arc furnaces has been well documented [37-41].

Major interharmonic-producing loads are power electronic-based devices and static-frequency converters such as VFDs and cycloconverters. Flicker-generation characteristics from interharmonic-producing loads are rather different from the fluctuating loads because voltage fluctuation is caused by interharmonics[1]. The

---

[1] IEC 61000-4-30 [5] defines an interharmonic as "any frequency which is not an integer multiple of the fundamental frequency".

flicker caused by interharmonic-producing loads can be understood with the help of Figure 5.1. This figure shows a waveform that has a 175-Hz interharmonic superimposed on a fundamental-frequency component (60-Hz). It can be seen that the waveform envelope has a noticeable fluctuation. This fluctuation is a form of flicker.

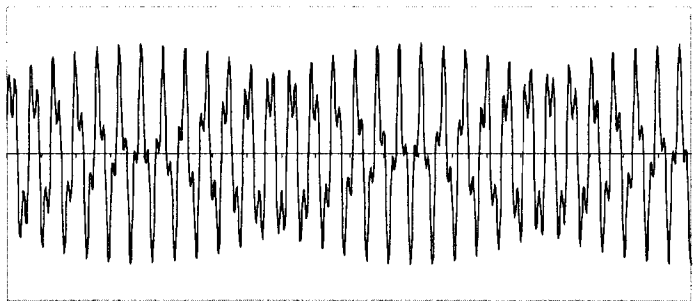

Figure 5.1: Waveform with a 175-Hz interharmonic and 60-Hz component

Interharmonic generation from interharmonic-producing loads can be explained as follows (more information on interharmonics will be provided in the next chapter). A current-source inverter VFD is used as an example here. A VFD converts a 60-Hz input into an output with a different frequency as shown in Figure 5.2.

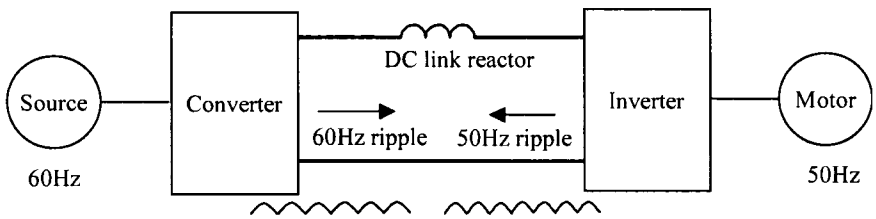

Figure 5.2: Generation of interharmonics from a VFD

If the motor is running at 50 Hz, this frequency will be seen at the DC link as 50-Hz ripples. As a result, the current of the DC link actually contains both 60-Hz ripples (due to supply voltage) and 50-Hz ripples (due to motor voltage). Since the supply-side current is related to the DC link current through the converter, the 50-Hz ripples will penetrate into the supply side and present themselves as interharmonics. This is because 50 Hz is not an integer multiple of 60 Hz. Figure 5.3 shows the voltage waveform from a VFD load. Fluctuating voltage magnitude can be clearly

seen in the enlarged section. As a result, devices that produce interharmonics have been considered as major sources of flicker [42].

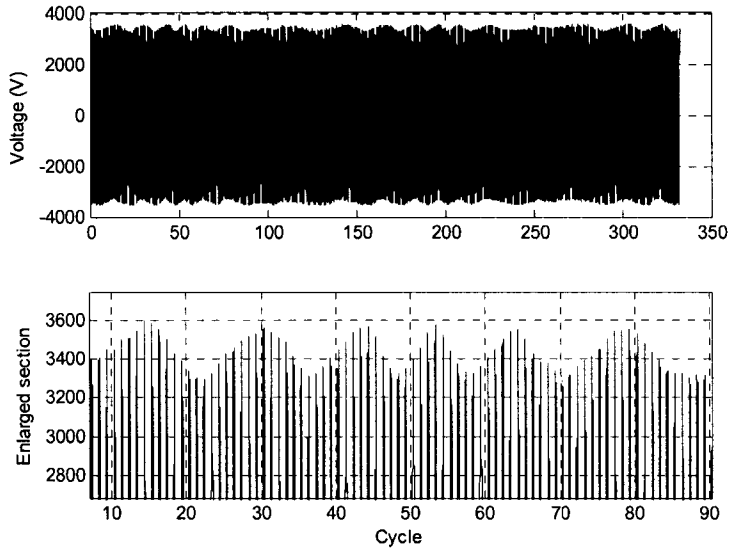

Figure 5.3: Voltage waveform of a VFD

5.2 System Identification–Based Method

Chapter 3 demonstrated that when changes of fundamental-frequency positive-sequence voltage and current are sufficient, the system identification-based method can be used to localize the sag source. This method does not limit the number of sags it can handle. If we view flickers as repetitive sags and assume that there is only one flicker source in the system, the system identification-based method can be applied to detect the flicker source. The method can be implemented as follows.

Step 1: Perform Fourier transform and symmetrical components transformation to extract the fundamental-frequency positive-sequence components from the available voltage and current waveforms.

Step 2: Separate real and imaginary parts of voltage and current in Step 1 and calculate equivalent resistances based on real and imaginary parts

Step 3: Localize the disturbance source from equivalent resistance signs as follows. If resistance signs are negative, the sag source is downstream; if resistance signs are positive, the sag source is upstream. No conclusion can be drawn when resistance signs do not agree.

It is recommended to record the flicker data with an adequately long period, i.e. over many cycles, so that the fluctuation of the waveform magnitude can be seen and analyzed. The following case studies are given to show the validity of the proposed flicker-source detection method.

5.2.1 Case Study 1: Fluctuating Load

An experiment was setup in the laboratory to represent the load fluctuation (Figure 5.4). An induction motor coupling with a DC generator has a rating of 7.5 HP. The voltage fluctuation was created by switching resistance load R_{Load} (32.5 ohms) on and off continuously. Point M is the measurement point which collects the downstream flicker data for this test. Figure 5.5a shows voltage and current waveforms and Figure 5.5b plots fundamental-frequency root-mean-square (RMS) magnitudes recorded at M.

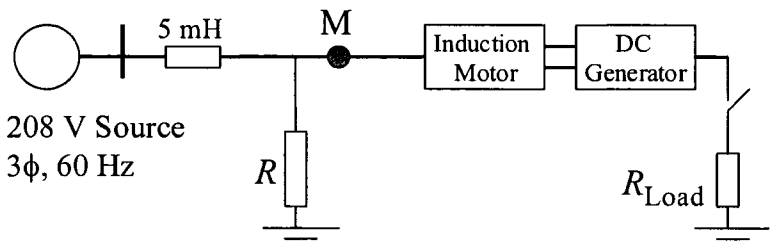

Figure 5.4: Test circuit for flicker from a fluctuating load

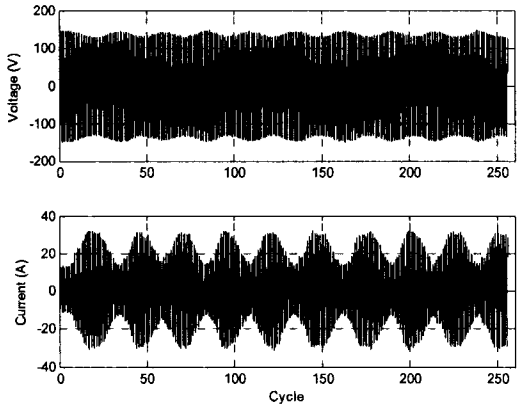

(a) Voltage and current waveforms

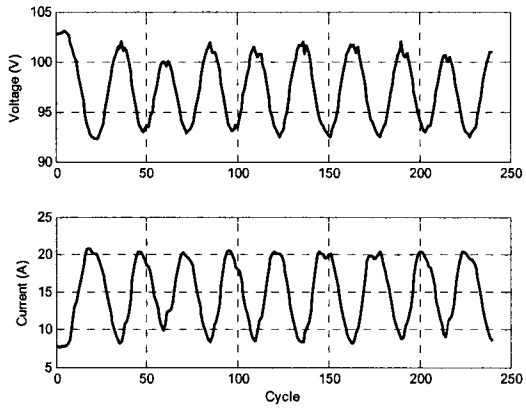

(b) Fundamental-frequency RMS magnitudes

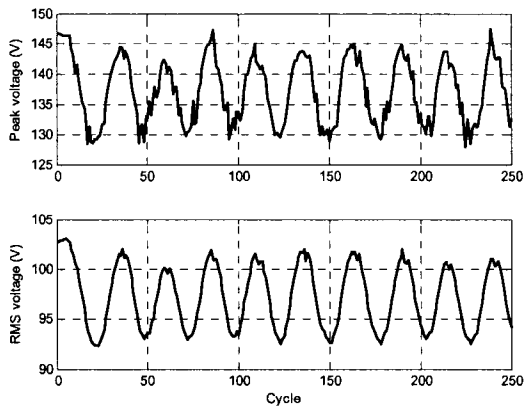

(c) Peak and RMS voltage magnitudes

Figure 5.5: Voltage and current waveforms, fundamental-frequency RMS magnitudes, and peak and RMS voltage magnitudes of a fluctuating load

Fluctuations in both voltage and current waveforms and fundamental-frequency RMS magnitudes can be clearly seen. This fluctuation is the main cause for flicker generation so a parameter related to the voltage fluctuation is required to assess the flicker level. The most recognized parameter for the flicker assessment is the relative voltage fluctuation or $\Delta V/V$. This parameter represents the change in the voltage magnitude divided by the average fundamental-frequency voltage. If this parameter is sufficiently large and the fluctuation frequency is between 0.5 Hz to 30 Hz, flicker will occur. The definition of relative voltage fluctuation according to [43] is given as follows:

$$\frac{\Delta V}{V} = \frac{(V_{\max} - V_{\min})/2}{V_1} \times 100\% \tag{5.1}$$

where

V_{max} the maximum peak or RMS voltage magnitude,

V_{min} the minimum peak or RMS voltage magnitude,

V_1 the average peak or RMS fundamental-frequency voltage magnitude.

The RMS and peak values are based on the following equations:

$$V_{RMS} = \sqrt{\frac{1}{N}\sum_{i=1}^{N} v_i^2} \qquad \text{and} \qquad V_{peak} = \max(v_i) \tag{5.2}$$

where

N the total number of samples in one cycle,

v_i the i^{th} sample of the voltage waveform, $1 \le i \le N$.

Figure 5.5c plots peak and RMS voltage magnitudes of a fluctuating load using equation (5.2). The fluctuation in both peak and RMS voltage magnitudes can be clearly noticed. From equation (5.1), peak and RMS relative voltage fluctuations are approximately 7.1% and 5.5%, respectively. These high relative voltage fluctuations represent significant changes in fundamental-frequency components. Therefore, the system identification-based method can be applied for the flicker-source detection. Equivalent resistances are estimated to be –0.04 and –0.28. Since both equivalent resistance signs are negative, the flicker source can be interpreted as in the downstream direction which agrees with the known flicker source.

5.2.2 Case Study 2: Interharmonic-producing Load

The second case study investigates the flicker source from interharmonic-producing loads. Figure 5.6 shows a diagram of a 25-kV distribution feeder typically seen in rural North America. The feeder length from the substation to the site is about 30 miles and the total feeder load is approximately 10 MVA. The feeder is equipped with a series capacitor and a voltage regulator. Customers A and B are the largest loads supplied by the feeder. Both use VFDs to pump gas pipelines. Customer A's VFD uses old current-source inverter technology, while Customer B uses the newer Pulse-Width-Modulation inverter technology to power its motor. Since the installation of Customer A load a few years ago, light flicker problems have been reported at various locations in the system, including the Customer A site, the town center, and Customer C (a small rural processing facility). In addition to light flicker, motor power pulsation and frequent replacement of light bulbs have been reported by the facility.

Figure 5.7a shows recorded voltage and current waveforms. The flicker source is analyzed by the system identification-based method the same way as it is analyzed in the fluctuating load. Equivalent resistances are estimated to be –0.04 and +0.03. Since resistance signs are not consistent, the flicker source could not be localized reliably. The cause of this incorrect flicker source is found as follows: the system

identification-based method uses fundamental-frequency voltage and current changes to estimate the fundamental-frequency resistance of the non-disturbance side. The interharmonic-caused flicker does not involve changes of fundamental-frequency components. As a result, it is not possible to estimate the resistance accurately. This can be justified from Figure 5.7b where the fundamental-frequency RMS changes are rather small. Peak and RMS relative voltage fluctuations from Figure 5.7c are approximately 4.5% and 0.6%, respectively. These relative voltage fluctuations are lower than the fluctuating load.

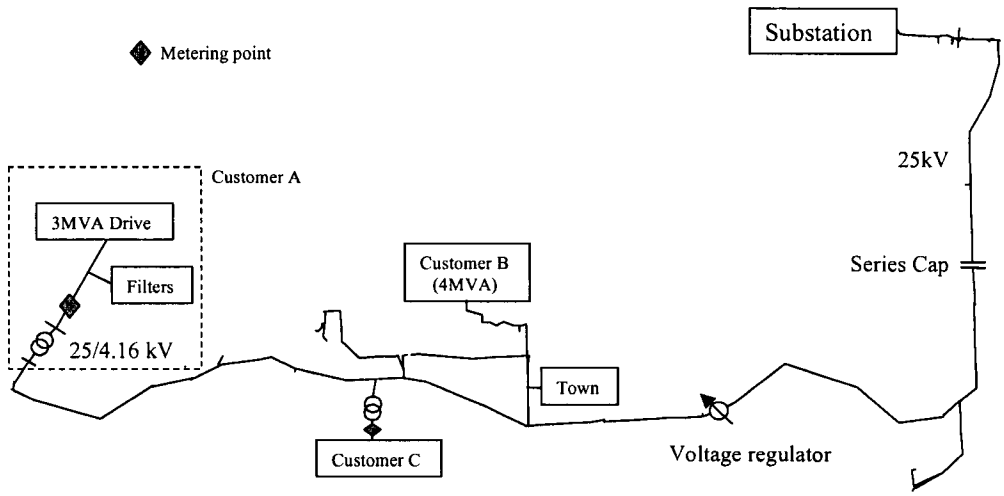

Figure 5.6: A 25-kV rural distribution system

The VFD results show that the system identification-based method has limitations for flicker-source detection. The main reason is that it relies on the changes of fundamental-frequency components, while interharmonic-caused flicker does not involve fundamental-frequency component changes. As a result, an alternative method is needed to detect sources of flicker caused by interharmonics.

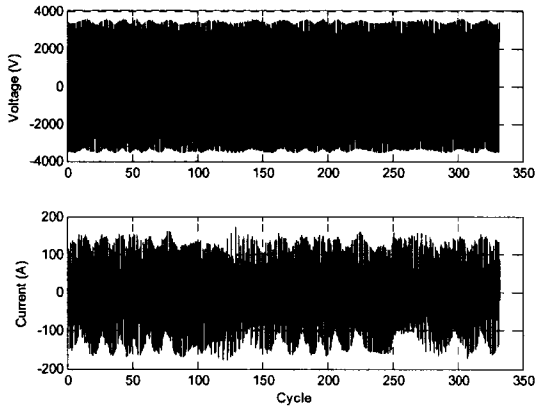

(a) Voltage and Current waveforms

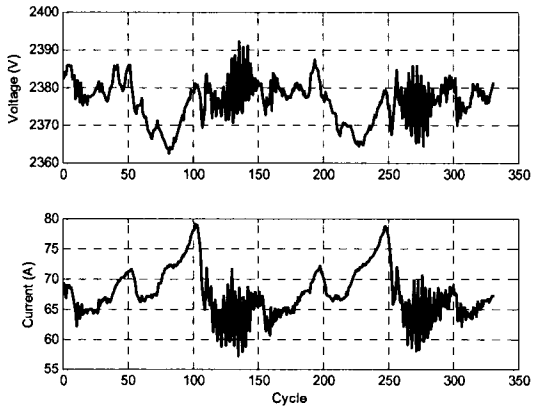

(b) Fundamental-frequency RMS magnitudes

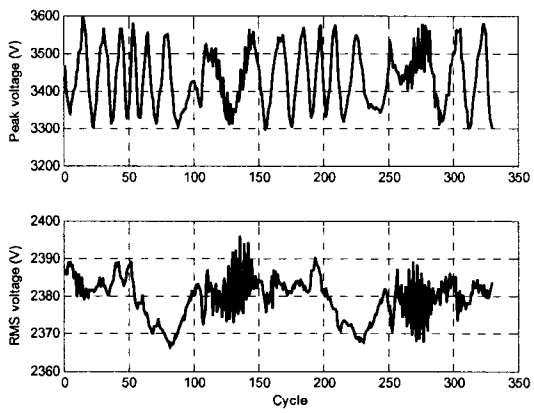

(c) Peak and RMS voltage magnitudes

Figure 5.7: Voltage and current waveforms, fundamental-frequency RMS magnitudes, and peak and RMS voltage magnitudes of a VFD load

5.3 Power Direction–Based Method

It is described in Section 5.1 that a VFD causes flicker by injecting interharmonics into the system. Therefore, the characteristics of the interharmonics should be explored to develop an alternative method for flicker-source detection. Since it is rare for a system to contain multiple interharmonic sources at the same frequency, the interharmonic source should be located on the side where the interharmonic power is generated. Thus, the main concept of the proposed method is to check the direction of interharmonic active powers. The method can be verified using the same VFD case study in Section 5.2.2. The frequency spectra (using 60-cycle window for DFT) of the recorded voltage and current (as the percentage of the fundamental-frequency RMS values) are shown in Figure 5.8. It can be seen that there are two dominant interharmonics at 117 Hz and 237 Hz. It is these interharmonics that cause the voltage fluctuation. The 60-Hz, 117-Hz and 237-Hz active powers are plotted together in Figure 5.9. It can be seen that the interharmonic active powers have the opposite signs to the 60-Hz active power (P_1). Since the 60-Hz active power flows from the supply system to Customer A, the interharmonics must come from Customer A. In other words, Customer A is the flicker source.

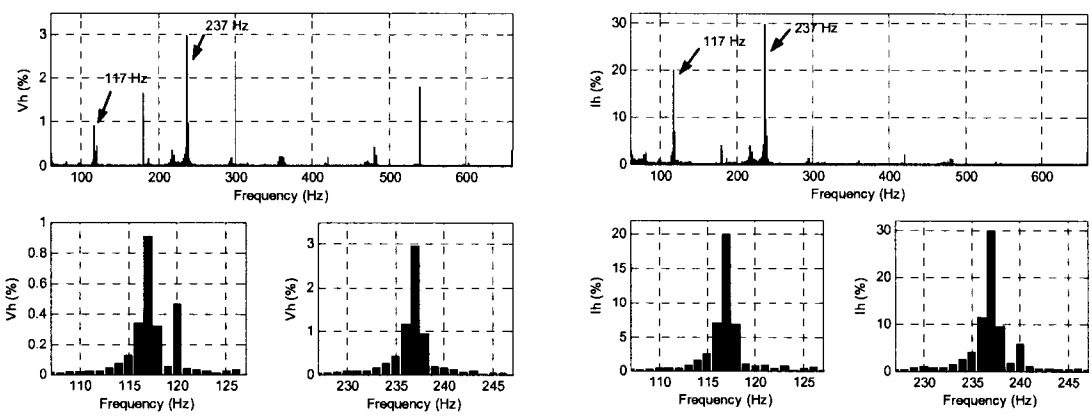

(a) Voltage spectra (b) Current spectra

Figure 5.8: Voltage and current spectra of a VFD load

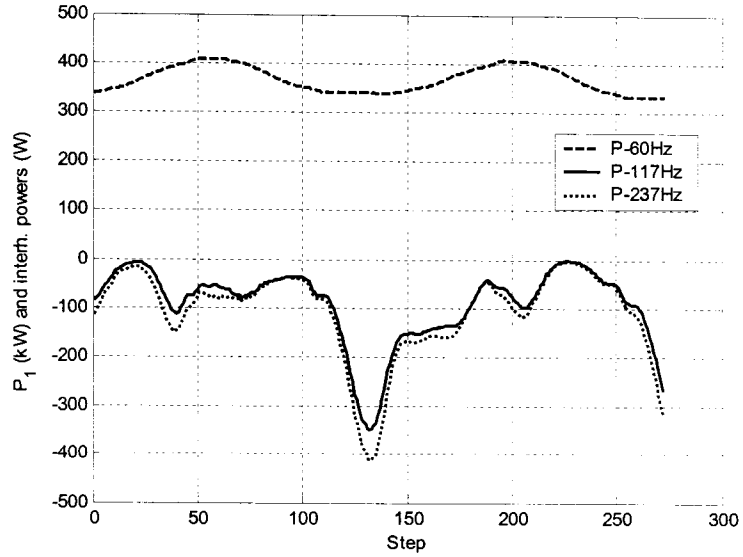

Figure 5.9: Active powers of 60-Hz and interharmonic components

The validity of the above conclusion can be further verified by correlating the interharmonic frequencies with the drive frequency as shown in Figure 5.10. Each dot in this figure represents one operating point of the drive. The symbols f1 and f2 represent the low and high interharmonic frequencies, respectively. It can be seen that there is an almost perfect correlation between the two frequencies. An increase of drive frequency leads to linear increase of interharmonic frequencies. The results confirm that the VFD at Customer A is the source of the interharmonics.

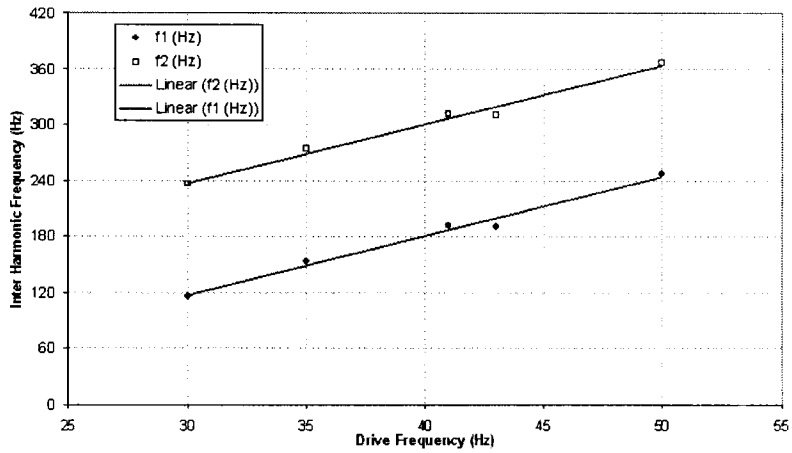

Figure 5.10: Correlation between interharmonic and drive operating frequencies

5.4 Combined Method for Flicker-Source Detection

Case study results have shown that two schemes are required to develop a general-purpose flicker-source detection method. If a flicker is caused by the fluctuation of the fundamental-frequency components, the system identification-based method should be used; if a flicker is caused by interharmonics, the power direction-based method should be used. The challenge thus becomes the development of a method that combines both methods for general-purpose flicker-source detection.

The combined method needs to determine which method to use. The selection criterion proposed by this thesis is based on the following observations:

1) If there are large fundamental-frequency voltage fluctuations, the flicker could be caused by fundamental-frequency components. It has been shown previously that the peak and RMS relative voltage fluctuations for the flicker caused by the fundamental-frequency components are larger than the flicker caused by interharmonics. Apart from the relative voltage fluctuation, the relationship between peak and RMS voltage magnitudes and fundamental-frequency voltage magnitude can also be checked if flicker is caused by fundamental-frequency components. Figure 5.11 correlates the peak voltage magnitude with the fundamental-frequency voltage magnitude for fluctuating and VFD loads. The fitting lines are plotted such that they minimize the sum of squares of the deviation using the principle of least squares. It can be seen that there is a strong linear correlation for the fluctuation load (5.11a), but not for the VFD load (5.11b). This strong correlation is caused by the fluctuations of fundamental-frequency components. The strength of the correlation can be assessed by the correlation coefficient (r) as follows [44]:

$$r = \frac{n\sum_{i=1}^{n} V_1(i)V_p(i) - \sum_{i=1}^{n} V_1(i)\sum_{i=1}^{n} V_p(i)}{\sqrt{\left[n\sum_{i=1}^{n} V_1^2(i) - \left(\sum_{i=1}^{n} V_1(i)\right)^2\right]\left[n\sum_{i=1}^{n} V_p^2(i) - \left(\sum_{i=1}^{n} V_p(i)\right)^2\right]}} \quad (5.3)$$

where V_1 and V_p are fundamental-frequency and peak voltage magnitudes of the n-cycle flicker data. The strongest linear correlation happens when the correlation coefficient equals one, while the weakest linear correlation occurs when the correlation coefficient is zero. According to equation (5.3), correlation coefficients between peak and fundamental-frequency voltage magnitudes for fluctuating and VFD loads are 0.97 and 0.03, respectively. Figure 5.12 shows the correlation between RMS and fundamental-frequency voltage magnitudes for both case studies. It can be seen that both case studies show strong correlation with the correlation coefficients of 0.999 and 0.995 for fluctuating and VFD loads, respectively.

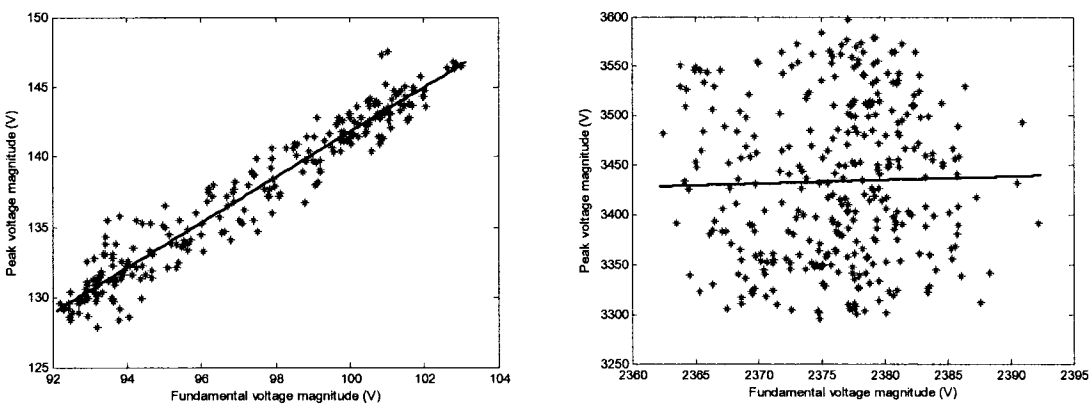

(a) Fluctuating load (b) VFD load

Figure 5.11: Plots between peak and fundamental-frequency voltage magnitudes

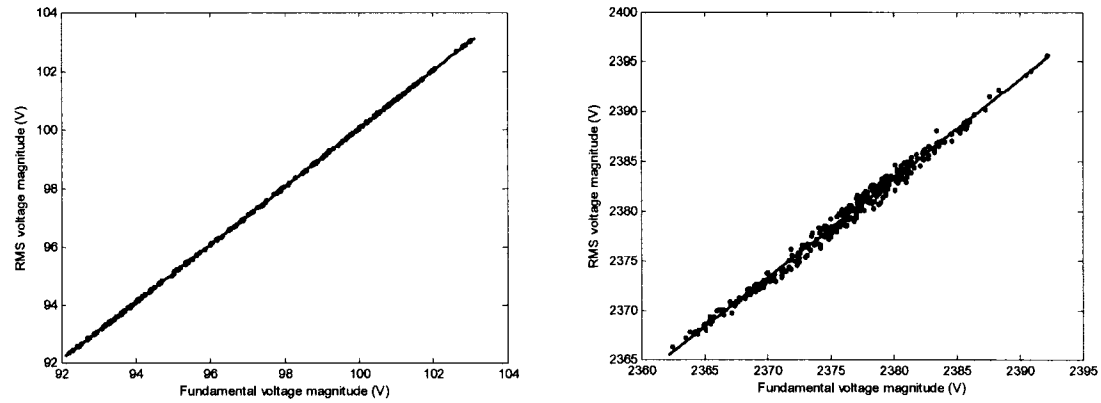

(a) Fluctuating load (b) VFD load

Figure 5.12: Plots between RMS and fundamental-frequency voltage magnitudes

Based on results from case studies, the criteria to judge if the flicker is caused by the fundamental-frequency components are proposed as follows: 1) Both peak and RMS relative voltage fluctuations are higher than 2.5% and 2) Correlation coefficient between peak and fundamental-frequency voltage magnitudes is higher than 0.9. Checking the correlation coefficient between peak and fundamental-frequency voltage magnitudes is sufficient because interharmonics are generally small in magnitude. This results in very high correlation coefficients (over 0.99) between RMS and fundamental-frequency voltage magnitudes for both flickers caused by fundamental-frequency components and interharmonics as shown in Figure 5.12.

2) The waveform spectra can be checked to determine if there are significant interharmonic components whose frequencies are greater than 100 Hz. Note that flicker caused by fundamental-frequency components will not have interharmonic components with frequencies greater than 100 Hz. The trend of the interharmonic frequency should also be monitored. Figure 5.13 shows the voltage spectra (using 60-cycle window for DFT) of fluctuating and VFD loads. It can be observed that some interharmonic components above 100 Hz, e.g. 117

Hz and 237 Hz, are significant for a VFD load, while there are no significant interharmonic components for a fluctuating load.

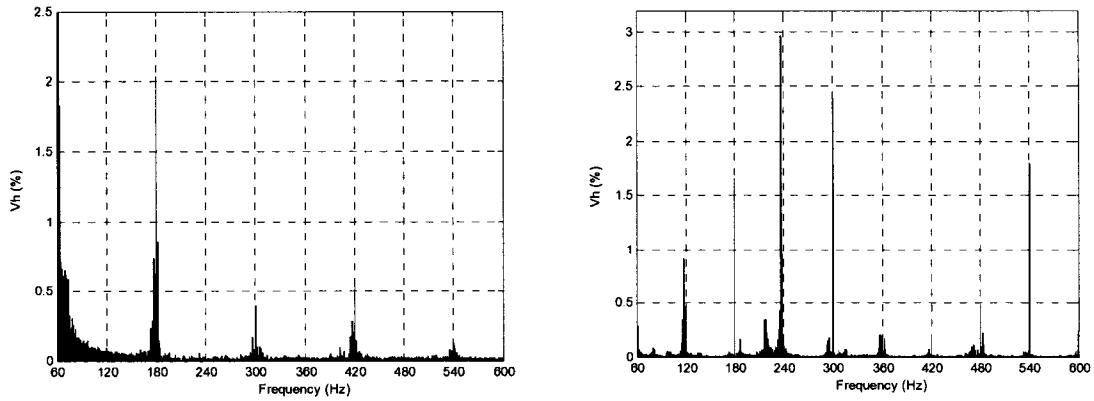

(a) Fluctuating load (b) VFD load

Figure 5.13: Voltage spectra comparison between fluctuating and VFD loads

3) Magnitude trends of existing interharmonic voltage and current should have the similar pattern. This is because the interharmonic-producing loads generate interharmonic currents which in turn cause interharmonic voltages drop across the supply impedance. Thus, magnitudes of interharmonic voltage and current should be correlated or have similar magnitude trends. Figure 5.14a illustrates magnitude trends of existing interharmonic voltages (sold line with left y-axis) and currents (dashed line with right y-axis) at 117 Hz and 237 Hz of the VFD case study. Interharmonic current magnitudes shown are multiplied by factors in order to make both interharmonic voltage and current magnitudes comparable. An alternative method to check the interharmonic authenticity is to plot interharmonic voltage magnitudes against interharmonic current magnitudes as shown in Figure 5.14b. It can be easily seen that they are strongly correlated.

Based on aforementioned discussions and observations, the following general-purpose flicker-source detection method is proposed. Figure 5.15 is a flowchart for the combined method.

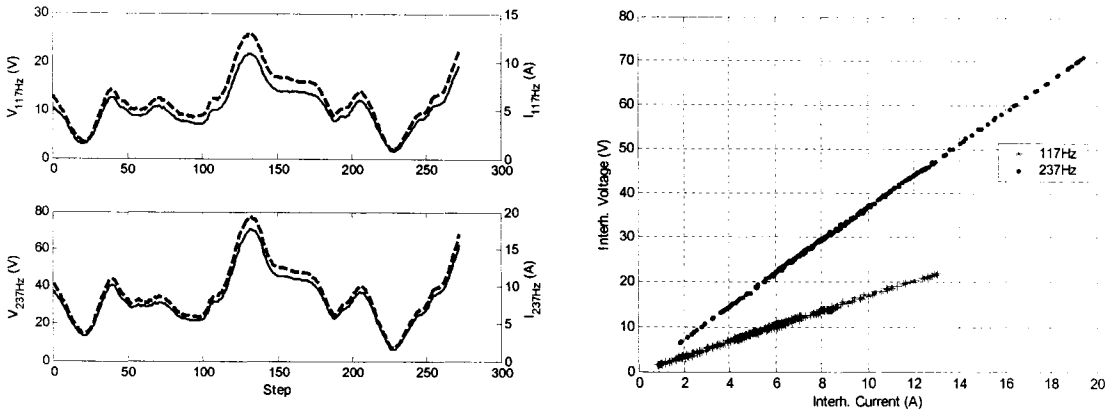

(a) Magnitude trends (b) Correlation plots

Figure 5.14: Magnitude trends and correlation plots of interharmonic voltages and currents at 117 Hz and 237 Hz of a VFD case study

Step 1: Check the impact of fundamental-frequency components on the flicker level. If the following criteria are satisfied, then the flicker is caused by the fundamental-frequency fluctuations: 1) Both peak and RMS relative voltage fluctuations are higher than 2.5% and 2) Correlation coefficient between peak and fundamental-frequency voltage magnitudes is greater than 0.9. If it is judged that the flicker is caused by the fundamental-frequency components, then the system identification-based method can be used to determine the flicker source reliably.

Step 2: If the fundamental-frequency components are judged not to be the cause of flicker, then the flicker source could be determined by the power direction-based method. Perform Fourier analysis on the flicker waveforms using 60-cycle window and one-cycle sliding window. Check interharmonic-frequency components (above 100 Hz[2]) from the spectra. Note the two largest components as the two dominant interharmonics.

[2] Interharmonics above 100 Hz will not cause changes in fundamental-frequency components.

Step 3: Calculate active powers of the dominant interharmonics obtained in Step 2 as a function of window position. The flicker source can be determined from the sign of the interharmonic active power.

Step 4: Verify the authenticity of dominant interharmonics in Step 3 by plotting interharmonic voltage and current magnitudes together as a function of window position. If both magnitude trends are similar, the flicker-source conclusion from Step 3 is correct, otherwise no conclusion can be drawn.

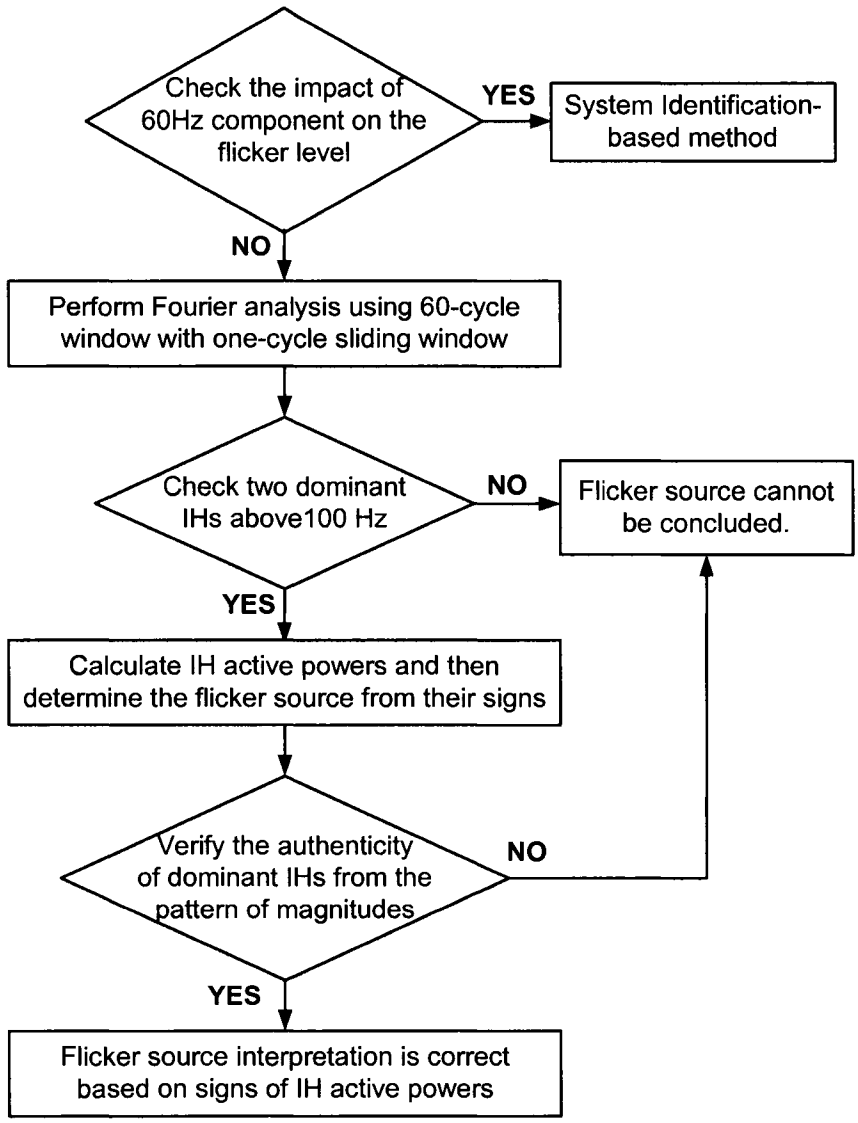

Figure 5.15: A diagram of guidelines for using the combined method

5.5 Summary

This chapter extended the system identification-based method in Chapter 3 to the problem of flicker-source detection. General information of flicker disturbances and their causes were provided. Two flicker-source detection methods were proposed based on unique characteristics of flicker-producing loads. Case studies were used to verify proposed methods. Guidelines for the combined method were also developed.

The flicker caused by the fundamental-frequency components can be judged by the values of both peak and RMS relative voltage fluctuations and the correlation coefficient between peak and fundamental-frequency voltage magnitudes. The thresholds for judgement criteria have been proposed based on results from case studies. If it is found that the flicker is caused by the fundamental-frequency components, then the system identification-based method can be applied to detect the flicker source reliably. The flicker source can be determined based on the fundamental-frequency positive-sequence resistance signs in the similar way as sag-source detection in Chapter 3. If the flicker is not caused by the fundamental-frequency components, the flicker could be caused by interharmonics. The flicker source could be determined using the power direction-based method because interharmonic-caused flicker does not involve changes of fundamental-frequency components. The flicker source can then be determined from active power signs of dominant interharmonics. Dominant interharmonics are significant interharmonic components above 100 Hz which can be easily found from the waveform spectra. It is proposed to verify the authenticity of interharmonics by checking the trend of interharmonic voltage and current magnitudes. Results from case studies have shown that both methods work reasonably well.

The next chapter will discuss another issue related to flicker and interharmonics. The main work is a systematic approach to derive limits for interharmonic magnitudes from published flicker limits. Results will be useful to assess the flicker impact from interharmonic-producing sources.

CHAPTER 6

Interharmonic–Flicker Curves[1]

The relationship between flickers and interharmonics is briefly mentioned in Chapter 5. In this chapter, the inherent relationship between flickers and interharmonics is further analyzed. The root-mean-square and peak voltage fluctuations caused by a single interharmonic are investigated. A limit for interharmonics by utilizing the published limits on voltage flicker is proposed. The limit is represented as an interharmonic-magnitude versus interharmonic-frequency curve and is called an interharmonic-flicker curve. A systematic method to derive limits for interharmonics from the flicker limits is presented. Potential applications and discussions are also provided.

6.1 Introduction

Interharmonics are spectra components whose frequencies are not integral multiples of the supply fundamental frequency. When a voltage waveform contains interharmonics, the root-mean-square (RMS) and peak magnitudes of the waveform

---

[1] The work in this chapter has been published: T. Tayjasanant, W. Wang, C. Li, and W. Xu, "Interharmonic-Flicker Curves," *IEEE Trans. Power Delivery*, Vol. 20, No. 2, April 2005, pp. 1017-1024.

will fluctuate. This is because the periods of the interharmonic components are not synchronous with the fundamental-frequency cycle. This fluctuating magnitude is essentially a form of voltage flicker. If the fluctuating magnitude is sufficiently large and the fluctuation frequency is in a range perceptible to the human eye, a light flicker will occur.

The relationship between voltage flicker and voltage interharmonics has become an active research area in recent years due to concerns of power quality. Reference [42] calculated a curve that relates the magnitude of voltage fluctuation to the magnitude of interharmonics. The characteristics of interharmonic–caused light flicker were investigated in [45] using the IEC flickermeter algorithm. The experimental study results of the light flicker in incandescent and fluorescent lamps caused by interharmonics were given in [46] and [47].

This chapter presents a further advancement in this area. It proposes a limit on the interharmonics based on voltage flicker standards. This work is motivated by the voltage flicker problems encountered by the variable frequency drive (VFD) manufacturers and users. Certain VFDs inject interharmonics into the supply system. The interharmonics, in turn, cause voltage flicker. It has become necessary to find what is the permissible level of interharmonics that a VFD can generate. Such information will be very useful for designing and evaluating mitigation measures to reduce the flicker impact of VFDs. The limit for interharmonics is presented as a magnitude versus frequency curve, much like the classical IEEE voltage flicker curve [48]. Since the limit is derived with the goal of reducing the flicker impact of interharmonics, the curve is called "Interharmonic–Flicker Curve".

It is worthwhile to point out that the concept of using a curve to limit interharmonics is introduced in [49] on the basis of the IEC flickermeter limits [50]. This chapter presents a systematic research on the subject and demonstrates that the IEC flickermeter needs improvement when dealing with interharmonic-caused flickers.

6.2 Interharmonics and Flicker

If an interharmonic is introduced in a voltage waveform, the magnitude of the combined waveform could fluctuate and flicker might occur consequently. Figure 6.1 shows a voltage waveform composed of a 60-Hz component and a 117-Hz component. The magnitude of the interharmonic component is 50%. It can be seen that the envelope has noticeable fluctuation.

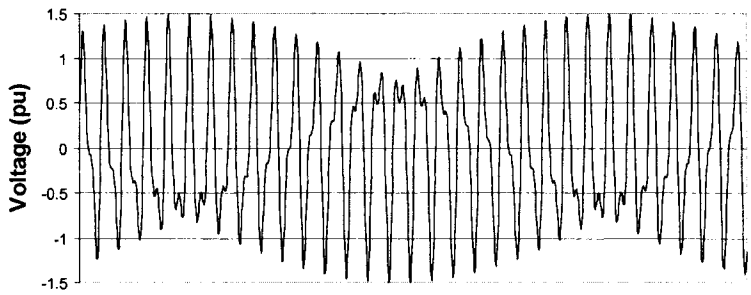

Figure 6.1: Voltage waveform containing a 117-Hz interharmonic

Flicker happens when the fluctuation is sufficiently large and the fluctuation frequency is in a range perceptible to the human eye (0.5 Hz to 30 Hz). The frequency of the fluctuation is called the modulation frequency [47] or beat frequency [49], [51] which can be determined by

$$f_{beat} = | f_{IH} - f_h | \tag{6.1}$$

where f_{IH} is the interharmonic frequency and f_h is the harmonic frequency closest to f_{IH}. For example, both interharmonic frequencies at 51 Hz and 69 Hz can cause 9-Hz modulation frequency for the 60-Hz system. The modulation frequency in the sensitive range of the flicker perception is normally called flicker frequency [43], [46].

6.3 Voltage Fluctuation Caused by A Single Interharmonic

A good starting point to analyze the relationship between flicker and interharmonics is to examine a signal containing only one interharmonic. Although this case is only an approximate representation of the actual situation, it can reveal a good deal of information for more sophisticated analysis. Consider a signal containing the fundamental-frequency component and a single interharmonic:

$$v(t) = V_1[\sin(2\pi f_1 t) + m\sin(2\pi f_{IH} t + \theta_{IH})] \tag{6.2}$$

where

V_1 the fundamental-frequency (peak) magnitude,

f_1 the fundamental frequency,

m the interharmonic relative magnitude,

f_{IH} the interharmonic frequency,

θ_{IH} the interharmonic phase angle.

The signal amplitude of equation (6.2) is modulated due to the existence of the interharmonic. The modulation can be explained as follows: let $f_{IH} = hf_1 + \Delta f_h$ where h is the harmonic order nearest to f_{IH}, then the voltage signal can be expanded as

$$\begin{aligned} v(t) = V_1 sin(2\pi f_1 t) + [V_1 m\, cos(2\pi \Delta f_h t + \theta_{IH})] sin(2\pi h f_1 t) \\ + [V_1 m\, sin(2\pi \Delta f_h t + \theta_{IH})] cos(2\pi h f_1 t) \end{aligned} \tag{6.3}$$

It can be seen that the voltage waveform contains harmonic components that have varying magnitudes of $V_1 m\, cos(2\pi \Delta f_h t + \theta_{IH})$ and $V_1 m\, sin(2\pi \Delta f_h t + \theta_{IH})$. If Δf_h equals zero, only the harmonic component exists. There will be no magnitude fluctuation in this case. However, if Δf_h does not equal zero, the interharmonic will

exist and this asynchronous component causes the magnitude to fluctuate and the fluctuation frequency is $|\Delta f_h|$. Waveforms when $V_I = 100$ V, $f_I = 60$ Hz, $m = 10$, and $\theta_{IH} = 0°$ for $f_{IH} = 57$ Hz (top) and 117 Hz (bottom) are shown in Figure 6.2. In this figure, the frequency of magnitude variation at 3 Hz is clearly seen. It is worth noting that if the interharmonic frequency is near the odd harmonics (57 Hz is near the 1st harmonic), the waveform envelope swells in both positive and negative directions. If the frequency is near the even harmonics (117 Hz is near the 2nd harmonic), the envelope changes in a sinusoidal form.

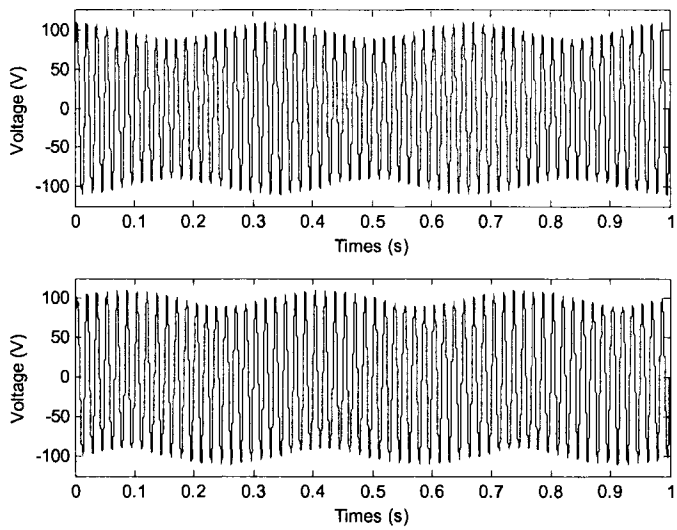

Figure 6.2: The waveforms with interharmonic frequencies at 57 Hz (top) and 117 Hz (bottom)

One can therefore conclude that when a signal contains interharmonics, both the RMS and peak values of the signal will vary. The definition of voltage fluctuation according to [43] is

$$\left.\frac{\Delta V}{V}\right|_x = \frac{(V_{x\_\max} - V_{x\_\min})/2}{V_{1\_x}} \times 100\% \tag{6.4}$$

where x represents either RMS or peak. The RMS magnitude fluctuation has an effect on incandescent lamp flicker [47], [52]. However, fluorescent lamps are more

sensitive to peak values [46], [47]. Relationships between both RMS and peak voltage fluctuations and the interharmonic magnitude are determined in the following subsections.

6.3.1 RMS Magnitude Fluctuation

The definition for RMS value is

$$V_{RMS} = \sqrt{\frac{1}{T_1}\int_0^{T_1} V_1^2\left[sin(2\pi f_1 t) + m\,sin(2\pi(f_1 + \Delta f)t + \theta_{IH})\right]^2 dt} \tag{6.5}$$

where $\Delta f = f_{IH} - f_1$ and T_1 is the period of the fundamental-frequency component. By using a trigonometric identity, equation (6.5) can be rewritten as

$$V_{RMS}^2 = \frac{1}{2}V_1^2(1+m^2) + \frac{mV_1^2}{\pi\Delta f T_1(1+\frac{\Delta f T_1}{2})}sin(\pi\Delta f T_1)cos(\pi\Delta f T_1 + \theta_{IH}) \tag{6.6}$$

The interharmonic magnitudes are typically much smaller than the fundamental-frequency component, namely $m << 1$. After neglecting the m^2 terms

$$V_{RMS}^2 = \frac{1}{2}V_1^2\left[1 + \frac{2m}{\pi\Delta f T_1(1+\frac{\Delta f T_1}{2})}sin(\pi\Delta f T_1)cos(\pi\Delta f T_1 + \theta_{IH})\right] \tag{6.7}$$

As θ_{IH} varies from 0 to 2π, the maximum and minimum RMS values can be determined as

$$V_{RMS\_max} = \frac{V_1}{\sqrt{2}}\sqrt{1+\left|\frac{2m}{(1+\frac{\Delta fT_1}{2})}\frac{sin(\pi\Delta fT_1)}{\pi\Delta fT_1}\right|}$$
$$V_{RMS\_min} = \frac{V_1}{\sqrt{2}}\sqrt{1-\left|\frac{2m}{(1+\frac{\Delta fT_1}{2})}\frac{sin(\pi\Delta fT_1)}{\pi\Delta fT_1}\right|} \quad (6.8)$$

Further considering $m << 1$ and $|(\sin x)/x| \le 1$, the RMS voltage fluctuation level can be determined as

$$\left.\frac{\Delta V}{V}\right|_{RMS} \approx \left|\frac{m}{(1+\frac{\Delta fT_1}{2})}\frac{sin(\pi\Delta fT_1)}{\pi\Delta fT_1}\right| = m\left|\frac{\sin\alpha}{\alpha\left[1+\frac{\alpha}{2\pi}\right]}\right| \quad (6.9)$$

where $\alpha = \pi\Delta fT_1$. The above equation shows that the magnitude of RMS fluctuation is proportional to the magnitude of the interharmonic. In addition, Δf plays an important role on the fluctuation level. The shape of equation (6.9) is plotted in Figure 6.3 for the case of 0.3% interharmonic magnitude (m). It can be seen that the modulation impact on the RMS fluctuation is significant if the interharmonic is close to the fundamental frequency. The RMS fluctuation gets smaller when the interharmonic frequency increases. The dotted line in Figure 6.3 shows the modulation or flicker frequency (right-axis scale) caused by the interharmonic. This flicker frequency can be calculated by using equation (6.1).

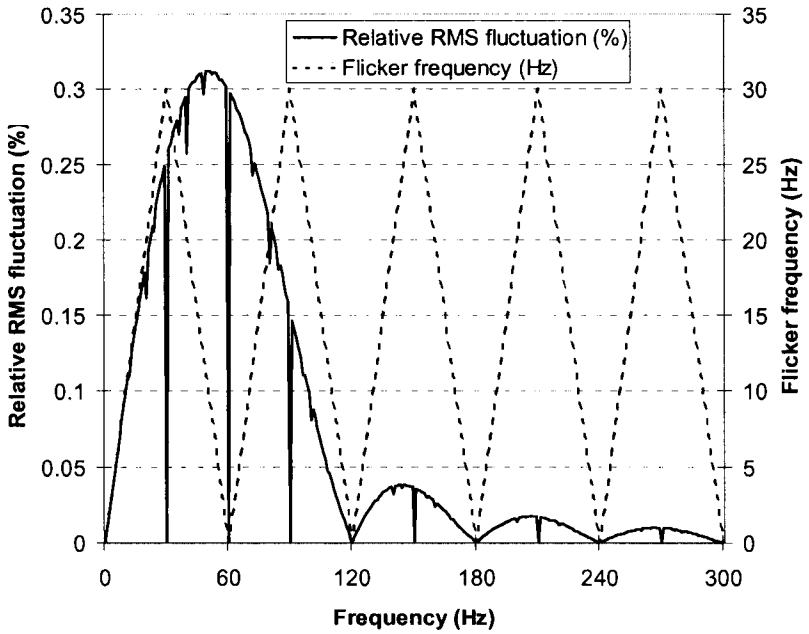

Figure 6.3: The relative RMS fluctuation with 0.3% interharmonic magnitude

6.3.2 Peak Magnitude Fluctuation

It is more complicated to determine the fluctuation level for the peak voltage. The signal of equation (6.2) has extreme values when $\frac{dv(t)}{dt} = 0$ or at $t = n/(4f_1)$, n = 1, 3, 5, ... when $m << 1$. The peak value has the following form:

$$V_{peak} = \left| V_1 \left[1 \pm m \sin\left(\frac{n\pi}{2} \frac{f_{IH}}{f_1} + \theta_{IH} \right) \right] \right| \tag{6.10}$$

Accordingly, the peak voltage will fluctuate between $V_1(1+m)$ and $V_1(1-m)$. The relative peak voltage fluctuation or $(\Delta V/V)_{peak}$ therefore equals m. It is important to note that this conclusion is independent of the frequency of the interharmonic component.

The above conclusions on RMS and peak fluctuation levels have been confirmed with numerical results. The numerical studies are performed as follows:

1) Generate a waveform defined in equation (6.2) numerically.

2) Calculate RMS and peak values based on the following equations:

$$V_{RMS} = \sqrt{\frac{1}{N}\sum_{i=1}^{N} v_i^2} \qquad \text{and} \qquad V_{peak} = \max(v_i)$$

where N is the total number of samples in one cycle and v_i is the i^{th} sample of the voltage waveform, $1 \le i \le N$.

3) Find the maximum and minimum RMS and peak values from the results.

4) Calculate the voltage fluctuation level defined in equation (6.4).

5) Repeat the above process by scanning through phase angles θ_{IH} from 0 to 2π and find the largest fluctuation.

Figure 6.4 shows the plot of the relative peak voltage fluctuation versus interharmonic frequencies ranging from 1 Hz to 300 Hz when interharmonic magnitude is 3% of the fundamental voltage. It can be seen that the peak is approximately the magnitude of the interharmonic.

A family of curves shown in Figures 6.3 and 6.4 can be obtained by varying interharmonic magnitudes. By checking this family of curves against the standard flicker curve, one can determine if an interharmonic component with given frequency and magnitude can cause perceptible flicker.

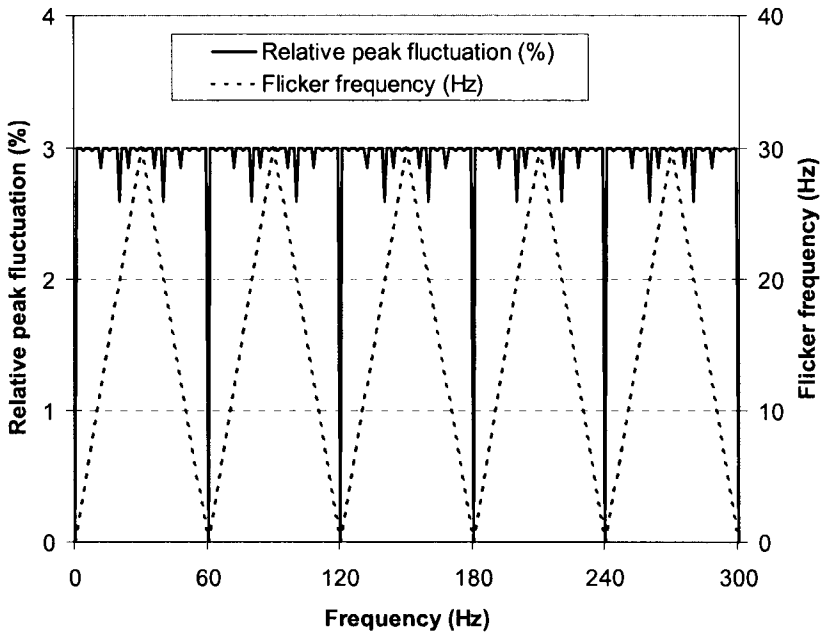

Figure 6.4: The relative peak fluctuation with 3% interharmonic magnitude

6.4 Interharmonic-Flicker Curves

Results presented in the previous section show that there is a definite relationship between voltage flicker level and interharmonic level. Since limits have been established for voltage flicker, one can derive a limit for the interharmonics by utilizing the flicker limits. Such information will be very useful for assessing the impact of interharmonics on voltage and light flickers. It also makes it easier to design mitigation measures since it is the interharmonic level that is directly affected by the measures. The problem of determining the limit for an interharmonic component can be formulated as follows.

Given fluctuation magnitude versus interharmonic magnitude and frequency relationship

$$(\Delta V / V)_x = f(m, f_{IH}) \tag{6.11}$$

flicker frequency versus interharmonic frequency relationship

$$f_{flicker} = g(f_{IH}) \tag{6.12}$$

and the maximum acceptable flicker magnitude versus flicker frequency relationship (i.e. the standard flicker curves)

$$(\Delta V / V)_x = \psi(f_{flicker}) \tag{6.13}$$

find the maximum acceptable interharmonic magnitude as a function of the interharmonic frequency

$$m = \phi(f_{IH}) \tag{6.14}$$

where $(\Delta V / V)_x$, and $f_{flicker}$ are the relative voltage fluctuation and flicker frequency, respectively. The curve characterized by equation (6.14) is called the interharmonic–flicker curve.

There are at least two sets of flicker limits published. One is the IEEE flicker curve [48]. The IEEE flicker curve shows acceptable flicker limits for incandescent lights. The curve represents values of the RMS voltage fluctuation or $(\Delta V/V)_{RMS}$ as a function of the fluctuation frequency. In recent years, the IEC flickermeter-based limits have attracted a lot of attention [43], [53]. In other words, there are two choices for equation (6.13). Both the IEEE and IEC flicker curves [49] are selected to derive the interharmonic-flicker curves. An analytical solution to the above equations is difficult to derive. The curve of equation (6.14) can be developed numerically as follows.

Step 1: Extract values of voltage fluctuation at a specific fluctuation frequency from the standard flicker curve.

Step 2: For a specific interharmonic frequency, find the corresponding flicker frequency using equation (6.1).

Step 3: At this frequency, find a critical interharmonic magnitude which causes RMS and peak magnitude fluctuations as found in Step 1. In other words, find the minimal magnitude of interharmonic to produce perceptible flicker with the frequency determined in Step 2.

Step 4: Repeat Step 2 and Step 3 to obtain the critical magnitudes for various interharmonic frequencies.

6.4.1 RMS Fluctuation-Based Interharmonic-Flicker Curve

Figure 6.5 shows the resultant interharmonic–flicker curve from 1 Hz to 240 Hz based on the RMS fluctuation and the IEEE flicker limit. For frequencies higher than 240 Hz, extremely high interharmonic magnitude is needed to produce perceptible flicker so it is excluded. Table 6.1 lists some values of the results (Appendix A provides all results from 1 Hz to 240 Hz). Note that the flicker frequency from the IEEE flicker curve stops at 20 Hz. This results in a discontinuity in the interharmonic–flicker curve.

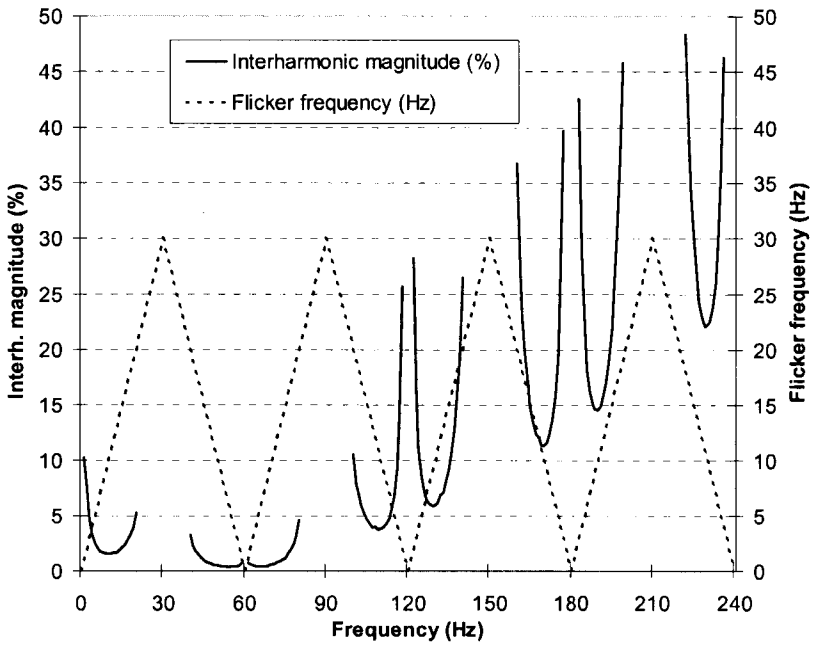

Figure 6.5: RMS fluctuation-based interharmonic–flicker curve

Table 6.1: Values of RMS-based and peak-based interharmonic-flicker curves

IH freq. (Hz)	Flicker freq. (Hz)	Critical IH mag.- RMS (%)	Critical IH mag. - Peak (%)
41	19	2.28	2.28
46	14	0.82	0.85
51	9	0.45	0.47
56	4	0.44	0.45
62	2	0.59	0.58
67	7	0.46	0.42
73	13	0.87	0.73
78	18	2.47	1.84
102	18	6.77	1.84
107	13	3.96	0.73
113	7	4.71	0.42
118	2	25.69	0.58
123	3	16.08	0.50
133	13	7.10	0.73
138	18	15.46	1.84
161	19	27.37	2.28
166	14	13.33	0.85
171	9	11.62	0.47
176	4	26.10	0.45
184	4	28.90	0.45
189	9	14.57	0.47
194	14	18.99	0.85
198	18	37.30	1.84
223	17	40.33	1.50
228	12	23.07	0.67
233	7	25.86	0.42

It can be seen that the limit for interharmonics increases with the interharmonic frequency. When the interharmonic frequency reaches 180 Hz, it is virtually impossible to experience RMS fluctuation-caused light flicker. This is because the interharmonic magnitude has to reach about 15% to cause the problem. This number is much higher than the limits established for harmonics. The lowest threshold for interharmonic level is near the fundamental frequency. This is due to the fact that the interharmonic component around the fundamental frequency can cause more RMS fluctuation than the one at higher frequencies [refer to equation (6.9)] The enlarged curve near the fundamental frequency (between 30 Hz and 90 Hz) is shown in Figure 6.9. By checking the curves, one can determine whether an interharmonic component can cause perceptible flicker. If the interharmonic component at a specific frequency is above the curve, the flicker problem is very likely to occur, while an interharmonic component under the curve would be unlikely to cause an RMS fluctuation-related flicker problem.

6.4.2 Peak Fluctuation-Based Interharmonic-Flicker Curve

Figure 6.6 presents the interharmonic–flicker curve derived from the waveform peak fluctuation. The IEEE flicker limit is used in this case too. It can be seen that the interharmonic magnitude that causes perceptible flicker does not increase with the interharmonic frequency, which is consistent with the observation that the peak fluctuation is independent of interharmonic frequency (see Figure 6.4). The limit near the equivalent flicker frequency of 9 Hz is the lowest. It is important to point out that the IEEE flicker curve is based on RMS values. When deriving the peak fluctuation-based interharmonic–flicker curve, the same IEEE flicker curve is used. The validity of this approach needs to be further verified. As will be shown next, the derived interharmonic–flicker curve has at least some reference value. This is because one cannot say that a particular lamp is sensitive to RMS fluctuation or peak fluctuation with certainty.

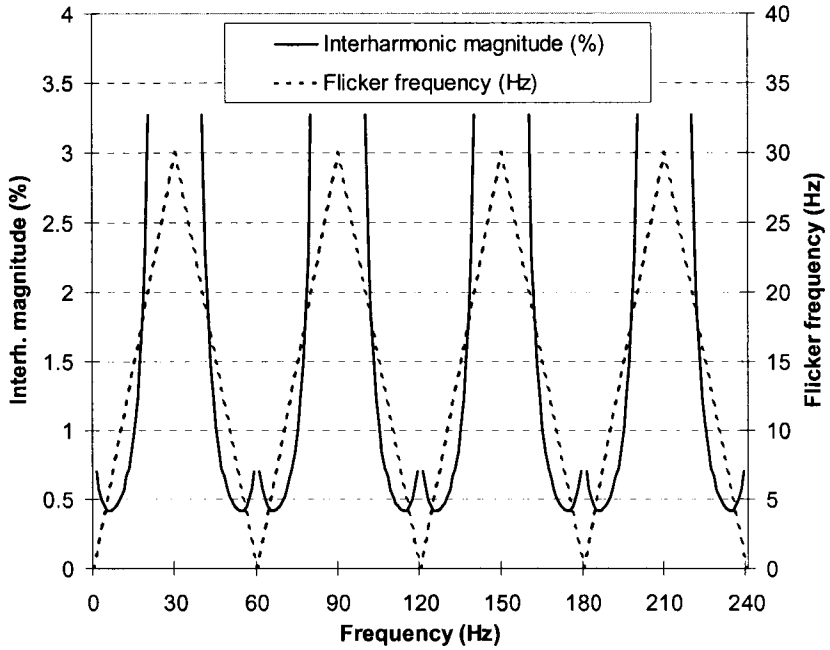

Figure 6.6: Peak fluctuation-based interharmonic–flicker curve

6.4.3 IEC Flickermeter-Based Interharmonic-Flicker Curve

The method to derive this curve is slightly different. In this case, one needs to program the IEC flickermeter algorithm [50] first. The algorithm is summarized in Appendix B. The waveform generated using equation (6.2) is then fed into the algorithm. The output of the algorithm is the short-term flicker level (P_{st}). The threshold of irritability is reached when P_{st}=1. At a certain interharmonic magnitude and phase angle, P_{st} will equal one. The minimum magnitude of the interharmonic that results in P_{st}=1 defines one point in the interharmonic-flicker curve. The curve is produced by changing the frequency of the interharmonic component and plotting the magnitudes resulting in P_{st}=1 against different interharmonic frequencies.

This exercise has led to the following finding: The IEC flickermeter cannot assess flickers that are caused by interharmonics with frequencies greater than 102 Hz. In other words, when such flicker-causing waveforms are fed into the

flickermeter, the P_{st} results will be significantly less than one, implying no flicker problem. Table 6.2 shows some of the test results.

Table 6.2: Flickermeter results for signals containing one interharmonic

Interharmonic Frequency (Hz)	$\Delta f = f_{IH} - f_1$ (Hz)	Value of m (%)	P_{st}
105	45	5	0.887
110	50	10	0.870
130	70	10	0.064
130	70	50	0.317
177	117	100	0.012
187	127	100	0.007

It can be seen that when f_{IH} is very high, the P_{st} is very small, indicating no flicker. This is the case even if the interharmonic magnitude is equal to the fundamental-frequency magnitude. This contradicts our field experiences. Fluorescent light flicker was witnessed for approximately 3% interharmonic at f_{IH} =189 Hz.

A careful analysis of the flickermeter algorithm reveals that the problem is caused by the bandpass filter of Block 3 of the flickermeter. The filter eliminates the DC and high-frequency components since it is judged that human brains are not sensitive to those frequencies. The filter has a cutoff frequency of 42 Hz as shown in Figure 6.7.

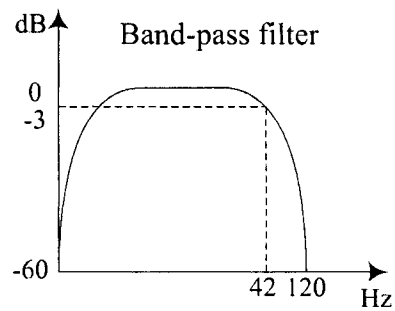

Figure 6.7: Response of the Block 3 filter of the IEC flickermeter

According to the IEC flickermeter, the input waveform is squared before it enters the bandpass filter. So the filter actually sees the following waveform:

$$
\begin{aligned}
x_{input} &= v^2(t) \\
&= V_1^2 \sin^2(2\pi f_1 t) + V_1^2 m^2 \sin^2[2\pi(f_1 + \Delta f)t + \theta_{IH}] \\
&\quad + V_1^2 2m \sin(2\pi f_1 t)\sin[2\pi(f_1 + \Delta f)t + \theta_{IH}] \\
&= \frac{1}{2}V_1^2 - \frac{1}{2}V_1^2 \cos(4\pi f_1 t) + V_1^2 m \cos(2\pi \Delta f t + \theta) \\
&\quad + V_1^2 m \cos[2\pi(2f_1 + \Delta f)t + \theta_{IH}] \\
&\quad + \frac{1}{2}V_1^2 m^2 - \frac{1}{2}V_1^2 m^2 \cos[2\pi(2f_1 + 2\Delta f)t + 2\theta_{IH}] \\
&\approx \frac{1}{2}V_1^2 - \frac{1}{2}V_1^2 \cos(4\pi f_1 t) + V_1^2 m \cos(2\pi \Delta f t + \theta) \\
&\quad + V_1^2 m \cos[2\pi(2f_1 + \Delta f)t + \theta_{IH}]
\end{aligned}
\tag{6.15}
$$

In the above approximation, the m^2 term is ignored. It can be seen from equation (6.15) that there are four frequency components in the signal: DC, $2f_1$, Δf, and $2f_1+\Delta f$. The bandpass filter will definitely filter out DC, $2f_1$, and $2f_1+\Delta f$. The only component left is Δf. The criteria to avoid this component being filtered out, without attenuation, is

$$\Delta f < 42 \text{ Hz} \quad \text{or} \quad f_{IH} < 60 + 42 = 102 \text{ Hz}.$$

In other words, the flickermeter will not be able to detect flickers caused by interharmonics whose frequencies are higher than 102 Hz.

As a further verification to the above finding, a waveform with f_{IH} =187 Hz and m = 50% is generated and shown in Figure 6.8. It can be seen that the waveform has noticeable flicker. The flicker frequency is 7 Hz ($=187-3\times60$). However, the spectral components of v^2 are all outside the passing band of the bandpass filter, which means that they are all filtered out.

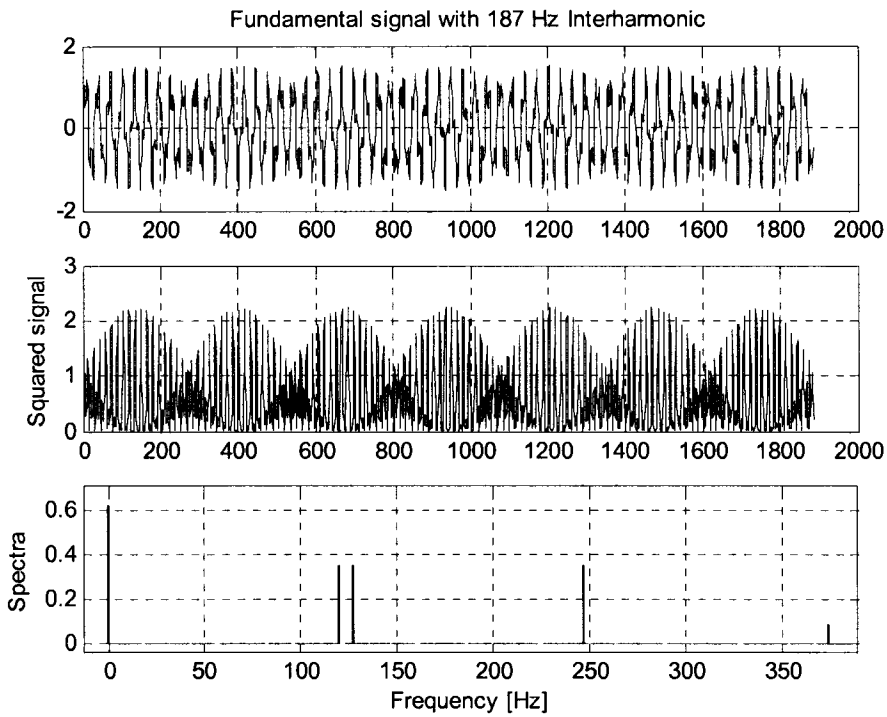

Figure 6.8: Waveform caused by a 187-Hz interharmonic and the spectrum of v^2 (DC, 120, 127, 247 and 374 Hz)

As a result, the IEC flickermeter-based interharmonic-flicker curve will not have a limit on interharmonics whose frequencies are higher than 102 Hz. But there is a limit below 102 Hz. The developed interharmonic-flicker curve is shown in Figure 6.9. This curve was originally presented in [54]. In Figure 6.9, RMS-based and peak-based interharmonic-flicker curves are also shown. It can be seen that limits are very similar. The IEC flickermeter-based limit is slightly more restrictive.

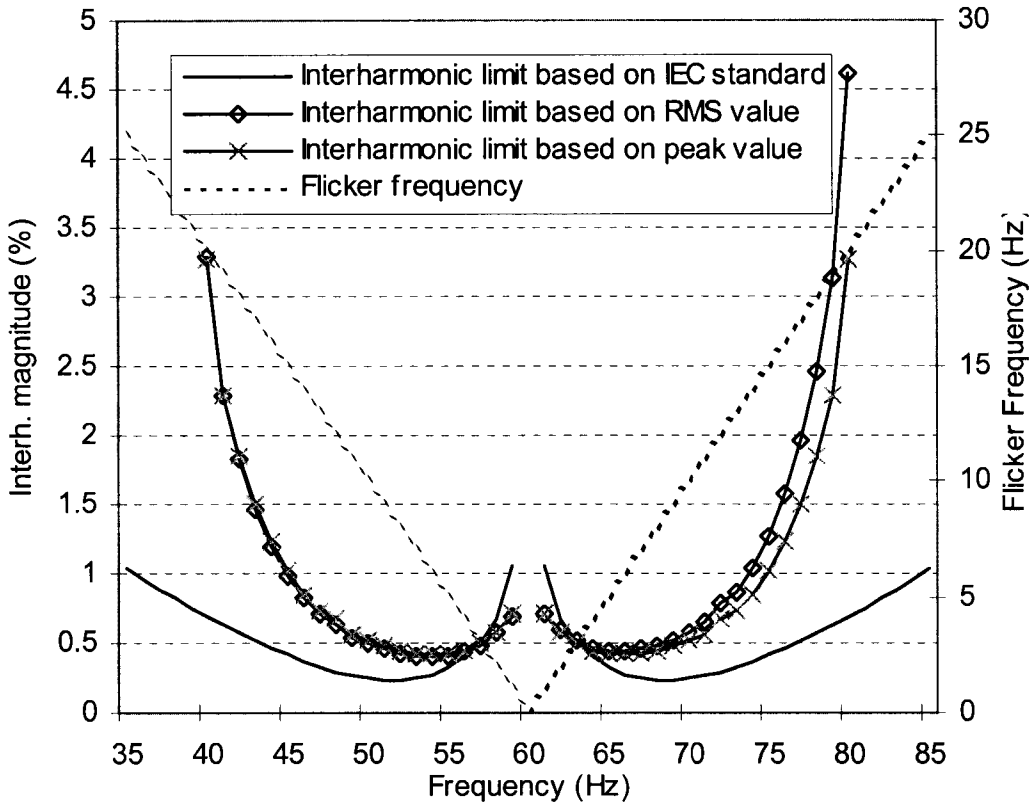

Figure 6.9: Comparison of three interharmonic-flicker curves

6.5 Potential Applications and Discussions

One of the potential applications of the proposed interharmonic–flicker curve is to evaluate flicker problems caused by VFDs or other static frequency conversion devices. As an example, the same real-life case in Chapter 5 involving a flicker–producing current source inverter-based VFD is evaluated using the developed curve. Figure 6.10 shows the characteristics of a voltage waveform snapshot measured at the drive terminal.

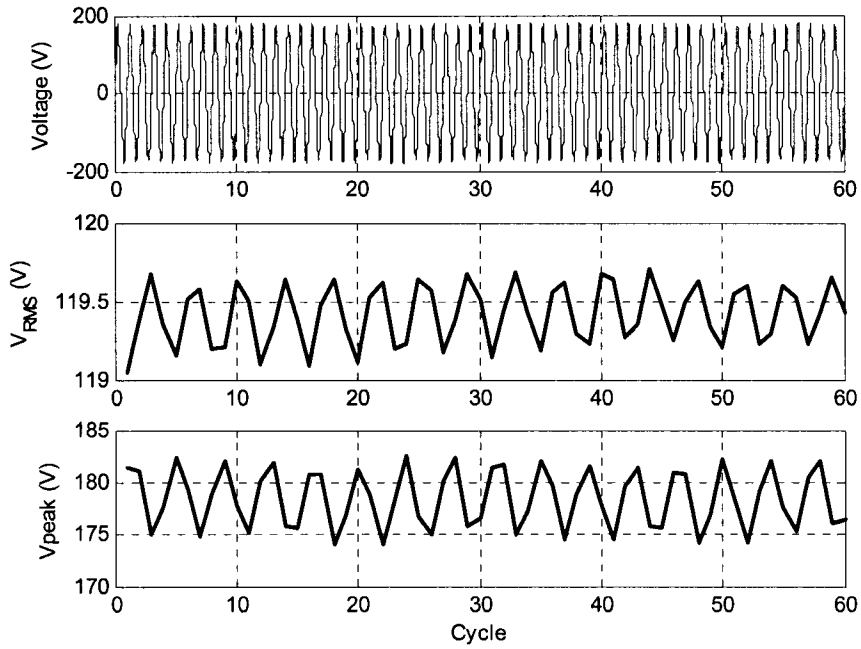

Figure 6.10: A sample waveform snapshot and its RMS/peak fluctuation pattern

A consistent fluctuation pattern can be seen from the waveform plot. This pattern can be more clearly observed from RMS and peak plots. The number of fluctuations in plots is about 16, which means that the flicker frequency is 16 Hz. The snapshot corresponds to a drive output frequency of 42.7 Hz. At this drive frequency, the most dominant interharmonic is at 196 Hz and the corresponding flicker frequency is 16 Hz. There is a good agreement between theory and observation.

When the drive operates at different frequencies, interharmonics with different magnitudes and frequencies are produced. Figure 6.11 shows the magnitude of the dominant interharmonic (the interharmonic with the lowest frequency) as a function of its frequency. The x–axis is also shown in terms of drive speed. The results were extracted from waveform snapshots measured in the field. During the measurements, fluorescent light flicker was observed at some operating points. These points are marked as stars in the figure.

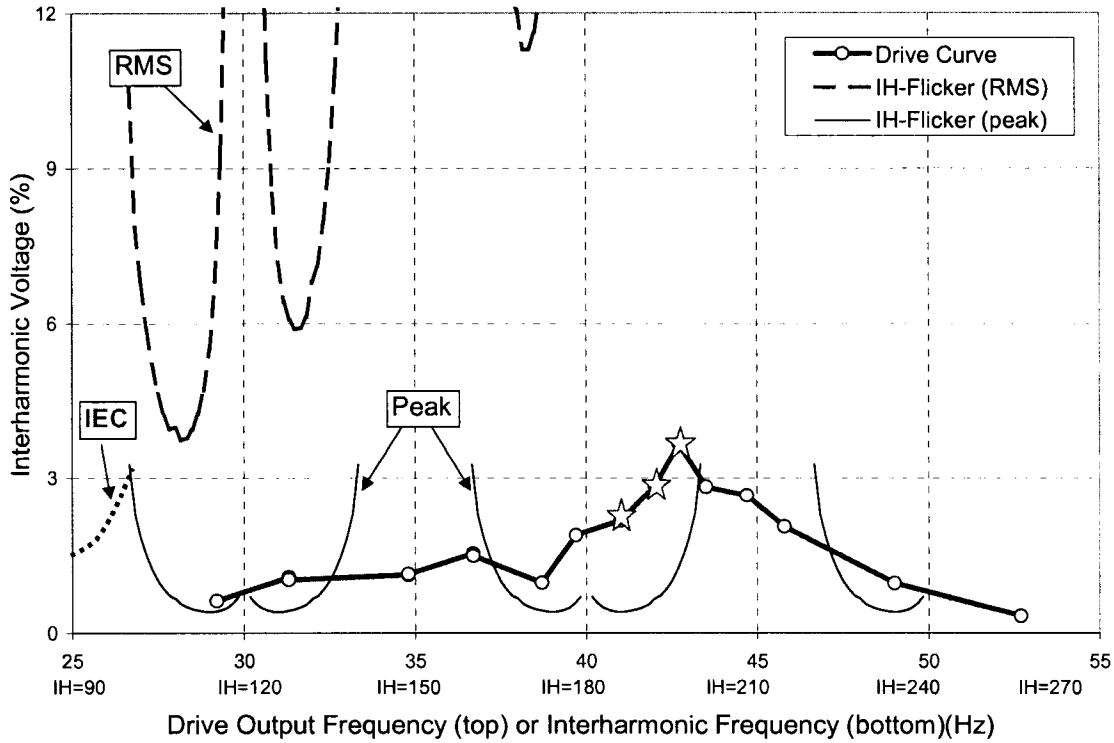

Figure 6.11: Interharmonic voltage profile of a VFD

To assess the severity of the interharmonic level, the proposed interharmonic–flicker curves were overlaid on top of the drive interharmonic curve. The following interesting observations can be made:

1) The drive curve is always below the RMS-based interharmonic-flicker curve. As a result, no flicker should be observed in theory if the lamps were sensitive to RMS fluctuations only.

2) The drive curve is above the peak-based interharmonic-flicker curve at several operating points. If the lamps were sensitive to peak fluctuations only, a number of flicker cases would have been observed.

3) The IEC flickermeter-based interharmonic-flicker curve has no limit for the drive operating points. As a result, the IEC flickermeter will indicate no flicker for all field cases.

4) The reality is that there are three cases exhibiting perceivable flicker. This implies that the actual lamp is neither sensitive solely to the RMS nor the peak fluctuation. Furthermore, the IEC flickermeter-based interharmonic-flicker curve is not useful at all to assess the problem.

5) A more likely scenario is that the limit for the interharmonic resides between RMS-based and peak-based interharmonic-flicker curves. In other words, the two interharmonic-flicker curves might define the range of possible flicker impact.

It is important to note that reference [47] has presented interharmonic-flicker curves using experimental results on fluorescent lights. The worst case curves are very close to the peak fluctuation-based interharmonic-flicker curve (Figure 6.6). This close agreement confirms that fluorescent lights are more sensitive to peak fluctuations. The lowest limits shown in [47] are about 1% for the frequency range of 100 Hz to 400 Hz, which agrees with our field experiences. Figure 6.6 shows lowest limits of 0.5%. Both limits are reasonably close. These results can be used to derive general limits on interharmonics. Note that the IEEE 519 [55] does not specify limits on interharmonics, but its new revision is expected to address this issue. One simple way to limit interharmonics is to set a conservative limit of 0.5% or an optimistic limit of 1% for individual interharmonic distortions. This approach, however, can be too restrictive. One can see from the interharmonic-flicker curves that the minimum interharmonic magnitude to cause flicker can be significantly higher than 1% when the interharmonic frequency is not close to harmonic frequencies. Experiences gained from solving the problem of Figure 6.11 indicate that it is very difficult to design a filtering scheme that can keep interharmonics below 1% level for all interharmonic frequencies. This is due to the fact that the interharmonics can appear at any frequency depending on the drive operating condition. There is no such problem for harmonics. As a result, a flat limit of 0.5% or 1% can be difficult to meet in reality.

6.6 Summary

This chapter has analyzed relationships between interharmonics and flickers. Limits for interharmonic voltages were established based on accepted flicker curves. There are two limit curves, one is based on RMS fluctuation and the other is based on peak fluctuation. The curves define the acceptable level of interharmonics as a function of their frequencies. A conservative limit of 0.5% on individual interharmonic distortion is recommended.

An application example has been shown in Section 6.5. The example also reveals that a lot more research work is needed to characterize the flicker impact of interharmonics. It appears that the actual limit for interharmonic is lamp dependent. However, the two proposed limit curves likely represent the upper and lower boundary to assess the severity of interharmonics from the perspective of light flickers.

This chapter also reveals some limitations of the IEC flickermeter when applied to measure interharmonic-caused flickers. The flickermeter cannot detect flickers caused by interharmonics whose frequencies are higher than 102 Hz. Significant work is needed to improve the IEC flickermeter algorithm in this area.

The interharmonic-flicker curve developed in this chapter is based on one interharmonic component. Variable frequency drives typically produce pairs of interharmonic currents with the same magnitude. These currents will interact with the system impedance, resulting in two interharmonic voltages of different magnitudes. How to limit interharmonic voltages for this more realistic case needs to be further investigated.

CHAPTER 7

Conclusions and Future Work

7.1 Conclusions

The topic of power quality (PQ) has received a lot of interest in recent years due to an increasing utilization of power electronic-based loads which are sensitive to minor changes in the power supply. PQ disturbances that had previously been considered insignificant can be severe enough to affect these sensitive loads. PQ problems are costly, especially to industrial customers, because of related production loss, production restart, and equipment damage. Consequently, PQ disturbance-source detection is the first step in diagnosing and solving PQ problems. Installing PQ monitors at various locations on the power system can provide useful information about the location of PQ disturbances. If sufficient PQ monitors are available, along with an accurate and reliable method for PQ disturbance-source detection, locations of PQ disturbance sources can be pinpointed. The location of disturbance sources is one important characteristic of PQ disturbances. The subject of this thesis is to develop a method that is theoretically justifiable and practically useful for the determination of PQ disturbance sources. In practice, if a PQ monitor is installed at the service entrance of an industrial plant, disturbance-source results from the analysis of recorded voltage and current data can determine whether the disturbance originates inside or outside of the industrial plant. This information would be very useful for diagnosing and solving PQ problems, as different solutions

or mitigation methods may be implemented depending on the source and characteristic of the problem. This thesis deals with methods to determine sources of voltage sags and flickers. The main conclusions and contributions of this thesis are summarized as follows:

- Due to its concrete background and sound concept of methods for transmission-line protection, the proposed method was motivated by the incremental-impedance concept. The method applied frequency-domain system identification and least-squares to estimate the equivalent impedance of the non-sag side from the recorded sag data. It was shown mathematically that the sign of the estimated resistance can reveal the direction of sag sources. A modification of the proposed method was also provided when nonlinear or constant power loads were presented. The proposed method was verified using data from simulations, experimental tests, and field measurements. Three major sag sources—faults, transformer energization, and induction motor starting—were considered. Results showed that the proposed method is effective and reliable.

- The proposed system identification-based method was then extended to the problem of flicker-source detection. Flickers can be viewed as repetitive sags so the proposed method can also be applied to flicker-source detection. However, it is necessary to check whether changes of fundamental-frequency voltages are sufficient to cause the flicker because unreliable flicker sources can be obtained from the system identification-based method if fundamental-frequency changes are insignificant. RMS and peak relative voltage fluctuations and the correlation coefficient between peak voltage magnitude and fundamental-frequency voltage magnitude were proposed to quantify the strength of changes of fundamental-frequency components. If relative voltage fluctuations and the correlation of changes are rather weak, the flicker source may be the interharmonic-producing loads. An alternative method based on the power direction was thus proposed in order to detect the flicker source from interharmonic-producing loads. The flicker source can be determined from the sign of the dominant interharmonic active

power generated by the loads. The validity of the proposed methods was verified by case studies. Guidelines for using the combined method were also developed based on discussions and observations from case studies.

- A systematic approach to derive limits for interharmonic magnitudes from the published flicker limits was presented. The limit was represented as an interharmonic-magnitude versus interharmonic-frequency curve and was called an interharmonic-flicker curve. The curve defines the acceptable level of interharmonics as a function of their frequencies. It was found that the actual limit for interharmonic magnitude is lamp dependent. The two proposed limit curves based on RMS and peak magnitude fluctuations likely represent the upper and lower boundary to assess the severity of interharmonics from the perspective of light flickers. Potential applications using a real-life VFD case were presented.
- The proposed PQ disturbance-source detection method has the following deliveries. When the disturbance happens in the power system, the developed method can help both the utility and customers to identify the location of that disturbance. If the monitoring point is at the utility-customer interface, it can be known that if the disturbance originates inside or outside of a particular customer. Any dispute about responsibility for the disturbance can then be fairly solved. The source location of the disturbance, as analyzed using the developed method, will help to specify the party who originates the disturbance. Proper penalty measures would be applied to the party who caused the damage.

7.2 Suggestions for Future Work

Some extensions and modifications for future work can be explored as follows:

- The proposed sag-source detection method is developed for radial systems where upstream and downstream subsystems can be identified clearly. Although the proposed method works reasonably well under this condition, it may not be

reliable for meshed systems. More investigation is needed in order to deal with the general system configuration.

- It would be useful to test the proposed sag-source and flicker-source detection methods on a larger set of data from field measurements, preferably with various types of modern loads, in order to discover and solve any practical problems that may arise when using the proposed methods for real-life applications.
- The proposed disturbance-source detection method focuses primarily on two types of PQ disturbances, voltage sags and flickers. While voltage sag is the most common PQ disturbance and voltage flicker is another type of important PQ disturbance, there are other common PQ disturbances in the power system such as voltage transients which require investigation. An extension of the disturbance-source detection method to cover other PQ disturbances should be researched. For example, the following concept might be useful for transient-source detection using the proposed system identification-based method. It is well known that voltage transients possess one unique characteristic, the predominant frequency (f_d). The typical predominant frequency for the transients in the distribution system is generally between 300 Hz and 1,000 Hz. Using the system identification-based method computed at the predominant frequency, the transient-source detection may be obtained, e.g. checking the sign of $\Re\text{eal}[\boldsymbol{Z}(f_d)]$.
- The interharmonic-flicker curve developed is based on a single interharmonic. However, two dominant interharmonics are likely in practice. Interharmonic-flicker curves based on two dominant interharmonics would be useful and more realistic for practical applications. In addition, it was found that flickers caused by interharmonics whose frequencies are higher than a certain frequency were actually observed from the real-life VFD case, however they could not be detected by the IEC flickermeter. Therefore, significant work is needed to remove this limitation of the IEC flickermeter algorithm.

References

[1] J. J. Burke, D. C. Griffith, and D. J. Ward, "Power Quality - Two Different Perspectives," *IEEE Trans. Power Delivery*, Vol. 5, No. 3, July 1990, pp. 1501-1513.

[2] J. E. Flory, T. S. Key, W. M. Smith, R. P. Stratford, J. C. Smith, J. M. Clemmensen, L. F. Saunders, C. D. Potts, G. L. Emmett, W. A. Moncrief, and B. Singletary, "The Electric Utility-Industrial User Partnership in Solving Power Quality Problems," *IEEE Trans. Power System*, Vol. 5, No. 3, August 1990, pp. 878-886.

[3] R. C. Dugan, M. F. McGranaghan, and H. W. Beaty, *Electric Power System Quality*, McGraw Hill, New York, 1996.

[4] *IEEE Recommended Practice for Powering and Grounding Electronic Equipment*, IEEE Standard 1100, 1999.

[5] *Electromagnetic Compatibility (EMC) – Part 4: Testing and measurement techniques – Section 30: Power Quality Measurement Methods*, International Electrotechnical Commission (IEC) Standard 61000-4-30, 2003.

[6] *Electromagnetic Compatibility (EMC) – Part 2: Environment – Section 5: Classification of electromagnetic environments*, International Electrotechnical Commission (IEC) Standard 61000-2-5, 1995.

[7] *IEEE Recommended Practice for Monitoring Electric Power Quality*, IEEE Standard 1159, 1995.

[8] M. F. McGranaghan, D. R. Mueller, and M. J. Samotyj, "Voltage Sags in Industrial Systems," *IEEE Trans. Industry Applications*, Vol. 29, No. 2, March/April 1993, pp. 397-403.

[9] M. M. Morcos and J. C. Gomez, "Flicker Sources and Mitigation," *IEEE Power Engineering Review*, November 2002, pp. 5-10.

[10] T. Tayjasanant and W. Xu, "A Case Study of Flicker/Interharmonic Problems Caused by a Variable Frequency Drive," Proceeding of the 11th International Conference on Harmonics and Quality of Power (ICHQP), Lake Placid, USA, Sept. 2004, pp. 72-76.

[11] J. Douglas, "Power Quality Solutions," *IEEE Power Engineering Review*, March 1994, pp. 3-7.

[12] K Price, "Practices for Solving End-User Power Quality Problems," *IEEE Trans. Industry Applications*, Vol. 29, No. 6, Nov/Dec 1993, pp.1164-1169.

[13] *Electromagnetic Compatibility (EMC) – Part 2: Environment – Section 8: Voltage dips and short interruptions on public electric power supply systems with statistical measurement results*, International Electrotechnical Commission (IEC) Standard 61000-2-8, 2002.

[14] Paul C. Y. Ling and A. Basak, "Investigation of Magnetizing Inrush Current in a Single-Phase Transformer," *IEEE Trans. Magnetics*, Vol. 24, No. 6, Nov. 1988, pp. 3217-3222.

[15] The Electricity Council, *Power System Protection, Volume 1-3*, Peter Peregrinus Ltd., United Kingdom, 1981.

[16] C. Li, T. Tayjasanant, and W. Xu, "A Method for Voltage Sag Source Detection by Investigating Slope of the System Trajectory," *Proc. Inst. Elect. Eng.-Gen. Transm. Distrib.*, Vol. 150, No.3, May 2003, pp. 367-372.

[17] A. C. Parsons, W. M. Grady, E. J. Powers, and J. C. Soward, "A Direction Finder for Power Quality Disturbances Based Upon Disturbance Power and Energy," *IEEE Trans. Power Delivery*, Vol. 15, No. 3, July 2000, pp. 1081-1086.

[18] N. Hamzah, A. Mohamed, and A. Hussain, "A New Approach to Locate the Voltage Sag Source Using Real Current Component," *Electric Power Systems Research*, Vol. 72, Issue 2, Dec 2004, pp. 113-123.

[19] A. G. Phadke and J. S. Thorp, *Computer Relaying For Power Systems*, John Wiley & Sons, 1988.

[20] A. K. Pradhan and A. Routray, "Applying Distance Relay for Voltage Sag Source Detection", *IEEE Trans. Power Delivery*, Vol. 20, No. 1, Jan. 2005, pp. 529-531.

[21] W. D. Stevenson, *Elements of Power System Analysis*, 4th ed., McGraw-Hill, 1982.

[22] P. G. McLaren, G. W. Swift, Z. Zhang, E. Dirks, R. P. Jayasinghe, and I. Fernando, "A New Directional Element for Numerical Distance Relays," *IEEE Trans. Power Delivery*, Vol. 10, No. 2, April 1995, pp. 666-675.

[23] G. Benmouyal and S. Chano, "Characterization of Phase and Amplitude Comparators in UHS Directional Relays," *IEEE Trans. Power Systems*, Vol. 12, No. 2, May 1997, pp. 646-653.

[24] *IEEE Guide for Protective Relay Applications to Transmission Lines*, IEEE Standard C37.113, 1999.

[25] T. S. Sidhu, H. Singh, and M. S. Sachdev, "Design, Implementation and Testing of An Artificial Neural Network Based Fault Direction Discriminator for Protecting Transmission Lines," *IEEE Trans. Power Delivery*, Vol. 10, No. 2, April 1995, pp. 697-706.

[26] F. H. Magnago and A. Abur, "Fault Location Using Wavelets," *IEEE Trans. Power Delivery,* Vol. 13, No. 4, Oct. 1998, pp. 1475-1480.

[27] K. S. Prakash, O. P. Malik, and G. S. Hope, "Amplitude Comparator Based Algorithm for Directional Comparison Protection of Transmission Lines," *IEEE Trans. Power Delivery*, Vol. 4, No. 4, Oct. 1989, pp. 2032-2041.

[28] A. Albert, *Regression And The Moore-Penrose Pseudoinverse*, Academic press, New York, 1972.

[29] V. Grigore, J. Hatonen, J. Kyyra, and T. Suntio, "Dynamics of a Buck Converter with a Constant Power Load," Proceedings of the 29th Power Electronic Specialists Conference (PESC), May 1998, pp. 72-78.

[30] D. J. Hill, "Nonlinear Dynamic Load Models with Recovery for Voltage Stability Studies," *IEEE Trans. Power Systems,* Vol. 8, No. 1, Feb. 1993, pp. 166-176.

[31] W. Xu and Y. Mansour, "Voltage Stability Analysis Using Generic Dynamic Load Models," *IEEE Trans. Power Systems*, Vol. 9, No. 1, February 1994, pp. 479-493.

[32] P. Ju, E. Handschin, and D. Karlsson, "Nonlinear Dynamic Load Modelling: Model and Parameter Estimation," *IEEE Trans. Power Systems,* Vol. 11, No. 4, Nov. 1996, pp. 1689-1694.

[33] W. Xu, E. Vaahedi, Y. Mansour, and J. Tamby, "Voltage Stability Load Parameter Determination from Field Tests on BC Hydro's system," *IEEE Trans. Power Systems,* Vol. 12, No. 3, Aug. 1997, pp. 1290-1296.

[34] *IEEE Standard Dictionary of Electrical and Electronic Terms*, IEEE Standard 100, 1984.

[35] P. G. Kendall, "Light Flicker in Relation to Power System Voltage Fluctuation," *Proc. IEE*, Vol. 113, No. 3, 1966, pp. 471-479.

[36] M. K. Walker, "Electric Utility Flicker Limitations," *IEEE Trans. Industry Applications*, Vol. IA-15, No. 6, Nov/Dec 1979, pp. 644-655.

[37] B. Bhargava, "Arc Furnace Flicker Measurements and Control," *IEEE Trans. Power Delivery*, Vol. 8, No. 1, Jan 1993, pp. 400-410.

[38] S. R. Mendis, M. T. Bishop, A. V. Do, and D. M. Boyd, "Investigation of Transmission System Voltage Flicker due to Multiple AC and DC Furnace Operations," *IEEE Trans. Power Delivery*, Vol. 10, No. 1, Jan 1995, pp. 483-496.

[39] S. R. Mendis, M. T. Bishop, and J. F. Witte, "Investigations of Voltage Flicker in Electric Arc Furnace Power Systems," *IEEE Industry Applications Magazine*, Jan/Feb 1996, pp. 28-34.

[40] G. Manchur and C. C. Erven, "Development of A Model for Predicting Flicker from Electric Arc Furnaces," *IEEE Trans. Power Delivery*, Vol. 7, No. 1, Jan 1992, pp. 416-426.

[41] L. Tang, S. Kolluri, and M. F. McGranaghan, "Voltage Flicker Prediction for Two Simultaneously Operated AC Arc Furnaces," *IEEE Trans. Power Delivery*, Vol. 12, No. 2, Apr 1997, pp. 985-992.

[42] IEEE Interharmonic Task Force Working Document, Draft 3 (2001, July 14), [Online]. Available: http://grouper.ieee.org/groups/harmonic/iharm/docs/ih519c.pdf

[43] M. Halpin, L. Conrad, and R. Burch, *IEEE Tutorial on Voltage Fluctuations and Lamp Flicker in Electric Power Systems*, IEEE Power Engineering Society Publication 01TP151, 2001.

[44] M. Beaver, *Introduction to Probability and Statistics*, 8th ed., PWS-KENT Publishing Company, 1991.

[45] T. Keppler, N. R. Watson, J. Arrillaga, and S. Chen, "Theoretical Assessment of Light Flicker Caused by Sub- and Interharmonic Frequencies," *IEEE Trans. Power Delivery*, Vol. 18, No. 1, Jan 2003, pp. 329-333.

[46] W. Mombauer, "Flicker caused by interharmonics," *etzArchiv Bd.* 12 (1990) H. 12, pp. 391-396.

[47] M. De Koster, E. De Jaeger, and W. Vancoetsem (2000, Jan 19), "Light Flicker Caused by Interharmonics", [Online]. Available: http://grouper.ieee.org/groups/harmonic/iharm/docs/ihflicker.pdf

[48] *IEEE Recommended Practice for Electric Power Distribution for Industrial Plants*, IEEE Standard 141, 1993.

[49] *Electromagnetic Compatibility (EMC) – Part 2: Environment – Section 2: Compatibility levels for low-frequency conducted disturbances and signalling in public low-voltage power supply systems*, International Electrotechnical Commission (IEC) Standard 61000-2-2, 2002.

[50] *Electromagnetic Compatibility (EMC) – Part 4: Testing and measurement techniques – Section 15: Flickermeter – Functional and design specifications*, International Electrotechnical Commission (IEC) Standard 61000-4-15, 2003.

[51] L. Tang, D. Hall, M. Samotyj, and J. Randolph, "Analysis of DC Arc Furnace Operation and Flicker Caused by 187 Hz Voltage Distortion," *IEEE Trans. Power Delivery*, Vol. 9, No. 2, April, 1994, pp. 1098-1107.

[52] L. Peretto and A. E. Emanuel, "A Theoretical Study of the Incandescent Filament Lamp Performance under Voltage Flicker," *IEEE Trans. Power Delivery*, Vol. 12, No. 1, Jan. 1997, pp. 279-288.

[53] S. M. Halpin, R. Bergeron, T. M. Blooming, R. F. Burch, L. E. Conrad, and T. S. Key, "Voltage and Lamp Flicker Issues: Should the IEEE Adopt the IEC Approach?," *IEEE. Trans. Power Delivery*, Vol. 18, No. 3, July 2003, pp. 1088-1097.

[54] R. Bergeron (2000, Jan 25), "Compatibility level for interharmonic voltages" [Online]. Available: http://grouper.ieee.org/groups/harmonic/iharm/docs/rbwg8.pdf

[55] *IEEE Recommended Practices and Requirements for Harmonic Control in Electrical Power Systems*, IEEE Standard 519, 1992.

Appendix A

Numerical Values of Interharmonic-Flicker Curves

Table A.1 tabulates numerical values of RMS-based, peak-based, and IEC flickermeter-based interharmonic-flicker curves illustrated in Chapter 6 between 1 Hz and 240 Hz. Blank cells in the table represent unavailable results. Note that results from IEC flickermeter-based interharmonic-flicker curve are only available from 20 Hz to 100 Hz.

Table A.1: Numerical values of RMS-based, peak-based, and IEC flickermeter-based interharmonic-flicker curves between 1 Hz and 240 Hz

IH freq. (Hz)	Flicker freq. (Hz)	Critical IH mag.- RMS (%)	Critical IH mag. - Peak (%)	Critical IH mag. - IEC (%)
1	1	10.23	0.70	
2	2	7.44	0.58	
3	3	4.97	0.50	
4	4	3.37	0.45	
5	5	2.53	0.42	
6	6	2.09	0.41	
7	7	1.83	0.42	
8	8	1.69	0.44	
9	9	1.60	0.47	
10	10	1.56	0.51	
11	11	1.58	0.57	

IH freq. (Hz)	Flicker freq. (Hz)	Critical IH mag. - RMS (%)	Critical IH mag. - Peak (%)
121	1		0.70
122	2	28.22	0.58
123	3	16.08	0.50
124	4	11.07	0.45
125	5	8.52	0.42
126	6	7.17	0.41
127	7	6.43	0.42
128	8	6.07	0.44
129	9	5.90	0.47
130	10	5.93	0.51
131	11	6.13	0.57

12	12	1.71	0.67	
13	13	1.73	0.73	
14	14	1.89	0.85	
15	15	2.11	1.01	
16	16	2.42	1.23	
17	17	2.78	1.50	
18	18	3.26	1.84	
19	19	3.85	2.28	
20	20	5.27	3.27	3.13
21	21			2.81
22	22			2.57
23	23			2.37
24	24			2.19
25	25			2.03
26	26			1.90
27	27			1.77
28	28			1.66
29	29			1.56
30	30			1.46
31	29			1.36
32	28			1.28
33	27			1.19
34	26			1.11
35	25			1.03
36	24			0.96
37	23			0.89
38	22			0.82
39	21			0.75
40	20	3.30	3.27	0.69
41	19	2.28	2.28	0.63
42	18	1.83	1.84	0.57
43	17	1.47	1.50	0.52
44	16	1.20	1.23	0.47
45	15	0.98	1.01	0.42
46	14	0.82	0.85	0.37
47	13	0.70	0.73	0.33
48	12	0.64	0.67	0.29

132	12	6.82	0.67
133	13	7.10	0.73
134	14	7.96	0.85
135	15	9.14	1.01
136	16	10.75	1.23
137	17	12.78	1.50
138	18	15.46	1.84
139	19	18.91	2.28
140	20	26.50	3.27
141	21		
142	22		
143	23		
144	24		
145	25		
146	26		
147	27		
148	28		
149	29		
150	30		
151	29		
152	28		
153	27		
154	26		
155	25		
156	24		
157	23		
158	22		
159	21		
160	20	36.82	3.27
161	19	27.37	2.28
162	18	23.00	1.84
163	17	19.54	1.50
164	16	16.90	1.23
165	15	14.84	1.01
166	14	13.33	0.85
167	13	12.28	0.73
168	12	12.07	0.67

49	11	0.54	0.57	0.26
50	10	0.49	0.51	0.24
51	9	0.45	0.47	0.23
52	8	0.43	0.44	0.23
53	7	0.41	0.42	0.24
54	6	0.40	0.41	0.28
55	5	0.41	0.42	0.33
56	4	0.44	0.45	0.40
57	3	0.49	0.50	0.51
58	2	0.57	0.58	0.67
59	1	0.70	0.70	1.05
60	0			
61	1	0.71	0.70	1.05
62	2	0.59	0.58	0.67
63	3	0.51	0.50	0.51
64	4	0.47	0.45	0.40
65	5	0.44	0.42	0.33
66	6	0.44	0.41	0.28
67	7	0.46	0.42	0.24
68	8	0.49	0.44	0.23
69	9	0.53	0.47	0.23
70	10	0.58	0.51	0.24
71	11	0.65	0.57	0.26
72	12	0.79	0.67	0.29
73	13	0.87	0.73	0.33
74	14	1.04	0.85	0.37
75	15	1.26	1.01	0.42
76	16	1.57	1.23	0.47
77	17	1.95	1.50	0.52
78	18	2.47	1.84	0.57
79	19	3.14	2.28	0.63
80	20	4.61	3.27	0.69
81	21			0.75
82	22			0.82
83	23			0.89
84	24			0.96
85	25			1.03

169	11	11.30	0.57
170	10	11.30	0.51
171	9	11.62	0.47
172	8	12.33	0.44
173	7	13.55	0.42
174	6	15.68	0.41
175	5	19.38	0.42
176	4	26.10	0.45
177	3	39.72	0.50
178	2		0.58
179	1		0.70
180	0		
181	1		0.70
182	2		0.58
183	3	42.57	0.50
184	4	28.90	0.45
185	5	22.03	0.42
186	6	18.26	0.41
187	7	16.15	0.42
188	8	15.05	0.44
189	9	14.57	0.47
190	10	14.54	0.51
191	11	14.89	0.57
192	12	16.16	0.67
193	13	17.04	0.73
194	14	18.99	0.85
195	15	21.79	1.01
196	16	25.42	1.23
197	17	30.37	1.50
198	18	37.30	1.84
199	19	45.81	2.28
200	20		3.27
201	21		
202	22		
203	23		
204	24		
205	25		

86	26			1.11
87	27			1.19
88	28			1.28
89	29			1.36
90	30			1.46
91	29			1.56
92	28			1.66
93	27			1.77
94	26			1.90
95	25			2.03
96	24			2.19
97	23			2.37
98	22			2.57
99	21			2.81
100	20	10.56	3.27	3.13
101	19	7.85	2.28	
102	18	6.77	1.84	
103	17	5.88	1.50	
104	16	5.21	1.23	
105	15	4.63	1.01	
106	14	4.23	0.85	
107	13	3.96	0.73	
108	12	3.99	0.67	
109	11	3.74	0.57	
110	10	3.79	0.51	
111	9	3.94	0.47	
112	8	4.25	0.44	
113	7	4.71	0.42	
114	6	5.49	0.41	
115	5	6.82	0.42	
116	4	9.26	0.45	
117	3	14.04	0.50	
118	2	25.69	0.58	
119	1		0.70	
120	0			

206	26		
207	27		
208	28		
209	29		
210	30		
211	29		
212	28		
213	27		
214	26		
215	25		
216	24		
217	23		
218	22		
219	21		
220	20		3.27
221	19		2.28
222	18	48.35	1.84
223	17	40.33	1.50
224	16	34.43	1.23
225	15	30.39	1.01
226	14	26.62	0.85
227	13	24.33	0.73
228	12	23.07	0.67
229	11	22.12	0.57
230	10	22.29	0.51
231	9	22.49	0.47
232	8	23.76	0.44
233	7	25.86	0.42
234	6	29.54	0.41
235	5	35.98	0.42
236	4	46.38	0.45
237	3		0.50
238	2		0.58
239	1		0.70
240	0		

Appendix B

IEC Flickermeter Algorithm

Figure B.1 shows a functional diagram of IEC flickermeter in IEC 61000-4-15. The flickermeter can be divided into two parts: simulation of the response of the lamp-eye-brain chain and on-line statistical analysis of the flicker signal and presentation of the results. The first task is accomplished by Blocks 2, 3 and 4, while the second task is performed by Block 5. Block details are briefly summarized next.

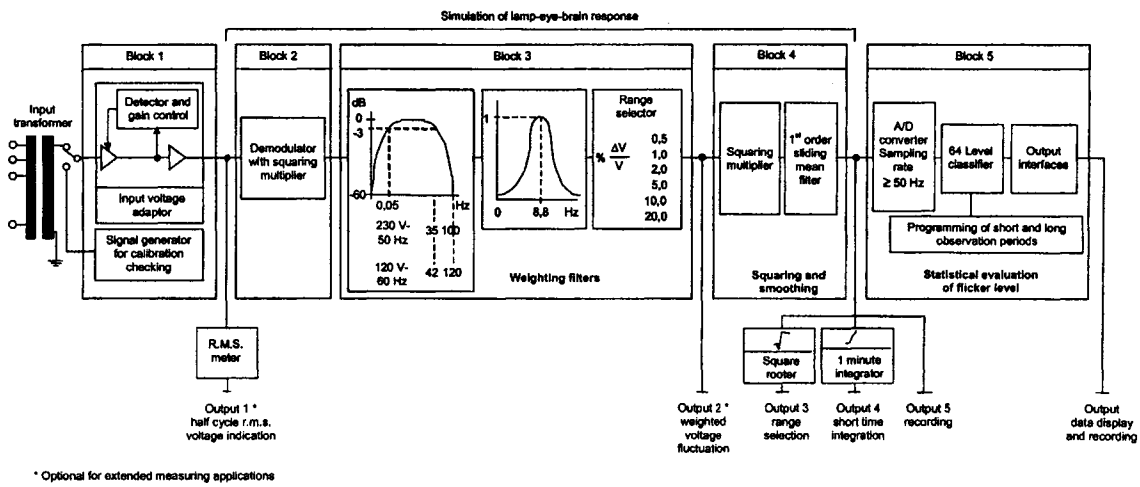

Figure B.1: A functional diagram of IEC flickermeter

Block 1: Input voltage adaptor and calibration checking circuit

The signal generator in this block checks the calibration of the flickermeter. A voltage adaptor scales the mean RMS value of the input voltage down to an internal reference level so that the subsequent analysis can work on any voltage rating. Taps of the input transformer provides suitable input voltage range to keep the input signal within its permissible range.

Block 2: Square law demodulator

The purpose of this block is to extract the voltage fluctuation by squaring the modulating voltage value scaled to the reference level, thus simulating the behavior of a lamp.

Blocks 3 and 4: Weighting filters, squaring and smoothing

There are two filters cascaded with a range selector in Block 3. The first filter eliminates the DC and network double frequency from the output of the demodulator. The second filter simulates the frequency response to sinusoidal voltage fluctuations of a coiled filament gas-filled lamp and of the human eye. The entire Block 3 can be realized by a transfer function specified in the standard. This transfer function can be modified to model different lamp responses. Block 4 consists of a squaring circuit and a first-order lowpass filter. This simulates the non-linear eye-brain perception and the storage effect in the brain. The output of this block is the instantaneous flicker sensation that varies with time.

Block 5: On-line statistical analysis

This block performs the on-line statistical analysis of the instantaneous flicker level obtained from Block 4 such as short-term flicker evaluation (P_{st}).